SAPIENZA
UNIVERSITÀ DI ROMA

# Wave effects in long-range connectivity: homogeneous and non-homogeneous periodicity

Doctorate school in Mechanical Engineering

Dottorato di Ricerca in Meccanica Teorica e Applicata – XXXIII Ciclo


Candidate

Amirsajjad Rezaei

ID number 1822398

Thesis supervisor

Prof. Antonio Carcaterra

Tutor

Dr. Federica Mezzani


November 2020

**Wave effects in long-range connectivity: homogeneous and non-homogeneous periodicity**
Ph.D. thesis. Sapienza-University of Rome



This thesis has been typeset by MS word.

Version: November 8, 2020
Author's email: amirsajjad.rezaei@uniroma1.it

# Contents

List of Figures ..... iii
List of Tables ..... v
Abstract ..... vi
Acknowledgements ..... viii
Chapter 1: Introduction and state of the art ..... 1
1.1. Background and state of the art ..... 1
1.2. Original contributions of the present investigations ..... 9
1.3. Thesis structure ..... 11
Chapter 2: Long-range and periodicity: an overview ..... 12
2.1. Introduction ..... 12
2.2. Graph-periodic structures ..... 12
2.3. Investigated structures ..... 16
2.4. Upcoming dynamic effects ..... 19
2.5. Relation between systems and effects ..... 21
2.6. Final remarks ..... 21
Chapter 3: Long-range homogenous configurations: leaf-periodicity and more ..... 23
3.1. Introduction ..... 23
3.2. Homogenous long-range waveguide with spring-like links ..... 23
3.2.1. Open interaction region ..... 24
3.2.1.1. A basic model for long-range waveguide ..... 24
3.2.1.2. Mistuned long-range connectivity ..... 31
3.2.2. Confined interaction region ..... 33
3.2.2.1. Integral model for long-range waveguides ..... 33
3.2.2.2. A summation model for long-range waveguides ..... 40
3.3. Resonator-based long-range homogenous waveguide ..... 41
3.3.1. Generalized mathematical model ..... 41
3.3.2. Single degree-of-freedom resonator unit ..... 44
3.3.3. Double degrees-of-freedom resonator unit ..... 48
3.4. Long-range homogenous membrane ..... 52
3.4. Final remarks ..... 56
Chapter 4: Nonlinear long-range homogenous waveguide ..... 57
4.1. Introduction ..... 57
4.2. Randomly excited nonlinear long-range waveguide ..... 57

4.2.1. General formulation and linearization procedure (random excitation) ..... 57
4.2.2. Periodically modulated coefficient and instability ..... 60
4.2.3. Fredholm's integral and entangled wavenumbers ..... 62
4.2.4. Approximate dispersion analysis ..... 63
4.3. Nonlinear long-range connectors ..... 64
4.4. Final remarks ..... 66
Chapter 5: Long-range non-homogeneous periodic configurations: tree-periodicity ..... 67
5.1. Introduction ..... 67
5.2. Waveguide with periodic nonlocalities ..... 67
5.2.1. Band structure identification ..... 68
5.2.2. Negative stiffness and low frequency stopbands ..... 72
5.2.3. Virtual experiment by insertion loss analysis ..... 73
5.2.4. Working mechanism and energy flow partition ..... 77
5.3. Elastic compound waveguide with periodic nonlocalities ..... 79
5.3.1. Band structure identification ..... 79
5.3.2. Insertion loss analysis ..... 83
5.4. Axisymmetric cylinder with periodic nonlocalities ..... 84
5.5. Final remarks ..... 89
Chapter 6: Concluding remarks ..... 90
Appendix A: On systems with temporal long-range effects ..... 93
A.1. Introduction ..... 93
A.2. Plane waves ..... 93
A.3. Frequency response analysis ..... 94
A.4. Modal analysis ..... 95
A.5. Results and discussion ..... 96
A.5.1. Wave propagation ..... 96
A.5.2. Frequency response analysis ..... 98
A.6. Final remarks ..... 99
References ..... 100

# List of Figures

## Chapter 1

Fig. 1. 1: A two degrees-of-freedom mass-in-spring system ..... 2
Fig. 1. 2: Bragg scattering mechanism ..... 3
Fig. 1. 3: Connectivity templates [51]: (a) one-all (b) all-all (c) random sparse (d) all-all limited ..... 4
Fig. 1. 4: Wavenumber-frequency curves in nonlocal medium [49] ..... 6
Fig. 1. 5: Path of an initial disturbance in different waveguides [96] ..... 6
Fig. 1. 6: Different propagation scenarios in long-range metamaterials [109] ..... 8
Fig. 1. 7: Sketch illustrating the graph-periodicity concept ..... 9

## Chapter 2

Fig. 2. 1: Sketch illustrating the graph-periodicity concept ..... 13
Fig. 2. 2: Linear long-range homogenous configurations ..... 16
Fig. 2. 3: Nonlinear long-range homogenous waveguide ..... 17
Fig. 2. 4: Long-range non-homogenous periodic one-dimensional configurations ..... 17
Fig. 2. 5: Long-range non-homogenous periodic cylindrical shell ..... 17
Fig. 2. 6: Overview of the systems and methods used in the thesis ..... 18
Fig. 2. 7: General map of relations among the systems and effects ..... 21

## Chapter 3

Fig. 3. 1: Schematic of the system ..... 25
Fig. 3. 2: Different propagation modes for long-range waveguide: (a) Real part of wavenumber (b) Imaginary part of wavenumber ..... 26
Fig. 3. 3: Dispersion curves for a long-range waveguide ..... 27
Fig. 3. 4: Group velocity curves for a long-range waveguide ..... 28
Fig. 3. 5: Phase velocity curves for a long-range waveguide ..... 28
Fig. 3. 6: Modal density for a long-range waveguide ..... 29
Fig. 3. 7: Modal density for a long-range waveguide ..... 29
Fig. 3. 8: Group velocity curves for a long-range waveguide ..... 30
Fig. 3. 9: Group velocity surface of mistuned long-range waveguides ..... 31
Fig. 3. 10: Group velocity curves of mistuned long-range waveguides ..... 32
Fig. 3. 11: Group velocity curves of randomly mistuned long-range waveguides ..... 33
Fig. 3. 12: Demonstration of rectangular confining interaction region ..... 34
Fig. 3. 13: Dispersion curves corresponding to a long-range waveguide ..... 35
Fig. 3. 14: Phase velocity curves for the long-range waveguide ..... 36
Fig. 3. 15: Group velocity curves for the long-range waveguide ..... 36
Fig. 3. 16: Modal density for the long-range waveguide ..... 37
Fig. 3. 17: Long-range waveguide with arbitrary number of rectangular interaction region ..... 37
Fig. 3. 18: Dispersion curves corresponding to a long-range with a single sub-window ..... 38
Fig. 3. 19: Change in $\chi cr$ against $N$ ..... 38
Fig. 3. 20: a) Nondimensional wave amplitude and b) the corresponding fast Fourier transform for a long-range waveguide ..... 39
Fig. 3. 21: Waveguide with unequally spaced nonlocalities ..... 40
Fig. 3. 22: Group velocity curves for the waveguide with unequally spaced nonlocalities ..... 41
Fig. 3. 23: waveguide with a generalized long-range resonator-based superstructure ..... 42
Fig. 3. 24: A simple model for long-range resonator-based waveguides ..... 44
Fig. 3. 25: Representation band structure of a resonator-based long-range waveguide (SDOF) ..... 46
Fig. 3. 26: Band structure of a resonator-based long-range waveguide ..... 47
Fig. 3. 27: Group velocity curves corresponding to the acoustic branch for different value of $\chi$ ..... 47
Fig. 3. 28: Group velocity curves corresponding to the optical branch for different value of $\chi$ ..... 48
Fig. 3. 29: Long-range waveguide with a rectangular interaction region ..... 49

Fig. 3. 30: Representation band structure of a resonator-based long-range waveguide (2DOF) ..... 50
Fig. 3. 31: Band structure of a resonator-based long-range waveguide ..... 51
Fig. 3. 32: Group velocity curves corresponding to the acoustic branch for different values of $\chi$ ..... 51
Fig. 3. 33: Group velocity curves corresponding to the optical branch for different values of $\chi$ ..... 52
Fig. 3. 34: Representation of a cylindrical window ..... 53
Fig. 3. 35: Dispersion surfaces for long-range membrane a) $\chi = 100$ b) $\chi = 1000$ ..... 54
Fig. 3. 36: Vector plot of phase velocity for long-range membrane ..... 55
Fig. 3. 37: Vector plot of group velocity for long-range membrane a) $\chi = 100$ b) $\chi = 1000$ ..... 55

## Chapter 4

Fig. 4. 1: Variation of the equivalent stiffness along the axis ..... 63
Fig. 4. 2: Nondimensional dispersion relation ..... 64

## Chapter 5

Fig. 5. 1**:** A unit cell of a uniform rod with nonlocalities ..... 68
Fig. 5. 2: Stiffness-frequency diagram ..... 71
Fig. 5. 3: Band structure for uniform waveguide with nonlocalities ..... 71
Fig. 5. 4: Critical stiffness as a function of frequency ..... 72
Fig. 5. 5: Stiffness-frequency diagram ..... 73
Fig. 5. 6: Semi-infinite uniform rod with nonlocalities with two inclusions ..... 74
Fig. 5. 7: Insertion loss for a semi-infinite uniform waveguide with nonlocalities ..... 75
Fig. 5. 8: Insertion loss and related eigenfrequency curves for a three-component semi-infinite rod ..... 76
Fig. 5. 9: Insertion loss for a uniform rod with nonlocalities ..... 76
Fig. 5. 10: Effect of stiffness on insertion loss for a uniform rod with nonlocalities ..... 77
Fig. 5. 11: Semi-infinite uniform rod with nonlocalities with two inclusions ..... 77
Fig. 5. 12: Energy flow partition ..... 79
Fig. 5. 13: A unit cell with nonlocalities and impedance mismatch ..... 80
Fig. 5. 14: Comparison between three different cases ..... 81
Fig. 5. 15: Change in critical frequencies due to the introduction of nonlocalities ..... 83
Fig. 5. 16: Insertion loss for an elastic compound rod with nonlocalities ..... 84
Fig. 5. 17: A periodicity cell of a cylindrical shell with periodic nonlocalities ..... 85
Fig. 5. 18: Band structure of an axisymmetric cylindrical shell with periodic nonlocalities ..... 87
Fig. 5. 19: Band structure of an axisymmetric cylindrical shell with periodic nonlocalities for two different values of nondimensional stiffness $K$ ..... 88

## Appendix A

Fig. A. 1: The wave attenuation curves for the waveguide with non-instant interactions ..... 96
Fig. A. 2: The phase velocity curves for the waveguide with non-instant interactions ..... 97
Fig. A. 3: The group velocity curves for the waveguide with non-instant interactions ..... 97
Fig. A. 4: The variation in the amplitude of the transfer function for the central point of a waveguide with non-instant interactions with respect to frequency ..... 98
Fig. A. 5: The phase response for the central point of a waveguide with non-instant interactions ..... 98

# List of Tables

## Chapter 2

Table 2. 1: List of the systems ..... 20
Table 2. 2: List of the effects induced by long-range interactions ..... 20

## Chapter 5

Table 5. 1: The low-frequency stopbands in an axisymmetric cylindrical shell with periodic nonlocalities ..... 88

# Abstract

Metamaterials are artificial composites, developed to exhibit specific properties. Their characteristics majorly stem from the tailored structure itself rather than its composing materials. What drew attention to this family is the exotic behaviours they inherently present, which is unusual with respect to those observed in nature. Acoustic metamaterials, in particular, could provide attractive features for practical purposes, including cloaking and noise cancelling. A second original viewpoint on metamaterials suggests the possibility of enjoying the tantamount effects by introducing a domain within which distant points interact mutually. Thus, developing distinct configurations through embedding long-range connectors within host structures could provide the potential to manipulate wave paths across the domain.

Bearing in mind the need for a wide variety of propagation phenomena in different applications, systems with long-range inclusions, which challenges the common notion of exclusive first neighbour interaction, could be a potential candidate. By initiating the graph-periodicity concept, two major categories of long-range configurations are introduced, namely long-range homogenous and non-homogenous systems. With reference to the graph-periodicity concept, genuine periodic configuration can be built, where the system captures the tree-periodicity property. In this case, due to the contribution of select groups of points in constructing the configuration, a non-homogenous periodic configuration is met. On the other hand, long-range homogenous configurations are those in which all points adhere to an identical connectivity template. Although such arrangements are not genuinely periodic (no tree-periodicity), they can be leaf-periodic depending on the template.

This thesis presents the analysis of wave propagation in conventional structures, namely waveguide, membrane and shell, integrated with long-range connector. Regarding long-range homogenous configurations, the long-range forces are modelled by summation and integral terms. The long-range operators are majorly modelled by simple spring-like connections, and in some instances by resonator units. Wave propagation behaviour of the system is comprehensively realized by examining the dispersion relation, obtained analytically. Several phenomena, including wave-stopping, negative group velocity, and redistribution of eigenstates, are observed under different circumstances depending on the comparative stiffness of long-range connections.

Next, the problem of wave propagation in long-range non-homogenous periodic configurations is investigated. Although extracting the dispersion curves for such systems is not a trivial task due to non-homogeneous distribution of long-range connectors, the adopted connectivity template provides the opportunity to take the advantage of the well-known Floquet theorem to identify the band structure. The emergence of gaps over the frequency band is confirmed. The model implies the possibility of pulling the gaps towards ultra-low frequencies and even generating stopbands, which could virtually open from zero, when connections assume negative stiffness. Insertion loss analysis is performed to roughly validate the arrangements of stopbands over the frequency band, yielded by the Floquet theorem.

Given the fact that human beings are social creatures, this creates several layers of human interactions yielding a giant network of intercommunications in societies. Thus, mathematical

modelling, analogous to the above, could be a big asset to shed light on behaviour of crowds in large scale. Correspondingly, dynamic memory, being the temporal counterpart of spatial long-range interactions, can be included in some long-established problems such as natural economic growth to achieve a more effective and accurate description of the system. Current study exclusively considers the effect of nonlocal interactions in the realm of physics and engineering though the underlying message conveyed by this concept can be extremely relevant in other fields as well.

# Acknowledgements

This thesis is the result of tremendous support and guidance that I received from many people directly or indirectly. I am greatly indebted to them for their guidance, advice, assistance, and contributions to the development of this work.

First and foremost, I present my sincere gratitude and special appreciation to my supervisor Professor Antonio Carcaterra, who put his trust in me, and provided the space for me to grow both personally and professionally. Despite his jam-packed schedule, he always tried to make some time for discussions and guiding me towards my path. Even after working for quite a long time with him, I am still surprised by his amazing intelligence, vision, and wisdom. His bold character convinced me to look at him as a mentor at certain instances of the past few years, and I wish I could acquire more of his qualities. I feel highly privileged to work under his supervision and shall always remain grateful for the support I received from him.

I would like to express my grateful acknowledgment to Professor Sergey Sorokin, who warmly welcomed me in Denmark during my sabbatical. Sergey was an integral part of my Ph.D. journey and came along to run subjects just when I was a bit disappointed at my choice of pursuing doctoral studies. He was always there for me in times of need and constantly helped me to sort out my personal and educational affairs during my stay in Aalborg. For all those matters, Sergey deserves a special thanks.

Special appreciation go to my favourite Italian, Dr. Federica Mezzani, who I forced to listen to my half-baked theories at times. She, alongside being a fantastic tutor, supported me with her friendship and understanding. I must also give a shout out to Dr. Silvia Milana, who repeatedly bailed me out of paperwork troubles by her remarkable negotiation skills.

Throughout the course of my Ph.D., I had the pleasure of meeting some of the most incredible people, those who their presence made my life exceptionally easier. I take this opportunity to thank my office mates/friends in Rome including:

- Lina, my real companion, in early days of confusion in Italy
- Leandro, the lively Italian dude, who is responsible for my recent interest in basketball
- Dorra for our epic conversations
- Maicol for giving my insight into Japanese culture
- Dario, the real engineer, who I learned a lot from
- Elena, the queen of COVOLUTION, for her everlasting nice attitude
- Simone, my half Iranian dude from Pomezia
- Manuel for tolerating my loud leaky headphones

I am forever thankful to tenant of *Boulevard of Broken Dreams* and countless friends that I met in Aalborg, especially:

- Neel, my cheerful dude, who has always been a shoulder to me
- Allan, the Brazilian Mohamed Salah, for creating numerous joyful moments
- Pedro, the Brazilian Pablo Escobar, for our hot political dialogues
- Hamed and Samaneh, the lovely couple, for showing me new perspectives of life

Selfishly, I would like to thank me for long working hours that are illegal under labour laws, and for never giving up when situation became tight on occasion. I thank Oreo biscuit and coffee, which had a central role in keeping me alive and energized along the past three years. I also must express my gratitude towards a few mathematical entities, namely Fourier, Floquet, and convolution theorems due to their undeniable contributions in making this work possible.

Last but not least, my sincere appreciation to my family for their continuous love, help and support. I am forever beholden to my parents; those who gave me the courage to step out of my comfort zone and seek my own destiny. This journey would not have been possible if not for them, and I dedicate this milestone to them.

# Chapter 1: Introduction and state of the art

## 1.1. Background and state of the art

Studying the wave propagation behaviour of systems integrated with long-range interactions is the major objective of the present work. A typical feature of molecular and supramolecular scaled systems, i.e. nonlocality is brought to the macro scale systems constructing a particular type of metamaterials called *elastic* metamaterials. The nature of elastic domains, which embrace the long-range forces, is profoundly changed with respect to the nature of that considering only standard interactions (short-range), generating potential supplemental propagation effects.

Early studies on the wave path in the artificially structured materials were conducted at the end of nineteenth century. Bose [1] investigated the status of electromagnetic waves propagating within a twisted structure, identified as *chiral* structure in the recent terminology, in terms of refraction and polarisation. Regarding the modern metamaterials, the pioneering studies by Veselago [2], Pendry [3] and Smith [4] incentivized many researchers to develop new contributions to achieve a better understanding of metamaterials' behaviour. Although the Greek word "*meta"* refers to emergence of new occurrences [5], nowadays, by attaching this prefix to a word, a further concept is created, possessing a more comprehensive essence with respect to its stem. Metamaterials yield beyond the common propagation behaviours, provided by the conventional materials, and exhibit brand new properties. Such anomalies primarily stem from the orientation and arrangement of their constructing blocks. In the light of the foregoing, a metamaterial, as accurately defined in [6], is a "macroscopic composite of periodic or non-periodic structures, whose function is due to both the cellular architecture and the chemical composition". The above definition highlights the meaning of: (1) connectivity template among the unit cells and (2) both individual and collective effects in the network. The constructing elements, which form the array should be smaller or equal with respect to the wavelength they are interacting with, for the metamaterial to be capable of manipulating the waves [6].

Two major classifications are available for metamaterials, namely *electromagnetic* and *acoustics*. Unlike the bulk materials, electromagnetic metamaterials grant the gradation of the refractive index, even negative values, providing the possibility to achieve some unconventional devices such as invisibility cloaks [7–9]. Negative index metamaterials, wherefore both permittivity and permeability are negative, felicitate the development of more enhanced equipment, in particular filters, antennas and phase shifters [10–13] though some natural substances such as noble metals display negative permittivity only in specific wavelength bands. Electromagnetic metamaterials also allow for designing lenses with elevated resolutions owing to their lack of diffraction limit with respect to that of classical optical devices [3,14,15].

The task of controlling the sound waves is afforded by acoustic metamaterials, for which the bulk modulus and the density could adopt a range of values, not applicable for conventional materials. The existence of double negative acoustic metamaterials, inspired by Veselago's medium in electromagnetism, was shown by Li and Chan [16] yielding a medium with negative refractive index. Effective negative bulk modulus and density are counterintuitive concepts in the context of classical mechanics since no natural-based substance presents such intrinsic characteristics, meaning the system experiences expansion when being compressed and out of phase acceleration with respect to the driving force. To gain an insight into how negative parameters could emerge, a simple two degrees-of-freedom mass-spring configuration, as shown in Fig. 1. 1, is considered.

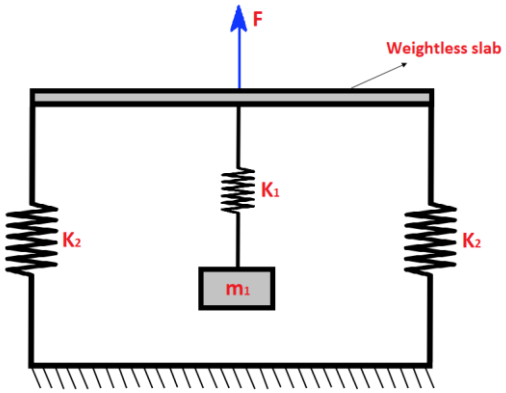


Fig. 1. 1: A two degrees-of-freedom mass-in-spring system

Assuming the existence of the interior resonator is not perceived by the observer, when the system is under harmonic excitation $F = F_0 e^{i\omega t}$, the associated effective stiffness of the system $\tilde{k}$ is obtained as:

$$\tilde{k} = 2k_2 + \frac{k_1}{1-\frac{\Omega^2}{\omega^2}} \qquad (1\text{-}1)$$

with $\Omega^2 = k_1/m_1$ being the resonant frequency of the resonator. Provided that $\Omega > \omega$ and $2k_2(\Omega^2/\omega^2 - 1) < k_1$, $\tilde{k}$ adopts a negative value. As an illustration a mass-mass configuration could be taken into account as a system possessing negative effective mass.

Analysis of *phononic crystals* (PCs), a special subcategory of acoustic metamaterials, reveals the existence of frequency bands within which the transmission of energy is prohibited [17–24], i.e. stopbands. Emergence of such gaps originates from the venture of wavefronts for adjusting their phase while crossing the interface between the constructing impedance mismatched elements of the crystal. Bragg scattering, which explains the working mechanism of PCs, was first submitted to discuss the x-ray diffraction from crystals and later utilized to identify their structure. As shown in Fig. 1. 2, the radiated waves from the scatterers, the parallel planes composed of periodic arrays of atoms, may interfere both constructively and destructively depending upon the characteristics of the diffracted waves as well as the spacing between the planes. Concerning periodic arrays, Bragg scattering defines a condition on the

length scale, to secure the occurrence of destructive interference. This implies the need for large size crystals for the sake of compatibility with the long wavelength of sound waves in the audible range, thereby limited applications. In contrast with PCs, *locally resonant acoustic metamaterials* (LRAMs), which take the advantage of dynamic local resonance [25], are disassociated from the preceding issue, providing the opportunity to design markedly smaller devices compared with the wavelength. Based on several contributions available in literature [25–31], stopbands are born due to the attachment of subunits to a host matrix, resonating and subsequently absorbing the energy propagating across the system within specific frequency bands, analogous to Fig. 1. 1. Various application including acoustic cloaking, acoustic diode, ultrasonic metamaterial lens etc. [32–36], are provided by the remarkable gift of acoustic metamaterials, capable of manipulating the mechanical waves.

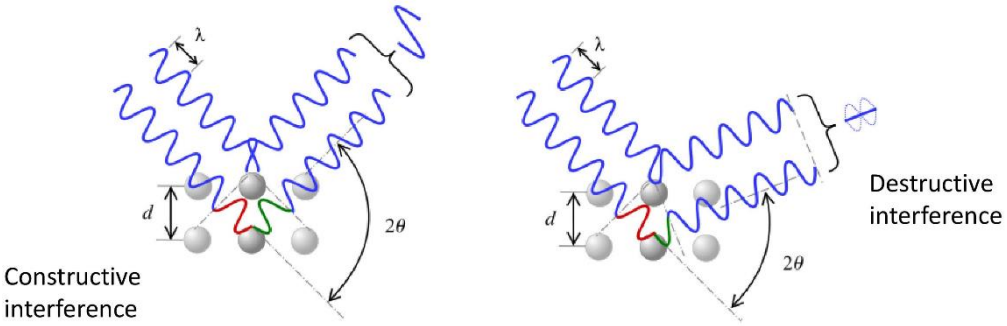


Fig. 1. 2: Bragg scattering mechanism

Apart from the wave propagation anomalies in metamaterials, distinct behaviours concerning the travelling waves within other domains are also engaging. For instance, light discloses peculiar effects concerning its propagation including slowing, stopping, time reversal and superluminality [37–42], when subjected to certain circumstances. As reported in [43–45], a phenomenon called near-irreversibility is met in conservative linear systems with singularities in their modal density. Since the function of near-irreversible configurations is tied with the conversion of mechanical energy to heat, not typical of linear systems and intrinsic to nonlinear ones, they could be beneficial for absorption purposes.

Another category of metamaterials could be developed by embracing the underlying ideas of nonlocal and micropolar elasticity [46–50], which tackles the problems in the micro and nano scale. To plainly state the idea, let us consider the nonlocal theory of elasticity law as:

$$\boldsymbol{t}_{kl,k} + \rho(\boldsymbol{F}_l - \ddot{\boldsymbol{w}}_l) = 0 \tag{1-2a}$$

$$\boldsymbol{t}_{ij}(\boldsymbol{X}) = \int_V \alpha(|\boldsymbol{X}' - \boldsymbol{X}|, \tau)\, \boldsymbol{\sigma}_{ij}(\boldsymbol{X}')dv(\boldsymbol{X}') \tag{1-2b}$$

$$\boldsymbol{\sigma}_{ij}(\boldsymbol{X}') = \lambda \boldsymbol{e}_{rr}(\boldsymbol{X}')\boldsymbol{\delta}_{kl} + 2\mu \boldsymbol{e}_{kl}(\boldsymbol{X}') \tag{1-2c}$$

$$\boldsymbol{e}_{kl}(\boldsymbol{X}') = \frac{1}{2}\left(\frac{\partial \boldsymbol{w}_k(\boldsymbol{X}')}{\partial x_l'} + \frac{\partial \boldsymbol{w}_l(\boldsymbol{X}')}{\partial x_k'}\right) \tag{1-2d}$$

where $\rho$, $\boldsymbol{F}$ and $\boldsymbol{w}$ are the mass density, body forces and the displacement vector, respectively. $\lambda$ and $\mu$ are the Lame's coefficients and $\boldsymbol{\sigma}$ denotes the classical stress tensor. Based on the presented theory, the state of stress $\boldsymbol{t}$ at a given point $\boldsymbol{X}$ is not essentially determined by the strain at the immediate neighbouring points. Indeed, the state of strain at all points $\boldsymbol{X}'$is instrumental in the response of the system. Clearly this formulation considers the effect on every single point placed within the nonlocal body $\boldsymbol{V}$ and the extent to which the stress at $\boldsymbol{X}$ is influenced by the strain at other points is tuned by the kernel $\alpha$. Extending this concept to elastic structures in the macro scale is the key to design a novel type of metamaterials, namely *elastic metamaterials*, which could potentially disclose unusual behaviour. The newly introduced nonlocalities induce new forces on points and consequently modify the dynamic response of conventional elastic solids in order to achieve a fruitful performance in terms of waves. Different tasks including attenuation, absorption and blocking are among the highly demanding applications, which may be afforded by this update.

To name the established composite a metamaterial, some criteria must be met based on the submitted definition. It is evident that the individual and collective actions of both the original configuration as well as the nonlocalities are vitally important in the overall response of the system. On the other hand, the promotion of a conventional elastic system to an intricate configuration may take place by considering various spatial templates for initiating long-range forces, which unequivocally deliver different topologies. This indicates that the points entitled to such mutual forces may be selected in accordance with a certain mathematical rule or no rule at all. Since all crucial factors involved in the definition play a key role in the response, the final arrangement is indeed a metamaterial.

Acknowledging the importance of the topology in the response of systems, the connectivity matrix demonstrates how constituents are linked within a lattice. The off-tridiagonal entries in long-range systems assume non-zero values since tridiagonal matrices generally characterize purely elastic lattices. Thus, the matrix adopts a specific form for a given topology. As explained in [51], different patterns for communication channels including, one-all, all-all, random sparse and all-all limited, as shown in Fig. 1. 3 could be adopted, each exhibiting a certain behaviour unlike that of conventional short-range elastic solids.

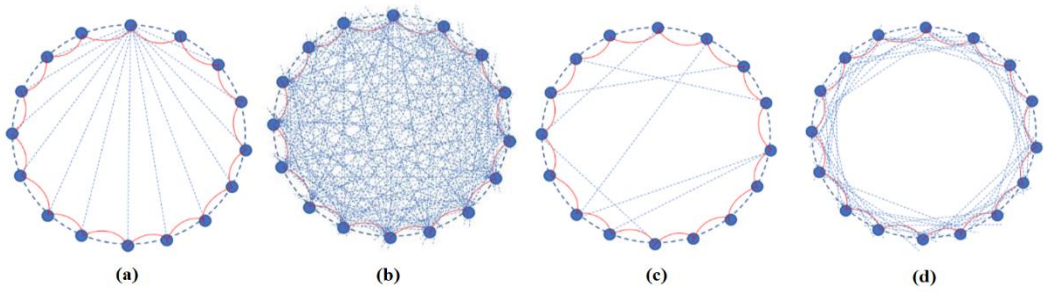


Fig. 1. 3: Connectivity templates [51]: (a) one-all (b) all-all (c) random sparse (d) all-all limited

The idea of "*action at a distance*" contributed substantially in the early mechanistic theories to achieve a better understanding of nature. For instance, the Newton's law of universal gravitation determines the instantaneous gravitational force between two agents, being

proportional to the inverse square of the distance. Although the underlying claims of the theory including instantaneous communication later challenged by the general and special relativity of Einstein, it still yields very plausible results in the low-gravity regime. Nowadays, it is evident that a force, which acts in a distance is transmitted with a delay due to the existence of an upper limit on the speed of travelling information. Several fields have borrowed the fruitful concept of long-range interactions in order to explain the challenges faced in the science world. For instance, a substantial number of studies have been devoted to realizing the effects induced by the distant elements in chemical substances [52–55] and biological agencies [56–58]. Long-range transport is proven to be a beneficial tool for modelling ecological populations [59–61], most important when separated groups are mixed. Quantum entanglement [62], the significant contribution of Einstein to quantum physics, demonstrates the bold link between the long-range interactions and physics. Further investigations in various branches of physics including quantum mechanics [63–65], chemical physics [66–68] and optics [69–71] are carried out. Long-range scheme brings also a variety of new features into the thermodynamics of the system. For example, the entropy in such systems is not proportional to the amount of material within the domain [72], i.e. non-extensive entropy, a key term in Tsallis statistical mechanics [73]. Other unconventional phenomena such negative specific heat and ergodicity breaking emerge in systems with slow decay of interactions [74], where strong long-range forces are present. The influence of a connectivity template among a mass of particles in an elastic medium has been underlined earlier. Similarly, the effect of communications among the non-adjacent agents in a crowd is vital as taken into account by several scholars in the fields of swarm dynamics [75–77], traffic flow [78,79] and population dynamics [80,81].

From a different angle, the dynamic evolution of some systems indicates the potential involvement of its time-history in the overall response suggesting the emergence of temporal long-range effects, i.e. dynamic memory. A case in point is the retarded action of the pressure fields induced by vortices on air foils, when the effect is perceived later in time. The memory effect is observed in the context of economics [82–84], where considering its influence provides more realistic predictions for the natural growth and foreign exchange rates. The introduction of delay has also shown to be a useful asset in understanding the conduct of a crowd of autonomous agents such as traffic and pedestrian flow [85–87], especially for control purposes. An integral term, usually of the convolution type, appears in the corresponding constitutive equations of viscoelastic media relating the response to the time-history of strain and this is implicitly confirmed by their macroscopic behaviour [88–90]. Studies on the transmission of optical waves in disordered media indicate the conservation of important information about the incident waveform during the passage [91–93], being the signature of memory effect.

Regarding the theory of elasticity, Kroner [94], for the first time, brought up the importance of electric cohesive forces in the state of stress within an elastic domain and was followed by Eringen [46,49] who presented an elegant mathematical framework to address the problems in this field. The results from the plane wave solution of the wave equation associated to a one-dimensional linear nonlocal elastic waveguide were virtually verified by an experimental study [49]. Even though no explicit wavenumber-frequency relation is presented in [49], the results provided by the experimental campaign underline the potent effect of long-range forces on the

response, as shown in Fig. 1. 4. Based on this figure, the trend of curves differs considerably with respect to that of the conventional waveguide (D'Alembert).

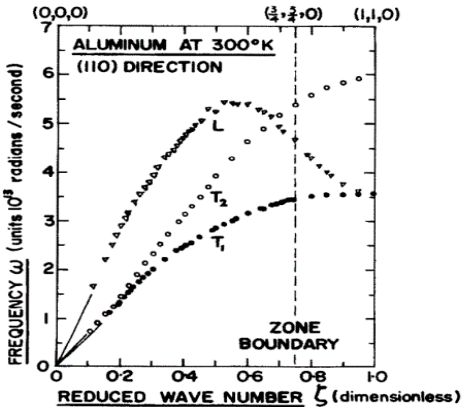


Fig. 1. 4: Wavenumber-frequency curves in nonlocal medium [49]

To overcome the difficulties facing the nonlocal theory of elasticity, mainly when the selected kernel yields fractional derivates in stress-strain relation, Zingales [95–99] developed new models to model the dynamic response of elastic configurations with long-range interactions. Discrepancies between his model and that of Eringen emerge when the analysis concerns the bounded medium for which the no spatially periodic wave forms is predicted by the present model. Based on his model, the following dispersion relation is formulated to tackle the problem of wave propagation in a long-range one-dimensional waveguide [96]:

$$\omega^2 = \beta_1 c_l^2 \kappa^2 + \frac{A}{\rho}\left[\int_{-\infty}^{\infty} g(x,\xi)(\cos\kappa x - \cos\kappa\xi)d\xi\right] \qquad (1\text{-}3)$$

In Eq. (1-3), the integral term, which is originally coming from an additional elastic potential energy corresponding to the nonlocal terms, modifies the dispersion relation associated with a conventional wave equation. The interaction of points with other counterparts within the domain is regulated by the kernel $g(x,\xi)$. The analysis suggests some changes in the response of the system including the shape modification of travelling disturbances, when the long-range forces are present (see Fig. 1. 5).

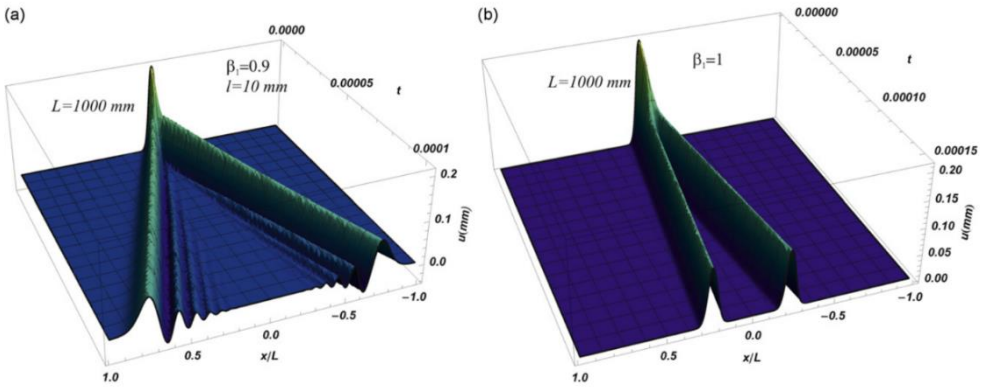


Fig. 1. 5: Path of an initial disturbance in different waveguides (a) a long-range waveguide (b) a conventional waveguide [96]

Although the given numerical analysis provides insight into the propagation of travelling pressure along a cantilever bar and subsequently the behaviour of long-range elastic materials, failure to deliver an analytical dispersion relation leaves the intrinsic characteristics of such systems uncertain. Among other major contributions in the field, Tarasov [100–103] puts forward a highly mathematical approach to realize the continuous dynamic description of long-range domains. The mathematical dexterity of the analysis is shown by considering a vast variety of interaction laws among the particles including power law and Grunwald-Letnikov-Riesz interactions. The investigations generally begin with a chain of oscillators with long-range interactions and their corresponding set of equations. The system of equations concerning a configuration with linear long-range force is transformed into the continuous medium equation employing a transform as [100]:

$$\frac{\partial^s}{\partial t^s}u(x,t) - G_\alpha A_\alpha \frac{\partial^\alpha}{\partial |x|^\alpha}u(x,t) - F\big(u(x,t)\big) = 0 \qquad (1\text{-}4)$$

where $\partial^\alpha/\partial|x|^\alpha$ is the Riesz fractional derivative with $\alpha$ being non-integer. The transform $\hat{T}$ is the combination of other three separate operations, which transforms discrete model to a continuous one. Eq. (1-4) is obtained in the infrared red limit, when the wavenumber tends to zero and thereby it is an approximate description. Besides, the approach claims achieving the fractional generalization of weak and strong nonlocal elasticity. This is examined by presenting the solution for a long-range continuum with fractional elasticity of Grunwald-Letnikov-Riesz type, as [103]

$$u(x) = \frac{f_0}{\pi\rho}\int_0^\infty \frac{\cos\lambda|x|}{C_e^2\lambda^2 + C(\alpha)\lambda^\alpha}\,d\lambda \qquad (1\text{-}5)$$

which reduces to the solution of the fractional integral elasticity for $0 < \alpha < 2$ and fractional gradient elasticity for $\alpha > 2$. His works typically is an attempt to show the robustness of the methodology since no specific dynamic behaviour of such systems is underlined, certainly not in terms of waves. To delve into the intrinsic dynamic characteristics of systems with embedded long-range connectivity, Carcaterra et al. [104] proposed a novel idea inspiring several articles and essays [105–112] including the present work. An analytical dispersion relation is available for the extracted equivalent partial differential equation, which stems from a set of equations describing the dynamics of a 1D lattice with particles interacting through electromagnetic forces, giving the possibility to reach an extensive knowledge of long-range systems. In [109], the equation of motion for a three-dimensional long-range elastic body is derived as:

$$\rho\boldsymbol{u}_{tt}(\boldsymbol{x},t) - \frac{E}{2(1+\nu)}\left[\nabla^2\boldsymbol{u}(\boldsymbol{x},t) + \frac{1}{1-2\nu}\nabla\big(\nabla\cdot\boldsymbol{u}(\boldsymbol{x},t)\big)\right] + \int_{\boldsymbol{\xi}\in\mathbb{R}^3} f(|\boldsymbol{r}|)\boldsymbol{r}\,dV = 0 \qquad (1\text{-}6)$$

Here the integral $\int_{\boldsymbol{\xi}\in\mathbb{R}^3} f(|\boldsymbol{r}|)\boldsymbol{r}\,dV$ represents the long-range forces between two arbitrary points, say $\boldsymbol{x}$ and $\boldsymbol{\xi}$, located at the distance $\boldsymbol{r}$ from one another. Remarkably, the linearized 1D version of the above equation, when Gauss-like and Laplace-like interaction laws are implemented, yields an analytical dispersion relation. This wavenumber-frequency relation provides rich propagation scenarios as compared with the D'Alembert waveguide, specifically in longer wavelengths. Based on Fig. 1. 6, different propagation regimes including superluminality and wave-stopping emerge for certain threshold of $\chi$, a nondimensional

parameter that characterizes the intensity of long-range forces with respect to the short-range forces.

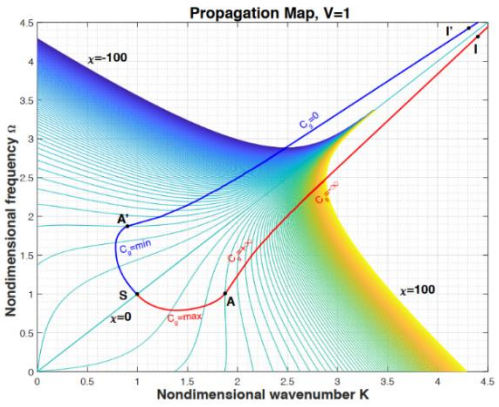


Fig. 1. 6: Different propagation scenarios in long-range metamaterials [109]

Recently some studies have been carried out to implement the idea of long-range forces into the context of locally resonant acoustic metamaterials [113,114] though no abnormality such as negative group velocity has been observed in the response. The need for utilizing a more general mathematical framework to treat the elastic metamaterials could be a rationale for researchers not to approach them. In fact, the common differential equations, which describe the dynamics of the conventional elastic solids are no longer sufficient when the distant points are interacting, for which integral terms represent such forces, reminiscent of Eq. (1-6).

Nowadays the popularity of metamaterial is rising due to the exotic behaviour they afford to present. Bringing the intrinsic features of Eringen's nonlocal elasticity [49] into the macro scale as proposed by Carcaterra et al. [104], promises the development of new kind of metamaterials, i.e. elastic metamaterials. Indeed, inserting nonlocalities into a conventional elastic solid could lead to forming two separate kind of configurations: long-range homogenous systems [109] and long-range non-homogenous systems, each capable of displaying specific phenomena. Although several works have been presented in the context of long-range metamaterials [110–112], this is the first time that a rough analysis is presented to investigate noise-induced wave propagation within a nonlinear domain with long-range interactions. The possibility of altering the propagation regime due to the change in the intensity of noise and nonlinearity is the key finding of this analysis.

One application yielded by metamaterials is the capability of filtering a range of frequencies, a major demand in a variety of industries and several periodic structures have been proposed to accomplish this objective [17,22,26,28]. This thesis is the pioneer in providing a basis for achieving an unconventional periodic structure by developing a model in which the periodicity arises from arrangement of external long-range links. The Floquet analysis of the proposed structure certifies the generation of stopbands in the associated band structure. The novel mechanism responsible for the birth of such gaps, different from the conventional periodic system with impedance mismatch, has been realized and underlined. Besides, a complementary

model of periodic configuration is provided, where the periodicity cell includes both high contrasts constructing blocks as well as nonlocalities.

Eventually, an effort has been made to include the idea of local resonance to the context of long-range metamaterials, which provides the possibility of generating stopbands without achieving a conventional periodic structure. In fact, this is an attempt to construct a model, which simultaneously benefits from the advantages of LRAMs and long-range metamaterials. The analysis suggests that the number of branches depends on degrees-of-freedom the employed external link, i.e. resonator unit, and the velocity of acoustic and optical phonons is highly impacted by the characterising parameters of resonator units including resonant frequencies and nondimensional relative stiffness.

## 1.2. Original contributions of the present investigations

This work is an attempt to provide a general understanding of occurring wave phenomena due to the introduction and combination of two notions: long-range interactions, and some sort of periodicity. The periodicity here presented under the name of *graph-periodicity* includes the classical periodic structures but generalizes this concept to cases in which the physical periodicity surprisingly does not imply necessarily periodic coefficients in the equations of motion.

In this study, spring-like links (massless elements) connects distant points along the waveguide following some prescribed connectivity pattern. However, a more general type of links comes afterwards by embracing the idea of local resonance.

Introducing the graph-periodicity concept (see Fig. 1. 7), the connectivity template is a graph made by tree and leaves, and this structure replicates itself along the waveguide. Replicating the tree-leaves structure periodically, leads to a standard periodic structure. However, if the trees are continuously distributed (i.e., not periodic) and the leaves are periodic, then a new kind of periodicity is borne, characterized by non-periodic coefficients for the equations of motion.

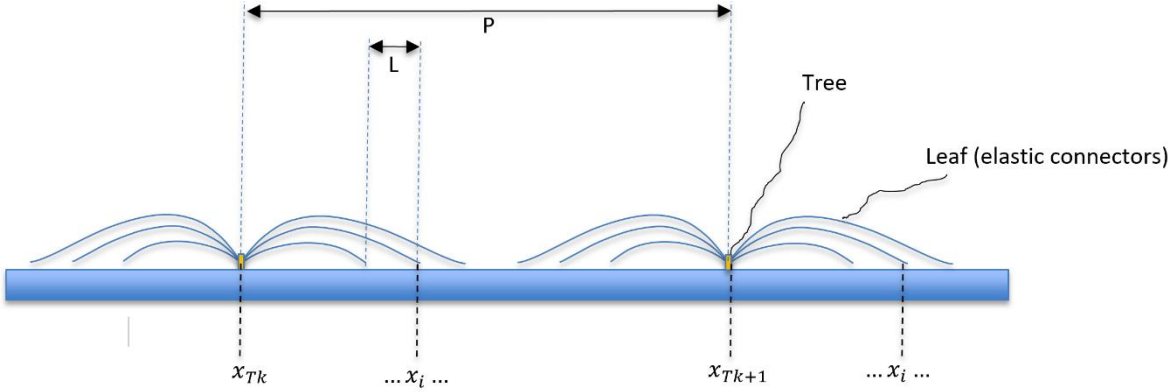


Fig. 1. 7: Sketch illustrating the graph-periodicity concept

For these reasons, two major categories of long-range configurations emerge. First, *long-range homogenous* (LRH) configurations, which consider identical connectivity template for all points. Second, *long-range non-homogenous* (LRNH) configurations, wherefore the connectivity template could differ from a point to another. Along this thesis, all cases associated with the second category are genuinely periodic, later cited as tree-periodic, due to the proper choice of connectivity templates, constructing *long-range non-homogenous periodic* arrangements. In a certain sense (not conventional), periodicity may also be present in LRH systems, later referred to as leaf-periodicity. In the first category, the particular form of dynamic description provides the opportunity for realizing the details of wave path by analytically expressing the dynamic description in the spatiotemporal Fourier domain, which enables a fruitful study on the envelope of waves. Other mathematical tools such as Floquet theorem are useful to understand the dynamic behaviour of the second category since the quest for obtaining the equation of motion is a challenging task and subsequently the derivation of the relation between the wavelength and the associated frequency is not immediate.

Regarding the *long-range homogenous* systems, the marriage of short-range and long-range interactions is beneficial for easing the path to develop technologies requiring anomalous wave propagation effects. In fact, short-range forces are ceased to be the dominant player in forming the dynamics due to the new mechanisms for energy transmission within the domain of interest, and thereby the violation from the standard behaviour of waves. Two separate long-range domains, namely waveguide and membrane, are taken into account and the emergent wave phenomena are discussed in detail. The existence of transcendental terms in the corresponding dispersion relations suggests that infinite values of wavenumber are available to produce a single frequency. The dispersion relations bring to light the emergence of different phenomena including the redistribution of eigenstates over the frequency domain, wave-stopping and negative group velocity, each scenario associated to a certain threshold of physical properties of the structures. Furthermore, along with previously mentioned phenomena, stopbands are generated in the band structure of the system, when resonator-based units are employed as long-range connectors. Moreover, a rough analysis on a randomly excited long-range 1D configuration with nonlinear connections shows that a shift in propagation regime of plane waves may be experienced given the proper circumstances with regards to the intensity of nonlinear effect and noise.

When the non-homogenous distribution of long-range connections results in conventional periodic structures, i.e., *long-range non-homogenous periodic* structures, stopbands emerge in the band structure of the systems. Two host elements, in particular rod and hollow shell, are chosen for studying the characteristics of such systems. A complementary analysis on the semi-infinite counterpart of the preceding demonstrates the interference between two sources. In fact, the difference in transmission speed across channels, i.e., rod and the spring-like links leads to the generation of sources and thus the stopbands. This effect is unique for the systems in which periodicity is induced by such long-range connectors and this mechanism is not present in conventional periodic configurations, where the impedance mismatch is responsible for the creation of gaps.

## 1.3. Thesis structure

The present chapter of the thesis declares explicitly the novel ideas we intend to bring in the scenario of long-range structures, and how it frames in the state of the art in the field.

Chapter 2 provides a bird eye view of the general conclusion drew from the analysis performed in the following chapters in order to gain a vision of the benefits submitted by long-range interactions and periodicity.

In Chapter 3, the plane wave analysis of the long-range homogenous domains is given, and the corresponding propagation schemes such as negative group velocity and wave-stopping are discussed in terms of group velocity. In the succeeding step, more general configurations are considered as long-range connectors, providing stopbands in the dispersion map of system together with the previously mentioned propagation effects.

Chapter 4 presents a detailed mathematical framework required to realize the effect of nonlinear long-rang interactions on a randomly excited system. Eventually, the effect of nonlinearity and noise on the status of travelling waves is examined by putting forward a rough approximate solution.

Chapter 5 is devoted to analysis of systems in which a periodic arrangement of external links leads to a periodic structure, a special type of long-range non-homogenous configurations. By means of Floquet theorem, the band structure of such systems is identified and the underlying mechanism responsible for the generation of stopbands is understood by investigating the energy flow across the system.

Conclusions and possible future developments are given in Chapter 6.

# Chapter 2: Long-range and periodicity: an overview

## 2.1. Introduction

The general purpose of this thesis is the identification of the wave effects promoted by the introduction of long-range connectors to elastic domains. Several types of long-range systems may be imagined thanks to the different arrangements that such connectors may adopt. This chapter is an attempt to provide an overview, as complete as possible, of a variety of systems and the corresponding effects.

Elastic metamaterials take the advantage of the concepts proposed in nonlocal elasticity and demonstrate the effects already observed in the context of electromagnetic metamaterials such as hypersonic travelling wave envelopes [115]. The core idea here is to establish long-range communications among the non-adjacent particles, which violates the notion promoted by the classical theory of elasticity allowing for interaction with the immediate neighbours only. Forces induced by nonlocal channels deeply influences the dynamics, and the response predictably deviates from the behaviour yielded by the conventional "short-range" systems. Clearly, the propagation regime could alter with the change in the intensity of the interactions. On the other hand, the connectivity template of the new communication channels, or long-range connectors, is another source of generation of new propagation phenomena. Development of conventional periodic configurations, when the periodicity is induced by nonlocal forces, is a new scenario. In fact, the proper attachment of long-range connectors to host structures such as waveguides forms periodic configurations capable of providing the frequency bands within which the wave propagation is inhibited.

In this chapter, a general overview of the results obtained in the following chapters is given. Although all phenomena are originated from the introduction of long-range forces into conventional systems, what causes the discrepancies is the way these nonlocalities are implemented. Since several long-range configurations have been considered along this thesis, the systems are presented as classified into two main categories: i) long-range homogenous (LRH) structure, and ii) long-range non-homogenous (LRNH) structures. Each class includes a few systems, contributing to better understanding of the arising effects. The closing remarks associated to each investigation are accommodated in the corresponding class, providing a scenic view of the entire study.

## 2.2. Graph-periodic structures

Notions of long-range interactions and periodicity, when suitably combined, lead to an interesting distinction between two different ways of building up long-range connectivity templates, enriching both the scenarios of nonlocal elasticity and periodic systems. This

distinction is important for the present investigation, enlightening a physical difference together with the related different mathematical approaches to the corresponding problems.

A classical periodic system shows, in general, a modular structure, where the characteristic module sequentially replicates itself along the system. This produces, as a mathematical counterpart, a differential equation of motion with periodic coefficients that characterize a conventional and genuine periodicity. We show ahead that a wider scenario discloses through the concept of graph-periodicity leading to some forms of periodicity even in the presence of constant coefficients.

For the sake of argument, let us consider a conventional infinite waveguide, described for simplicity by the standard wave equation $EA\frac{\partial^2 u}{\partial x^2} - \rho A\frac{\partial^2 u}{\partial t^2}$, with $u(x,t)$, $\rho$, $E$ and $A$ being the longitudinal displacement, mass density, Young's modulus, and the cross-section area, respectively. An additional archetypal long-range connectivity is superimposed, connecting, by a suitable long-range set of connectors, i.e., springs and in different possible fashions, distant points of the host waveguide.

For a given superimposed connectivity $G$ on a conventional waveguide, we can introduce its formal description through the symbol $G_T\left(x_{-N}, x_{-N+1,} \dots, x_{-1}, x_T, x_{1,}x_{2,} \dots, x_M\right)$. The graph $G_T$ specifies the set of connectors applied to the waveguide. Namely, the graph has a *tree* at $x_T$ connected to each of the selected points $x_{1,}x_{2,} \dots, x_M$ on its right, and to each of the points $x_{-N}, x_{-N+1,} \dots, x_{-1}$ on its left, that are the *leaves* of $G_T$. $M$ and $N$ are generally different, and the end points of leaves not necessarily equally spaced. In case the leaves are equally spaced, the spacing $L$ is named the *period of the leaves* and the related connectivity *leaf-periodic* (see Fig. 2. 1)

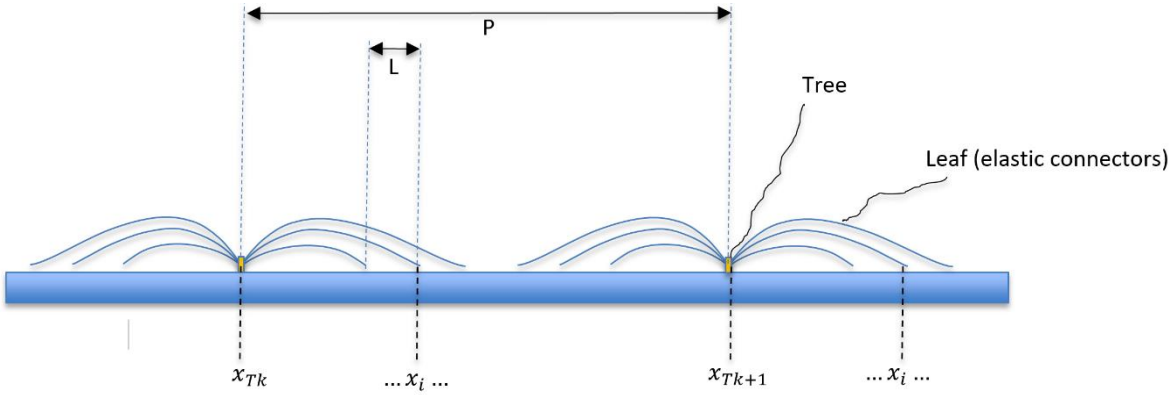


Fig. 2. 1: Sketch illustrating the graph-periodicity concept

The superposition of more connectivity graphs $G_{Tk}$ with different trees positions $x_{Tk}$, for $k = 1,2 \dots, M_P$, generates a new long-range connectivity graph $G$:

$$G = \cup_{k=1}^{M_P} G_{Tk} \qquad (2\text{-}1)$$

If the trees are equally spaced, the spacing $P$ is the *period of the trees*, distinct from the period of the leaves $L$ and the connectivity is *tree-periodic* (in some cases $P = L$).

The combination of tree-periodicity and leaf-periodicity leads to discuss several interesting cases, some of them considered in the present investigation.

A connectivity $G$ that is tree-periodic (independently of the leaf periodicity) produces a structure that is periodic in a genuine-conventional sense, i.e., its equation of motion has periodic coefficients. In fact, the connectivity $G$ applies only to specifically selected points along the waveguide, and we call for this reason the structure *long-range non-homogenous periodic* and its connectivity $G_{n-hom}$, a case analysed in this work.

If the connectivity is tree-periodic and leaf-periodic, we can generate a *long-range homogeneous periodic* structure through $G_{hom} = \lim_{P \to 0} G_{n-hom}$, that has a continuous distribution of trees. In fact, this means that the same connectivity applies identically to any point at *x* (the trees becoming infinitely dense), therefore producing homogeneity, and the presence of constant coefficients in the equation of motion (not periodic anymore). However, although in this way the tree-periodicity disappears, the leaf-periodicity still holds. Therefore, we have a constant coefficients equation of motion, but still characterized by a residual leaf-periodicity, that is an intriguing new concept investigated in the present part.

If the leaves are non-periodic, $G_{hom} = \lim_{P \to 0} T_{n-hom}$ produces simply a *long-range homogenous* connectivity without elements of periodicity, that is another case investigated in the present work.

The case $G_{hom} = \lim_{P \to 0, L \to 0} T_{n-hom}$ produce finally a continuous distribution of trees and leaves, periodicity is absent, and again a simply a *long-range homogenous* connectivity is defined.

Let us illustrate, by elemental examples, the equations of motion related to the previously introduced graph-periodicity.

The modified waveguide equation, when including the presence of the long-range elastic links, becomes:

$$EA\frac{\partial^2 u}{\partial x^2} - \rho A\frac{\partial^2 u}{\partial t^2} + \Lambda(x,t) = 0 \qquad (2\text{-}2)$$

Let us consider, as a first example, a periodic-tree and periodic-leaf connectivity, with an infinite number of trees along the waveguide, each with *N* leaves. The single-tree connectivity $G_T$, with its tree at $x_T$, is associated to the connector $\Lambda_T(x,t) = -\kappa\sum_{i=-N}^{+N}\delta(x - x_T)[u(x,t) - u(x - iL,t)]$. Simple consideration, including serially repeated trees, shows the long-range term $\Lambda_{n-hom}(x,t)$ reads:

$$\Lambda_{n-hom}(x,t) = -\kappa\sum_{r=-\infty}^{+\infty}\sum_{i=-N}^{+N}\delta(x - rP)[u(x,t) - u(x - iL,t)] \qquad (2\text{-}3)$$

The nature of the equation $EA\frac{\partial^2 u}{\partial x^2} - \rho A\frac{\partial^2 u}{\partial t^2} + \Lambda_{n-hom}(x,t) = 0$ is differential, with periodic coefficients: the differential part is $EA\frac{\partial^2 u}{\partial x^2} - \rho A\frac{\partial^2 u}{\partial t^2}$, the periodic coefficients are $\kappa\delta(x - rP)$, and:

$$\Lambda(x,t) = \Lambda(x + nP,t), \quad \forall n \in N \qquad (2\text{-}4)$$

This is an example of *long-range non-homogenous periodicity*. The most acknowledged method for periodic coefficients equations is the Floquet theorem.

However, as seen through the graph-periodicity concept, one can conceive a different way of using the same connectivity template that is not selective, i.e., does not involve only special points along the waveguide (as those at $x_{Tr} = rP$ as in the previous case) but it applies serially and homogenously to each point *x* of the structure (that means *P* becomes infinitely small). Hence, the name *long-range homogeneous periodicity*. In this case, the equation of motion does not exhibit periodic coefficients anymore. In fact:

$$\Lambda_{hom}(x,t) = -\kappa \sum_{i=-N}^{N} [u(x,t) - u(x - iL, t)] \quad (2\text{-}5)$$

This connector shows a different nature with respect to the form (3) previously presented. Using the form (5), Eq. (2-2) becomes a differential-delay equation with constant coefficients, i.e., $EA\frac{\partial^2 u}{\partial x^2} - \rho A\frac{\partial^2 u}{\partial t^2} + -\kappa \sum_{i=-N}^{N} u(x,t) - u(x - iL, t) = 0$. Although a periodically delayed term appears as $\sum_{i=-N}^{N} u(x - iL, t)$, the coefficients are constant. In this case the Floquet theorem, the typical tool for genuine periodic structures, can be skipped and replaced by a simpler direct double Fourier transform of the equation of motion.

More precisely, the first tree-periodicity case requires, because of the non-homogenous nature of the structure, a piecewise solution, each part living within any module of the system, i.e.:

$$u^{(i)}(x,t) = \left(A^{(i)} e^{jkx} + A^{(i)*} e^{-jkx}\right) e^{j\omega t}, \;\; x \in [x_i, x_i + P] \quad (2\text{-}6)$$

Different solutions satisfy continuity conditions at the module's boundaries, i.e., at $x_i \; and \; x_i + P$, and the Floquet's theory finds the non-trivial solutions for the unknown coefficients $A^{(i)}$. A set of eigenvalues follows for the wavenumbers, and their nature establishes the chance of propagating waves or inhibiting them (stopband effects).

The second case, with homogenous nature, due to the constant coefficients, permits a direct double Fourier transform, space and time, with a continuous solution along the entire waveguide (no need to express a piecewise solution as for periodic coefficients):

$$u(x,t) = \int_{-\infty}^{+\infty} \int_{-\infty}^{+\infty} W(k,\omega)\, e^{jkx} e^{j\omega t} dk \; d\omega \quad (2\text{-}7)$$

Its substitution into the equation of motion produces the dispersion relationship $k(\omega)$ and its nature determines the chance of wave propagation or its inhibition, and additionally the group velocity behaviour of the waveguide is determined.

Although the two methods do not admit any mathematical interchange, and each type needs its own technique, on the physical ground, the interpretation of the results of the two methods are comparable. In fact, they both rely of the nature of the complex wavenumber (whatever its mathematical origin, i.e., the eigenvalues analysis or the dispersion relationship), as an indicator of the kind of waves established along the waveguide.

For both the different kinds of periodicity, some transition effects are expected when the wavelength $\lambda$ becomes much smaller than *P*, and/or of *L* i.e., $kP >> 1$, and/or $kL >> 1$ where the wave energy remains trapped into the periodic inclusions, conferring to the system properties of energy propagation disruption in some frequency range.

In both cases, namely long-range homogenous and non-homogenous configurations, uncommon wave propagation effects emerge that include stopbands, wave-stopping, negative

group velocity and instabilities that amount to a rather rich scenario investigated in detail in the next sections.

## 2.3. Investigated structures

As stated in the previous section, two major categories of structures are considered. The first category, namely long-range homogenous structures, is the one wherefore every single point within the domain interacts nonlocally with other counterparts according to a specific connectivity law, and thereby homogenous. Four different systems are included in this class, three of which being composed of linearly elastic materials, two long-range one-dimensional waveguides with different long-range connectors, and a long-range membrane. Examples of such systems are shown respectively in Fig. 2. 2a, Fig. 2. 2b, and Fig. 2. 2c. The fourth structure displayed in Fig. 2. 3, is the nonlinear counterpart of the long-range waveguide with simple spring-like links as the long-range connectors (see Fig. 2. 2a).

These four systems are divided into three distinct minor groups based on the effects they represent, in the following sections. In fact, the minor classification facilitates to distinguish between novel effects induced by nonlinearity and the type of connections used in developing configurations. Plane wave solution is the key tool to carry out analyses on genuine long-range structure. Applying the plane wave solution yields analytical dispersion relations, containing key information about the propagation velocity of plane waves with different wavelengths as well as the wave envelope of mixed wavelengths. Regarding the nonlinear long-range waveguide, linearization of the dynamic description has been carried out with the help of statistical linearization method and rough estimation of the effect of noise and nonlinearity is obtained by applying the same solution to the homogenized version of the linearized problem. Further features of the system are extracted by employing the Fredholm theory.

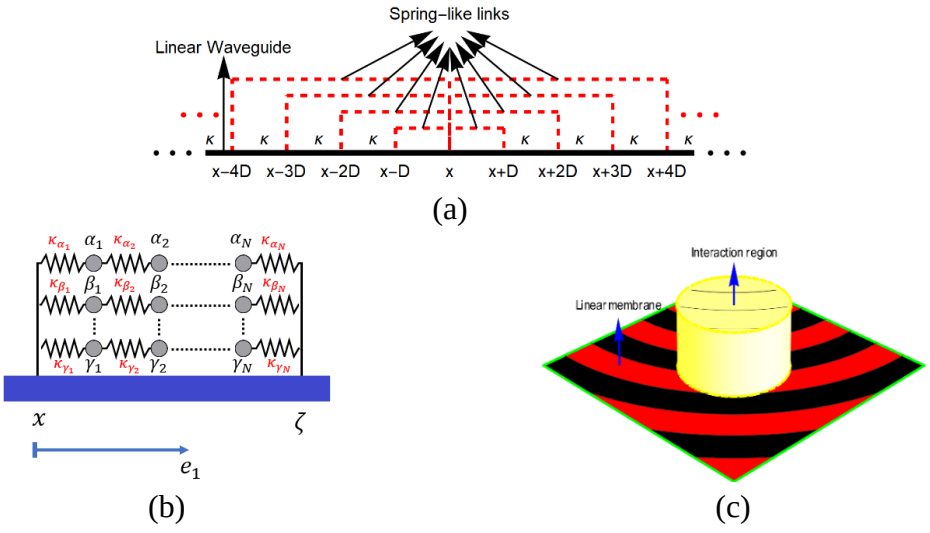


Fig. 2. 2: Linear long-range homogenous configurations (first and second minor groups): a) waveguide with spring-like links, b) waveguide with resonator units, and c) membrane

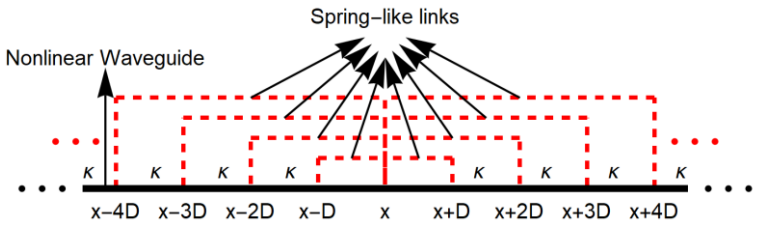


Fig. 2. 3: Nonlinear long-range homogenous waveguide (third minor group)

When only a selected group of particles contributes to constructing a long-range system, the configuration may give rise to totally different phenomena with respect to that of the first category. The second category being the long-range non-homogenous periodic structures assumes a special case, where the long-range connectors connect a selected group of points distributed periodically across the systems, generating a conventional periodic configuration. Therefore, all long-range non-homogenous configuration in thesis are periodic. To unveil the consequences of such connectivity law, three different systems are studied, shown in Fig. 2. 4 and Fig. 2. 5 The first two will later form a new minor group due to the similarity of effects they produce. In addition to these effects, the proposed periodic cylindrical shell (see Fig. 2. 5) present another effect, making it qualified to own its minor group.

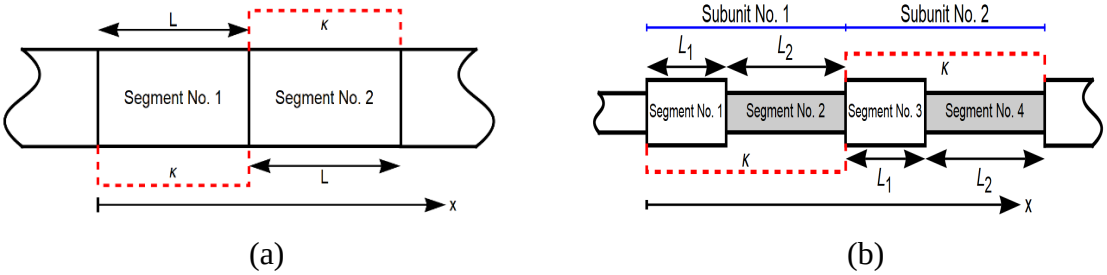


(a) (b)

Fig. 2. 4: Long-range non-homogenous periodic one-dimensional configurations: a) conventional waveguide b) compound waveguide

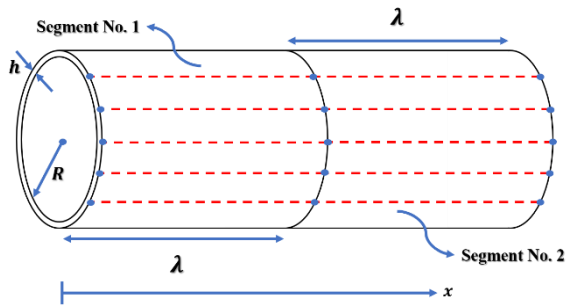


Fig. 2. 5: Long-range non-homogenous periodic cylindrical shell

In such cases, where the arrangement of spatial nonlocalities results in a periodic array, other methods must be selected for treating the corresponding dynamics. This stems from the intrinsic characteristics of the mathematical model, which contains periodic coefficients. Therefore, the band structure of these periodic configurations, namely conventional waveguide, compound waveguide and cylindrical shell, has been determined by Floquet

theorem. Other characteristics of such systems as well as the underlying mechanism for birth of the stopbands is identified by assessing the energy flow across different channels within the structures.

Fig. 2. 6 presents a general overview of contents mentioned in this section. Note that only the main classes are displayed in this figure. This research is devoted to analysing the propagation of waves in structures with spatial long-range interactions, shown in blue and orange. Other materials including the types of structure and the methods utilized for the investigations are also highlighted in the figure. All the configurations are assumed to be linear unless stated otherwise.

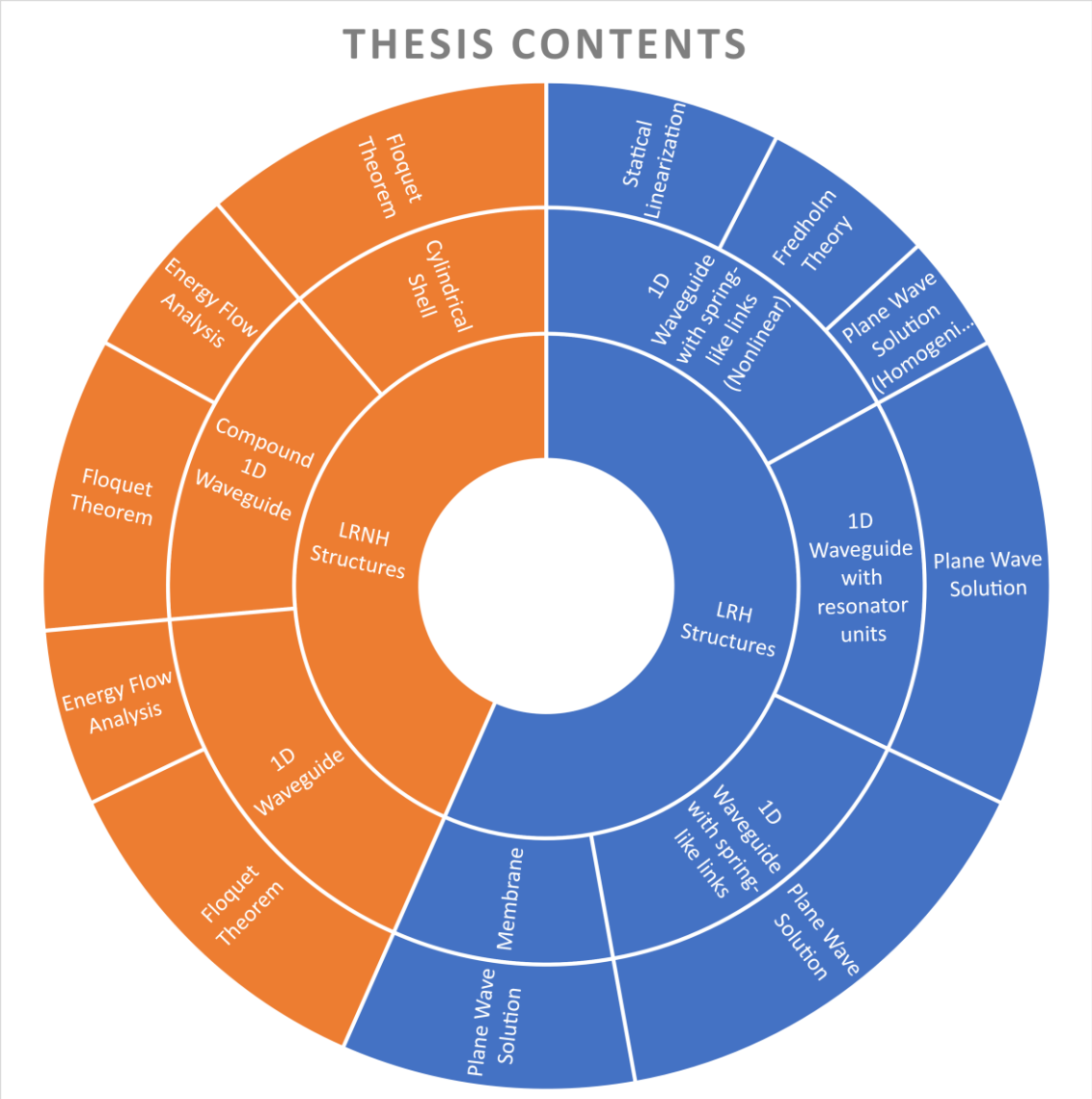


Fig. 2. 6: Overview of the systems and methods used in the thesis

As earlier mentioned, by breaking main classes, minor classification will be introduced based on the effects promoted by each system. This helps to reach a clear understanding of the relation between each system and the associated effects.

## 2.4. Upcoming dynamic effects

A few key concepts must be clarified before discussing the effects observed in systems mentioned above. To begin with, the concept of group velocity is essential to many of the topics investigated in this thesis. Plane waves of different wavelength form a packet, and group velocity is the measure, which determines the speed of the generated packet. The mathematical description of a general envelope of waves is of the form:

$$\alpha(x,t) = \int_{-\infty}^{\infty} A(k) e^{i(kx-\omega t)} dk \qquad (2\text{-}8)$$

Assuming the packet $\alpha(x,t)$ to be peaked at the wavenumber $k_0$, above relation, with linear expansion of $\omega(k)$ around $k_0$, takes the form:

$$\alpha(x,t) = e^{i(k_0 x-\omega_0 t)} \int_{-\infty}^{\infty} A(k) e^{i(k-k_0)(x-\omega_0' t)} dk \qquad (2\text{-}9)$$

The first factor $e^{i(k_0 x-\omega_0 t)}$ describes a waveform travelling at the phase speed $\omega_0/k_0$, and the integral term represents the packet propagating across the domain at the group velocity $\omega_0' = \frac{d\omega}{dk}\Big|_{k_0}$. This measure is of high significance, especially while intending to manipulate the flow of energy. In fact, the energy is not carried by individual waves of different wavenumbers, rather by an infinite set of them. Thus, the effects such as wave-stopping, and negative group velocity are referring to behaviour of the explained packet under specific circumstances.

The second concept to be addressed is related to the identification of ranges of frequency within which the transportation of energy is allowed, namely band structure. This consequential concept regains its importance when the elastic configuration under studying is periodic. For instance, the governing dynamics for a one-dimensional compound waveguide with the period $p$ is:

$$\frac{d}{dx}\left(E(x)\frac{du(x)}{dx}\right) + \omega^2 \rho(x) u(x) = 0 \qquad (2\text{-}10)$$

Since the configuration is periodic, Floquet theorem gives the interfacial condition for a unit cell of the structure as:

$$u(x+p) = e^{ikp} u(x) \qquad (2\text{-}11)$$

with $k$ being the Bloch parameter. This provides the chance to extract the band structure giving the information about the frequency ranges, whereby the propagation is permitted and forbidden. The forbidden bands, majorly known as stopbands or stopbands are highly beneficial for practical purposes including filtration.

Several distinct phenomena have been highlighted in this thesis, all emerged due to the modification of dynamics because of long-range interactions. As mentioned earlier, in this section, a new grouping system, called minor classification, is introduced for the systems. This classification, as brought in Table 2. 1, is based on the type of effects each group presents. All effects, as listed in Table 2. 2, are also presented in five distinct groups. Besides, a number is assigned to each single system as well as the effects, and their concise description are provided in the tables as well. The systems accommodated in the first group of both main classes

generate some effects included in the group with same indicator in Table 2. 2. The same holds for the second group of each class along with the effects related for the corresponding first group. Eventually, the effects promoted by the third minor group of the HLR structures are brought under group #3 in Table 2. 2. Note that the stopband effect is listed twice in Table 2. 2 for demonstration purposes.

Table 2. 1: List of the systems

| System No. | Description | Minor Groups | Main Groups |
|---|---|---|---|
| System #1 | Long-range waveguide with spring-like links | Group #1 | LRH Structures |
| System #2 | Long-range membrane (2D) | | |
| System #3 | Long-range waveguide with resonator units | Group #2 | |
| System #4 | Nonlinear long-range waveguide with spring-like links | Group #3 | |
| System #5 | Long-range waveguide (periodic) | Group #4 | LRNH Structures |
| System #6 | Long-range compound waveguide (periodic) | | |
| System #7 | Long-range cylindrical shell (periodic) | Group #5 | |

Table 2. 2: List of the effects induced by long-range interactions

| Effect No. | Description | Groups |
|---|---|---|
| Effect #1 | Wave-stopping | Group #1 |
| Effect #2 | Negative group velocity | |
| Effect #3 | Eigenstate redistribution | |
| Effect #4 | Stopband | Group #2 |
| Effect #5 | Propagation regime shift induced by nonlinearity and noise | Group #3 |
| Effect #6 | Wavenumber entanglement | |
| Effect #7 | Stopband | Group #4 |
| Effect #8 | Ultra-low frequency stopbands | |
| Effect #9 | Multiple source generation | |
| Effect #10 | Coupled mode filtering | Group #5 |

Having introduced to concepts of group velocity and stopbands, one may follow most effects presented in Table 2. 2. In fact, a major number of effects concerning the long-range homogenous system are related to group velocity. For instance, in chapter 3, it is shown that the zero/negative group velocity is met under certain circumstances. Additionally, the introduction of nonlinearity to a system brings some other phenomena such as coupling of the wavenumbers into the light (see chapter 4). Regarding long-range non-homogenous periodic system, where genuine periodicity is promoted by long-range connectors, the emergence of stopbands in the band structure of the systems is the predominant effect. However, dexterity of the concept of long-range interactions provides the chance to block the energy transported by coupled modes of different nature for the case of long-range cylindrical shell (periodic).

## 2.5. Relation between systems and effects

Although the existence of some delicate links is realized among effects represented by systems in different main classes, not all these occurrences are shared for a given configuration. For instance, it is demonstrated that the generation of multiple sources is inherent to periodic waveguide, when the periodicity is induced by the spring-like external links; therefore, it does not seem further from mind to conjecture the advent of this effect in other long-range configurations.

To ensure no confusion, a map of the effects promoted by long-range interactions in each system is given in Fig. 2. 7. The naming convention initiated in Table 2. 1 and Table 2. 2 has been taken into account, while providing the map. As observed, two sets of data are emphasized in Fig. 2. 7: i) the definite effects (marked with blue dots), those directly deduced from mathematical analyses, and ii) the anticipated effects (marked with orange dots), which are expected to occur due to the similarity with other analysed systems though are not explicitly demonstrated in the presented results. The alternative possibility for an effect to be accommodated in the latter is non-robustness of the method that implied its emergence. For the sake of clarification, two separate examples may be considered. First, the analysis on the long-range waveguide (periodic) suggests the possibility of pulling the stopbands towards arbitrary low frequencies (Effect #8) by adopting negative stiffness for long-range connectors. System #6 is expected to present the identical behaviour because of comparable configurations. The other example comes from the rough plane wave analysis put forward for the nonlinear long-range waveguide, and however the study indicates the emergence of wave-stopping, negative group velocity and eigenstate redistribution, here it is taken as a hypothesis for the sake of accuracy.

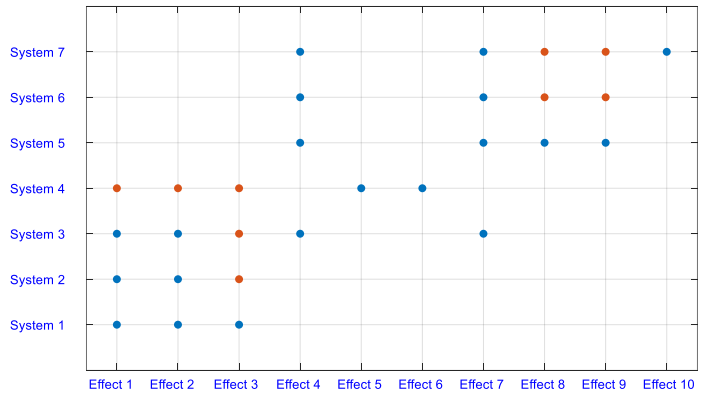


Fig. 2. 7: General map of relations among the systems and effects

## 2.6. Final remarks

This chapter delivers in a broad sense the effects promoted by the long-range interactions, when integrated with a conventional elastic solid. This helps to avoid the confusion for readers, while proceeding with the analyses brought in the following chapters. The phenomena are categorized in different groups; each corresponds to a specific class of systems though subtle

extension of some occurrences to other groups of systems is anticipated. This overview is inclined towards highlighting the extensive benefits of long-range interactions.

# Chapter 3: Long-range homogenous configurations: leaf-periodicity and more

## 3.1. Introduction

Above all, the current chapter tends to unveil how imposition of forces induced by long-range connectors alters the dynamics of elastic solids subjected to such interactions. Interaction among distant points can take place via different means including electromagnetic forces, simple elastic links and resonator units. Throughout this thesis, the long-range forces are majorly modelled by spring-like connectors, connecting distant points based on certain connectivity laws.

This chapter is devoted to studying the *long-range homogenous media*. The term *homogenous* is beneficial to distinguish the key difference between the systems presented in this part of thesis and those investigated in the chapter 5. *Homogenous* refers to systems in which all points interact nonlocally based on the corresponding connectivity template as opposed to long-range systems, where a limited number of particles communicate remotely with their counterparts. Also, some structures considered in this chapter are homogenous periodic based on the concept of graph-periodicity, which was discussed in the previous chapter. It should be noted that this term "periodic" does not refer to the periodicity of the entire configuration. Capturing this quality drastically influences the dynamics yielding distinct occurrences.

The chapter contains straightforward analyses on homogenous long-range domains, namely one-dimensional (1D) waveguides and a membrane. First, the dynamic description of two 1D waveguides with different distribution of long-range links is formulated and the arising phenomena are realized from the associated dispersion relations. Then, similar study is conducted on long-range system, where the spring-like links are replaced by resonator units. Eventually, the analysis is extended to a two-dimensional (2D) long-range domain and performance of the system in terms of waves is investigated.

## 3.2. Homogenous long-range waveguide with spring-like links

In this section, a 1D waveguide is considered as the host structure. The wave equation describing the motion of mechanical waves in a 1D elastic domain is:

$$\rho A \frac{\partial^2 u(x,t)}{\partial t^2} = EA \frac{\partial^2 u(x,t)}{\partial x^2} \qquad (3\text{-}1)$$

where $\rho$ and $E$ are the mass density and Young's modulus, respectively; and $u$ represents the axial displacement. In this context, the authors intend to modify the above equation so that the corresponding system to include the effects promoted by spatial long-range likes. First, a few analyses are provided for systems with open interaction region. This means that any arbitrary

point within the domain can establish communication with other non-adjacent points regardless of their distance. Then, the interaction region corresponding to each point is considered to be no longer open, which is a realistic assumption; and accordingly, some examples are provided to realise the associated effects.

## 3.2.1. Open interaction region

In the following, the behaviour of the waveguide is considered assuming that the long-range interaction region for any point is not confined to its vicinity but is arbitrarily wide, ideally infinite; and thereby an open interaction region. Primarily, the focus of this section is to develop a simple model, which possesses this characteristic; as presented in the first subsection. Subsequently, the system of interest is analysed comprehensively in terms of waves, and the arising phenomena are discussed in detail. Afterwards, in the second subsection, a comparable system is taken into account for which the connectivity template is mistuned to highlight the possibility of altering the propagation regimes by introducing a mistuning parameter to the system.

Note that, with reference to the graph-periodic concept, in subsection 3.2.1.1., we analyse the case of long-range homogenous periodic structure, characterized by the periodicity of the leaves, while the periodicity of the trees is lost because their continuous distribution ($P$ tends to zero). In section 3.2.1.2., the leaf-periodicity is lost making leaves non-equally spaced or continuously distributed, constructing a long-range homogenous structure.

### 3.2.1.1. A basic model for long-range waveguide

Here, the connection between non-adjacent cross-sections of the waveguide is made possible via spring-like links, as pointed out beforehand. A very simple model for a long-range waveguide is considered, as shown in Fig. 3. 1. Based on this connectivity template, each point of the waveguide at $x$ interacts with the equally spaced points $x_i = x \pm iD$ by simple spring-like links.

Although the model implies that each particle can ideally interact with an infinite number of its counterparts (open interaction region), a limited number of long-range exchanges is also a valid case. The equation describing the dynamics of the system is:

$$\rho \frac{\partial^2 u(x,t)}{\partial t^2} = E \frac{\partial^2 u(x,t)}{\partial x^2} - \sum_{i=-N}^{N} \frac{\kappa}{2^{|i|}} [u(x,t) - u(x+iD,t)] \qquad (3\text{-}2)$$

where $D$ is the closest distance between two particles interacting remotely, and $\kappa$ denotes a constant with the quality of stiffness. Based on the model, the intensity of interactions decreases by the factor $1/2^{|i|}$ as the distance between two points increases. Note that any other factor satisfying this condition is justifiable. The summation term represents the contribution of long-range forces, altering the dynamics of the conventional waveguide.

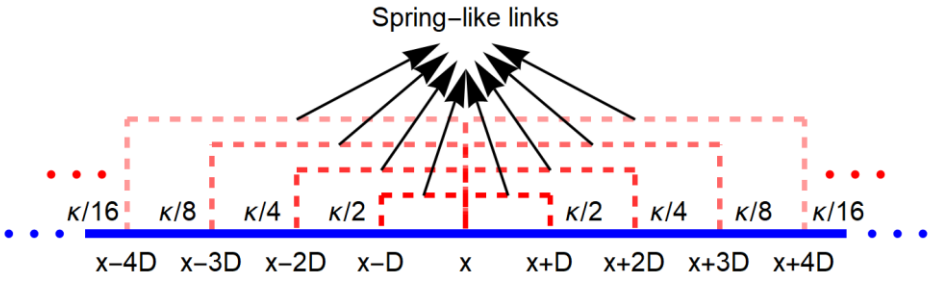


Fig. 3. 1: Schematic of the system

Since the summation term in Eq. (3-2) is valid for any arbitrary $x$, the external links responsible for distant communication are action at all points of domain according to the adopted connectivity template. Therefore, the configuration is homogenous due to the contribution of all cross-sections of the system to long-range interaction within the domain. Besides, leaf-periodicity still holds in the current case, and thereby a long-range homogenous periodic waveguide. Note that these two points are valid for all systems studied along the current chapter.

Assuming the displacement of the form $u(x,t) = u_0 e^{j(kx-\omega t)}$ with $u_0$, $k$ and $\omega$ being the amplitude, wavenumber and frequency, respectively; the associated dispersion relation is:

$$Ek^2 - \rho\omega^2 + \sum_{i=-N}^{N} \frac{\kappa}{2^{|i|}} \left[1 - e^{jikD}\right] = 0 \qquad (3\text{-}3)$$

This equation contains rich information about the intrinsic characteristics of the system such as propagation speed of the wave envelope. Introducing the nondimensional parameters $K = kD$, $\Omega = \omega D\sqrt{\rho/E}$ and $\chi = \kappa D^2/E$, Eq. (3-3) takes the form:

$$K^2 - \Omega^2 + \chi \sum_{i=-N}^{N} \frac{\left[1-e^{jiK}\right]}{2^{|i|}} = 0 \qquad (3\text{-}4)$$

The parameter $\chi$ uniquely characterizes the intensity of interactions with respect to that of short-range forces. A close examination of Eq. (3-4) reveals that no explicit expression is available to express the nondimensional wavenumber $K$ as a function of the nondimensional frequency $\Omega$. In fact, the transcendental nature of the dispersion relation owing to the presence of exponential terms implies the existence of infinite number of $K$ for every single value of $\Omega$. As Fig. 3. 2 shows the different values of $K$ that are extracted numerically for fixed values of $\Omega$, validating the correctness of the claim raised above. In the figures, only the first seven branches are taken into account, and since complexed-valued wavenumbers are detected, the real and imaginary part of the wavenumber are separately displayed in Fig. 3. 2a and Fig. 3. 2b, respectively.

Almost all the branches are composed of complex-valued roots (marked in blue); nevertheless, solely real-valued wavenumbers contribute to forming a unique branch (marked in red), denoting the possibility of pure propagation over the domain. Each branch is associated to a specific propagation mode and certainly among all branches, the propagation mode marked in red is capable of transporting energy.

Although the dispersion relation does not permit to obtain $K$ in terms of $\Omega$, i.e., $K(\Omega)$, it is straightforward to act conversely, yielding $\Omega(K)$ as:

$$\Omega = \pm\sqrt{K^2 + \chi \sum_{i=-N}^{N} \frac{[1-e^{jiK}]}{2^{|i|}}} \qquad (3\text{-}5)$$

Simple examination of Eq. (3-5) suggests that the expression under the square root is always positive for any given real-valued $K$. It is noteworthy that the frequencies generated by the preceding create the red branch shown in Fig. 3. 2.

Two parameters are involved in determining the arising phenomena and consequently their role should be studied. First, the indicator related to the number of interactions for each point, i.e., $N$. Secondly, the parameter regulating the relation between frequencies and the wavenumber, i.e. $\chi$. The change in value of $N$ implies the development of a new dynamics yet alerting $\chi$ means the manipulation of the mechanical and geometrical features of a specific system.

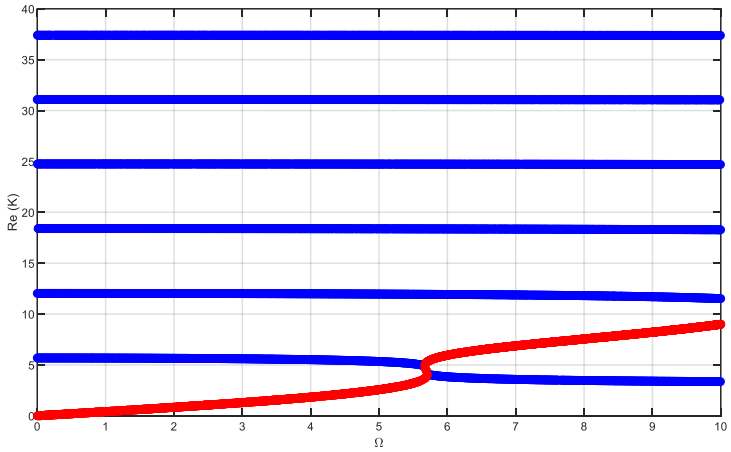


(a)

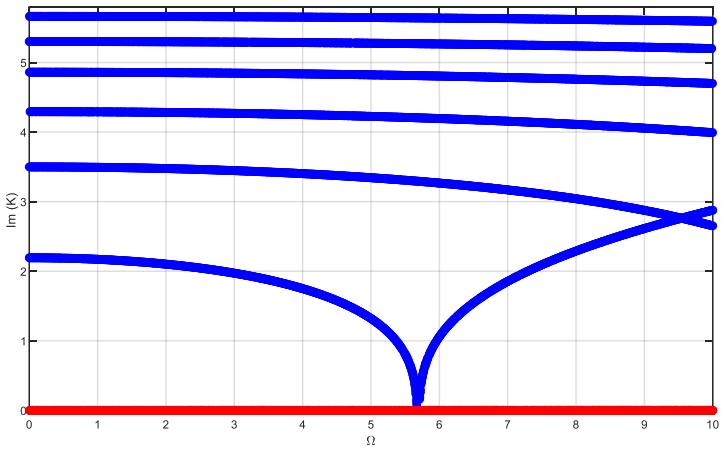


(b)

Fig. 3. 2: Different propagation modes for long-range waveguide: (a) Real part of wavenumber (b) Imaginary part of wavenumber ($N = 1, \chi = 5$)

In accordance with Eq. (3-5), the phase and group velocities are obtained as:

$$c_p = \frac{\Omega}{\mathrm{K}} = \frac{\sqrt{K^2+\chi\sum_{i=-N}^{N}\frac{\left[1-e^{jiK}\right]}{2|i|}}}{K} \tag{3-6a}$$

$$c_g = \frac{d\Omega}{d\mathrm{K}} = \frac{2K+\chi\sum_{i=-N}^{N}\frac{-ij}{2|i|}e^{jiK}}{2\sqrt{K^2+\chi\sum_{i=-N}^{N}\frac{\left[1-e^{jiK}\right]}{2|i|}}} \tag{3-6b}$$

For a system with $N = 1$, the dispersion curves are displayed in Fig. 3. 3, where the variation the nondimensional frequency is plotted against the nondimensional wavenumber for different values of $\chi$. Although the curves approach to that of the D'Alembert waveguide as the wavelength grows shorter, in general, considerable changes in the trend of curves is observed.

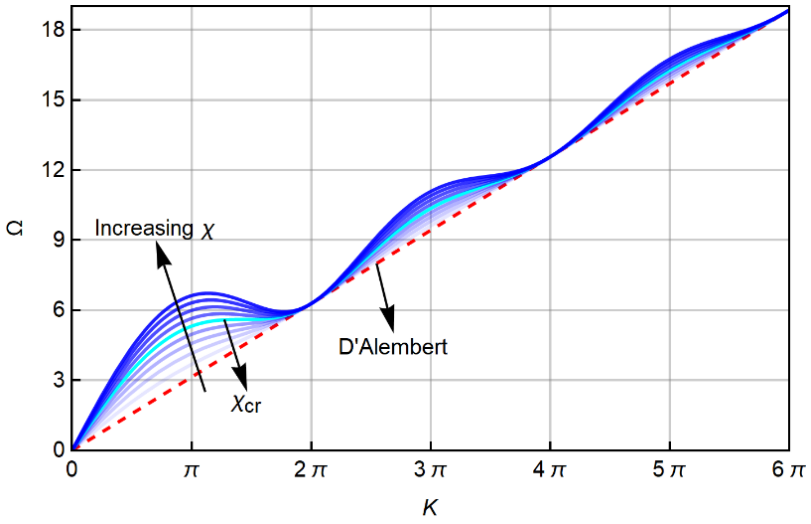


Fig. 3. 3: Dispersion curves for a long-range waveguide ($N = 1$)

The figure shows, as $\chi$ rises, two group of curves are evident: i) those lying beneath a critical value $\chi_{cr} = 9.207$, for which the slope is always positive, and ii) those sitting above the critical value, which experience negative slope along their path. In order to gain insight into the implications of this classification, the group velocity curves corresponding to above dispersion curves is provided in Fig. 3. 4. The highlighted region accommodates the first group curves, where the group velocity is always positive, typical of conventional system. Once $\chi$ adopts the critical value, the packet of waves is forced to stop propagating at a particular frequency, i.e. wave-stopping frequency, the first irregular phenomenon induced by long-range interactions is featured. This is exclusive to the packet of the waves implying that the plane waves of different wavelength keep travelling across the domain. Another unconventional effect called negative group velocity is met, when $\chi$ increases slightly beyond the critical value. This takes place within a frequency range between two wave-stopping frequencies, causing backward moving wave envelopes. The phenomena such as wave-stopping and negative group velocity were already reported by Eringen [49] and Carcaterra et al. [109].

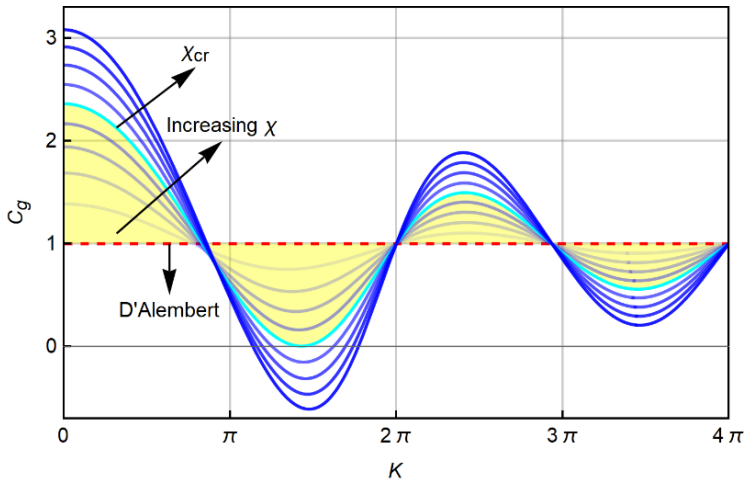


Fig. 3. 4: Group velocity curves for a long-range waveguide ($N = 1$)

Although sharp variations in the value of phase velocity is evident, as presented in Fig. 3. 5, no specific irregularity such as backward propagation is occurred. It is apparent that propagation occurs at higher speed, when the stiffer spring-like links act as long-range connectors. The introduction of long-range interactions dominantly impacts the waves of comparatively longer wavelength and thereby the effect weakens as the wavelength becomes shorter.

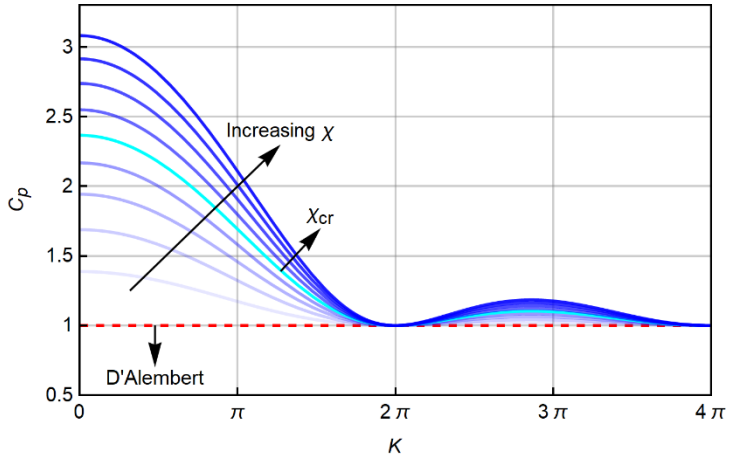


Fig. 3. 5: Phase velocity curves for a long-range waveguide ($N = 1$)

A supplementary feature of long-range systems is realized via modal density analysis $n(\Omega)$, providing information regarding the mean number of modes per unit frequency bandwidth [116]. The term *mode* is essentially meaningful for systems with discrete distribution of wavenumbers and consequently the concept of modal density is inherent to finite-size systems, not unbounded domains [110]. The boundaries of finite configurations generate phase shift, while reflecting the waves and this shift is normally negligible for high frequency perturbations [116]. Since the effect of boundaries are not significant under this condition, the behaviour of finite systems resembles an infinite one. Asymptotic treating of the governing resonance condition yields a general expression for any one-dimensional dispersive medium. For 1D domains, this measure is inversely proportional to the group velocity, i.e. $n(\Omega) \propto 1/C_g$ [116].

Fig. 3. 6 plots the variations of modal density as a function of frequency for an arbitrary subcritical value of $\chi$.

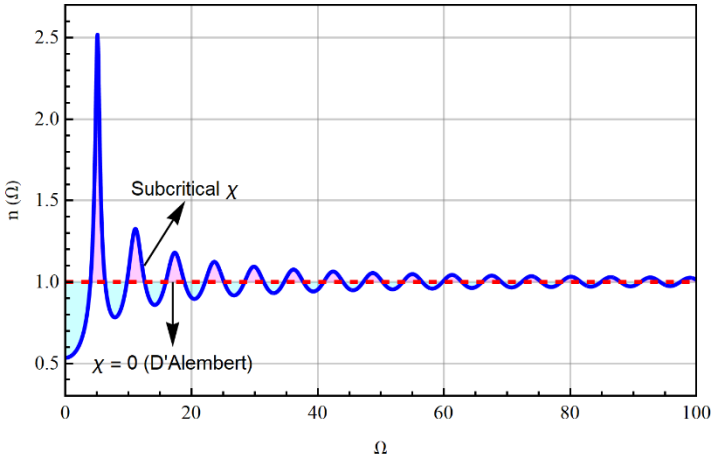


Fig. 3. 6: Modal density for a long-range waveguide ($N = 1$)

Through the use of colouring, two distinct kinds of regions are underlined: i) those highlighted in magenta refer to the bandwidths within which modal distribution is denser with respect to that of a D'Alembert waveguide, and ii) those marked with cyan, which possess the opposite quality. An interesting phenomenon called *modal migration* is revealed by examining the area under each group of regions. Surprisingly, the overall area corresponding to first group is equivalent to the area associated to the second group, suggesting the migration of the exact same number of modes from the less dense regions to the ones with higher density. However, a question remains whether the modes of high frequency relocate to lower frequency range or vice versa. To clarify this ambiguity, a crop of Fig. 3. 6 is illustrated in Fig. 3. 7, consisting of the first six region.

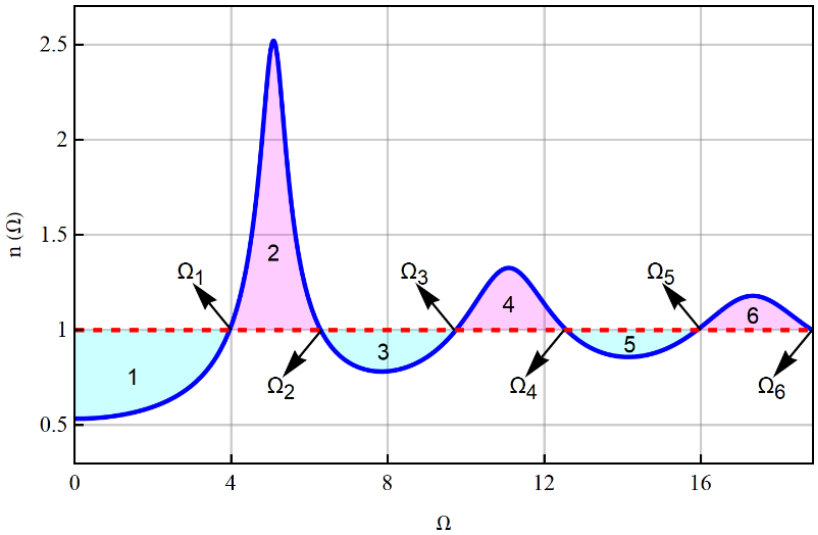


Fig. 3. 7: Modal density for a long-range waveguide ($N = 1$)

It is interesting that the area confined between two curves within the band $[0, \Omega_1]$ is exactly equal to the area of region number two, and the same holds for the next two pairs of regions.

By mathematical induction, this is a valid pattern for other following pairs. Thus, the analysis implies the redistribution of the modes from low frequency band to higher ranges. Note that this remark is only true for long-range waveguide with subcritical $\chi$, and clearly singularities appear on the modal density curves of systems with $\chi \geq \chi_{cr}$.

Up to this point, the parameter $N$ was fixed and all the effects discussed above emerged due to the change in intensity of forces exerted by the long-range connections. Although such configurations generally submit to the concept of long-range interactions, new dynamics are developed as $N$ varies. On the other hand, the magnitude of the forces decreases as the number of links rises due to the considered modulation in the interaction law and thereby negligible effect on the response. In the light of all this, it is reasonable to examine the limiting behaviour of the term responsible for long-range interactions $\sum_{i=-N}^{N} \frac{[1-e^{jiK}]}{2^{|i|}}$, when $N$ tends to infinity. Existence of a closed-form expression for the limit promotes a new dispersion relation as:

$$K^2 - \Omega^2 + 3\chi \left(1 - \frac{1}{5-4\cos K}\right) = 0 \qquad (3\text{-}7)$$

Variation of the group velocity $C_g$ associated to this system is plotted against the nondimensional wavenumber $K$ in Fig. 3. 8. Analogous to the waveguide with specific $N$, in this case, the emergence of wave-stopping, negative group velocity and redistribution of modes is confirmed as well. Furthermore, the curves indicate the chance of having several wave-stopping frequencies, given strong enough elastic links. For this system, the threshold is defined by the critical value $\chi_{cr} = 4.352$. A significant decrease in value of $\chi_{cr}$ is realized as compared to that of the long-range waveguide with $N = 1$, implying the need for less stiff links to drive the system towards exhibiting irregular behaviours.

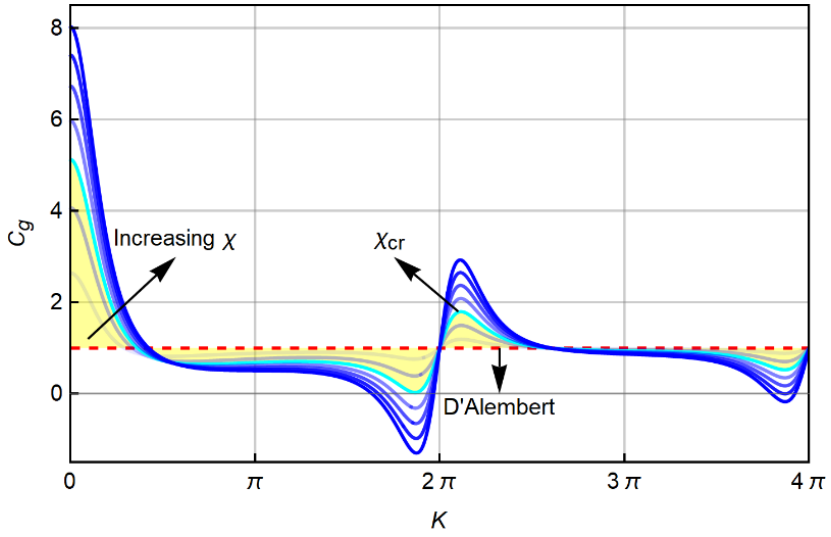


Fig. 3. 8: Group velocity curves for a long-range waveguide ($N \to \infty$)

### 3.2.1.2. Mistuned long-range connectivity

Mistuning is an effect that has been the subject of many investigations [117,118]. In structures with periodicity, the presence even of small perturbations in the periodicity pattern produces the effect of blocking the wave propagation. It is interesting to investigate how the presence of deterministic and random perturbations in the regular texture of the long-range connections, that essentially reminds the phenomenon of mistuning, affects the long-range propagation characteristics and namely the group velocity. Here the mistuning parameter changes the position, where second end of the spring-like links attaches to the waveguide, at the distance $iD$ from the central point $x$ in the unperturbed configuration. In this case, the leaf-periodicity is lost and the structure under studying is a simple long-range homogenous one.

The model considered here is an extension of what discussed in the previous subsection (see Fig. 3. 1) though spring-like links of the identical stiffness $\kappa$ are taken into consideration as long-range connectors. Here, a nondimensional mistuning parameter $\epsilon$ is introduced that modifies the attachment point of the long-range link. Note that $\epsilon$ may either adopt a deterministic or a random value, in the following analysis.

The equation of motion for a long-range waveguide with mistuned connectivity is:

$$\rho\frac{\partial^2 u(x,t)}{\partial t^2} = E\frac{\partial^2 u(x,t)}{\partial x^2} - \kappa\sum_{i=-N}^{-1}\left[u(x,t) - u\left(x + iD - \epsilon D(-1)^i, t\right)\right] - \kappa\sum_{i=1}^{N}\left[u(x,t) - u\left(x + iD + \epsilon D(-1)^i, t\right)\right] \quad (3\text{-}8)$$

The summation in Eq. (3-8) is split into two summations due to the factor $(-1)^i$, inducing a reciprocating distance between the extremes of each link.

In this case, the corresponding dispersion relation is:

$$K^2 - \Omega^2 + \chi\{\sum_{i=-N}^{-1}[1 - e^{jK[i-\epsilon(-1)^i]}] + \sum_{i=1}^{N}\left[1 - e^{jK[i+\epsilon(-1)^i]}\right]\} = 0 \quad (3\text{-}9)$$

Here, the definition of the nondimensional parameters $K$, $\Omega$ and $\chi$ are identical to those of the previous subsection.

The mistuning effect is evaluated by altering the parameter $\epsilon$, and analysing the associated change in group velocity for a waveguide with $N = 3$ and $\chi = 10$. The plot of the group velocity in terms of $K$ and $\epsilon$ is provided in Fig. 3. 9.

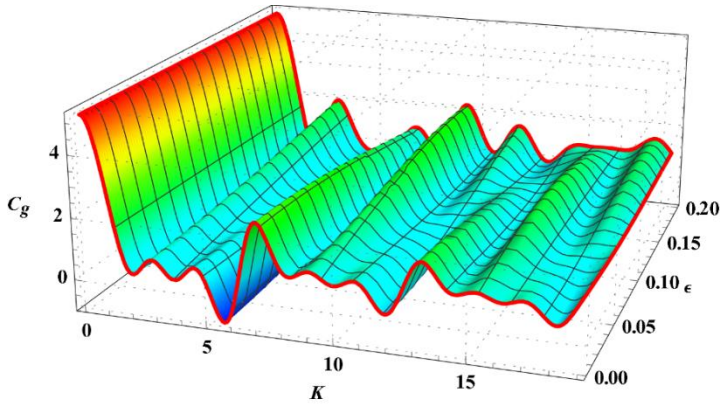


Fig. 3. 9: Group velocity surface of mistuned long-range waveguides ($\chi = 10$, $N = 3$)

It appears the group velocity is highly sensitive to the mistuning effect, since $\epsilon$ affects the oscillatory trend of the group velocity, when changing the wavenumber. More precisely, the presence of mistuning effects enriches the number of bandwidths within which the wave-stopping, and backwards energy propagation phenomena appear.

Fig. 3. 10 shows that, in the absence of mistuning, i.e., $\epsilon = 0$, the long-range waveguide shows a single wavenumber bandwidth within which the backward energy transfer is allowed, and correspondently two wave-stopping frequencies. In the presence of mistuning ($\epsilon = 0.4$), three bands with such characteristic are identified, together with six frequencies at which the wave-stopping occurs. This shows that the mistuning permits to emphasize the unusual wave propagation effects, originated owing to the presence of the long-range connections. Furthermore, it is demonstrated that such effects can emerge even in the presence of smaller number of connections $2N$, and of less stiff spring-like links.

Finally, the effect of considering a randomly mistuned connectivity is studied in Fig. 3. 11. For that matter, depending on $N$, different values for $\epsilon$ are selected by a random generator in a specific interval, and thereby no identical $\epsilon$ for all the long-range links. Note that $\epsilon$ should adopt identical values for pairs of links identified with multipliers of the same absolute value, otherwise dispersion relation will not yield any purely propagating modes. As shown in Fig. 3. 11, by implementing random mistuning parameter into the Eq. (3-9), the unconventional behaviour can be emphasised. In fact, multiple wave-stopping frequencies, and subsequently multiple bandwidths of backwards propagation can be reached. This implies that one may assume different $\epsilon$ for different pairs of long-range links to achieve a certain behaviour

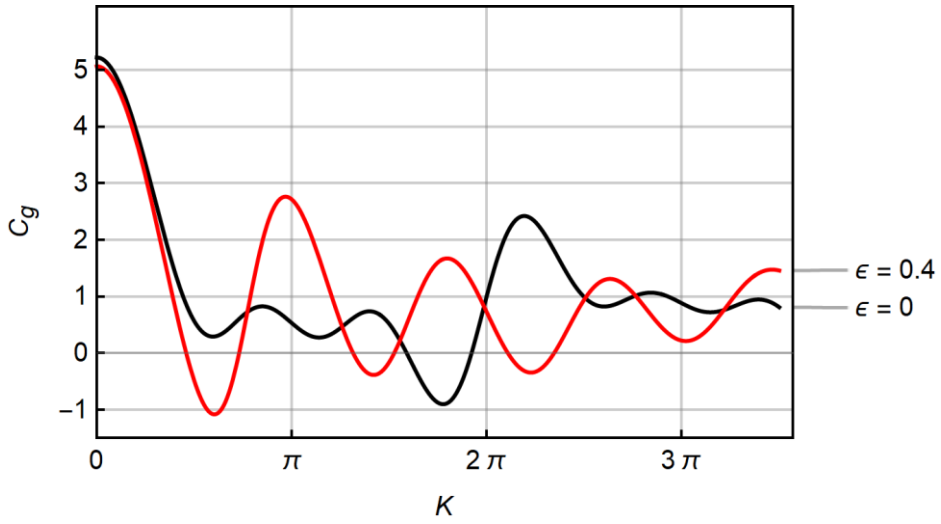


Fig. 3. 10: Group velocity curves of mistuned long-range waveguides ($\chi = 10$, $N = 3$)

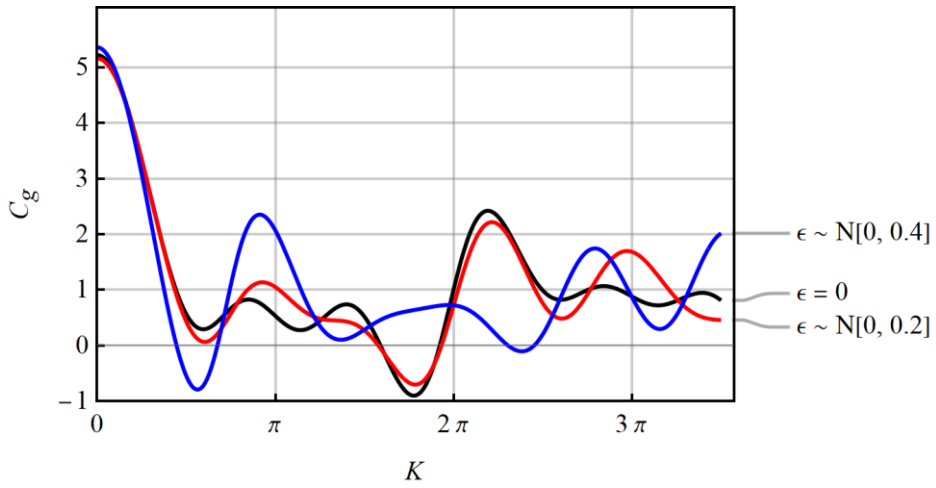


Fig. 3. 11: Group velocity curves of randomly mistuned long-range waveguides ($\chi = 10$, $N = 3$)

## 3.2.2. Confined interaction region

The previous examples assume no constraints on the width of the interaction region for each point. It is realistic to assume (in view of possible applications) that the interaction region is confined. In the following two subsections, two general models are presented, wherefore each point is allowed to interact with distant points within confined regions of interaction. In the first subsection, an integral formula, which includes a restricting window is presented for modelling the long-range forces. The second subsection develops a model, similar to those of the previous section, to demonstrate the possibility of reaching a confined interaction region without adopting integral formulation. Note that, neither leaf-periodicity nor tree-periodicity holds for the following examples, and hence long-range homogenous structures.

### 3.2.2.1. Integral model for long-range waveguides

In the previous case, although an arbitrary number of connections can be imagined for each point, only a specific group of particles can communicate with the central point $x$. The following model takes the advantage of integral formulation to consider all possible connections within a confined interaction region. For that matter, a rectangular window $H(x)$ of the length $2D$ defines the bounded region of interaction (see Fig. 3. 12).

The general equation of motion for such a system may be stated as:

$$\rho \frac{\partial^2 u(x,t)}{\partial t^2} - E \frac{\partial^2 u(x,t)}{\partial x^2} + \kappa \int_{-\infty}^{\infty} [u(x,t) - u(\xi,t)]\, H(x-\xi) d\xi = 0 \qquad (3\text{-}10)$$

where $\rho$ and $E$ are the mass density and Young's modulus of the waveguide, respectively; and $\kappa$ represents the stiffness of the spring-like links (assumed to be constant).

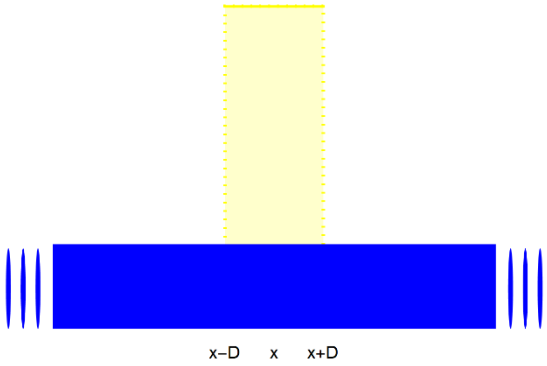


Fig. 3. 12: Demonstration of rectangular confining interaction region

The integral expression $\kappa \int_{-\infty}^{\infty}[u(x,t)-u(\xi,t)]\,H(x-\xi)d\xi$ explains the forces induced by the external elastic links, the underlying cause for generation of special dynamic behaviours. Through mathematical manipulations, Eq. (3-10) takes the equivalent form:

$$\rho\frac{\partial^2 u(x,t)}{\partial t^2}-E\frac{\partial^2 u(x,t)}{\partial x^2}+2\kappa D u(x,t)-\kappa H(x)*u(x,t)=0 \qquad (3\text{-}11)$$

Here the symbol $*$ represents the convolution operation. To study the response of the system in terms of waves, the dispersion characteristics must be analysed. Again, the system is long-range homogenous since both *P* and *L* tend to zero, based on the discussion given in chapter 2.

By expressing Eq. (3-11) by its Fourier transform (both in frequency and wavenumber domain), the dispersion relation is:

$$\rho\omega^2=Ek^2+2\kappa D(1-\operatorname{sinc} kD) \qquad (3\text{-}12)$$

with $\omega$ and $k$ being the angular frequency in $rad/s$ and spatial frequency in $rad/m$, respectively. Note that the nonunitary form of the spatiotemporal Fourier transform is utilized here. For the sake of simplicity, the dispersion relation (3-12) is rewritten in the nondimensional form as:

$$\Omega^2=K^2+2\chi(1-\operatorname{sinc} K) \qquad (3\text{-}13)$$

with

$$\Omega=\omega D\sqrt{\rho/E} \qquad (3\text{-}14a)$$

$$K=kD \qquad (3\text{-}14b)$$

$$\chi=\kappa D^3/E \qquad (3\text{-}14c)$$

Similar to the previous case, the dynamics of the system and hence the propagation regimes can be then discussed in terms of $\chi$ only. This parameter provides a measure of the strength of long-range interactions with respect to the classical short-range ones. The dispersion relation (3-13) includes a cardinal *sin* function (or *sinc* function), which brings the transcendental feature to this system akin to the exponential terms in Eq. (3-4).

Fig. 3. 13 presents the dispersion behaviour of the system for a wide range of $\chi$. Since the response is in terms of *sinc* function, several ripples are observed on curves. Curves located within the yellow shaded region do not deviate considerably from the D'Alembert response and thus roughly similar behaviour is declared. Once the value of $\chi$ violates the critical value $\chi_{cr} = 34.815$, the corresponding curves capture new characteristics recognized by the local extrema.

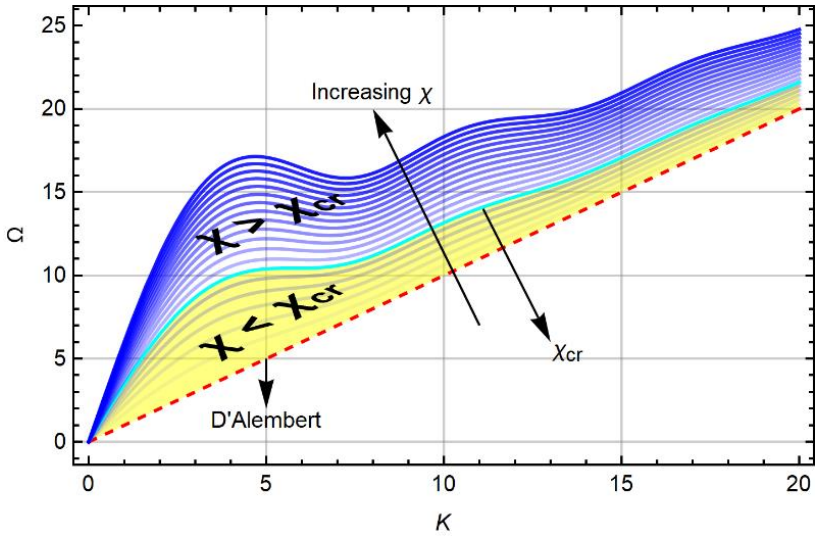


Fig. 3. 13: Dispersion curves corresponding to a long-range waveguide

Fig. 3. 14 and Fig. 3. 15 report, respectively, the phase velocity and group velocity curves. Changes in phase velocity $C_p$ are similar regardless of the value $\chi$ adopts and it is demonstrated that $C_p$ approaches to the response of the conventional waveguide (D'Alembert) as the wavelength shortens. Fig. 3. 15 confirms the claim raised above regarding the development of new propagation phenomena for $\chi \geq \chi_{cr}$. Based on the figure, any curve, which falls outside the shaded area crosses the axis at two distinct $K$ implying the possibility of stopping the packet of waves. Furthermore, the group velocity is negative for any $K$, which locates within the interval defined by the aforementioned wavenumbers. Again, the system proceeds towards the conventional path, that of the D'Alembert waveguide, as the wavenumber becomes larger. Identical phenomena were already observed for the systems discussed in the previous subsection.

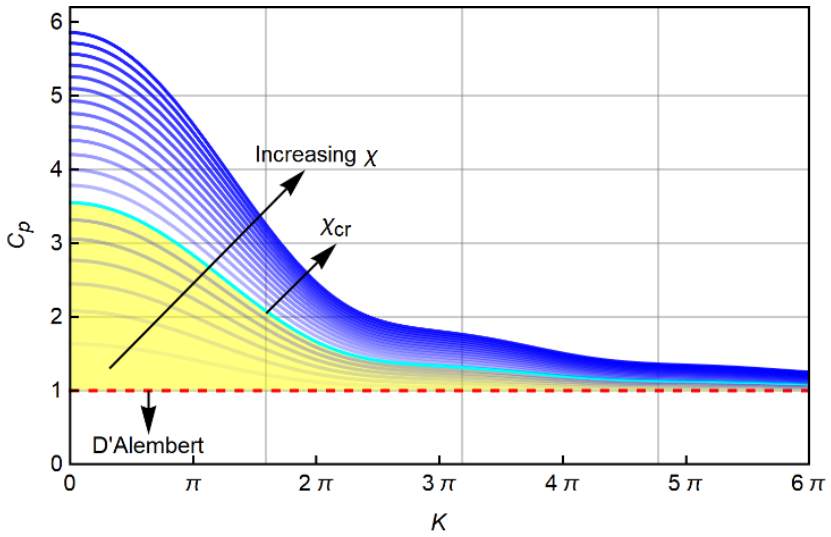


Fig. 3. 14: Phase velocity curves for the long-range waveguide

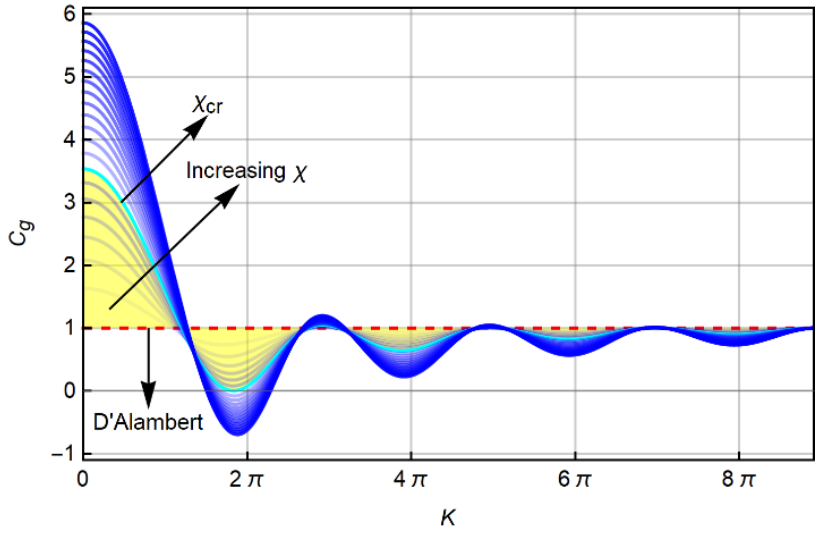


Fig. 3. 15: Group velocity curves for the long-range waveguide

To verify the occurrence of modal migration in current system characterized by subcritical value of $\chi$, the variation of modal density $n(\Omega)$ against the nondimensional frequency $\Omega$ is shown in Fig. 3. 16. Several regions have been created due to the intersection of curves associated to the modal density of long-range and conventional waveguide in a similar manner to Fig. 3. 6. The overall area caught between these two curves is zero, denoting the redistribution of modes across the frequency domain. However, it is not clear how this redistribution is directed since the modes of the less dense regions (marked in cyan) are assigned to different denser regions (marked in magenta).

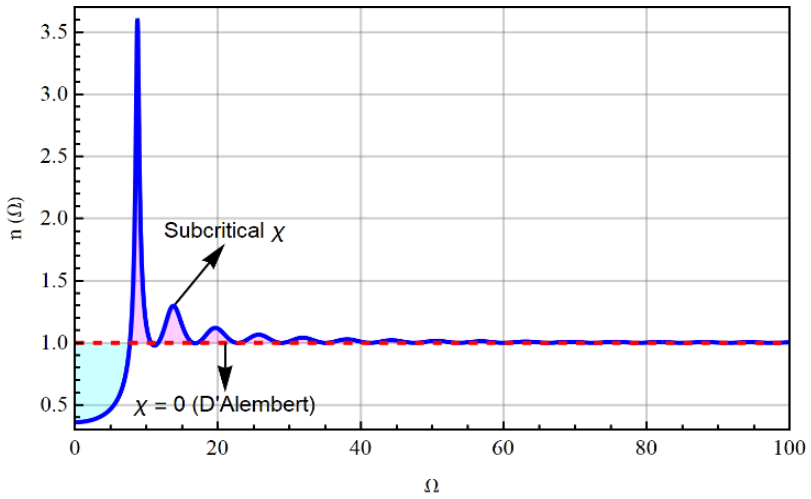


Fig. 3. 16: Modal density for the long-range waveguide

Note that what comes in the remaining part of this section is built around the study performed above, which was also reported in Ref. [111]. In that regard, the problem is generalized by considering a window, which itself contains several sub-windows identical to that showed in Fig. 3. 12. The definition of window is modified as (see Fig. 3. 17):

$$H(x) = \begin{cases} 1, & (4n-1)D \le x \le (4n+1)D \\ 0, & (4n+1)D < x < (4n+3)D \end{cases} \tag{3-15}$$

with $n$ being the numbers, which fall within a symmetric closed interval from the integer domain. Considering an unbounded waveguide with limited number of sub-windows $N$ (a natural odd number), Eq. (3-10) takes the form:

$$\rho \frac{\partial^2 u(x,t)}{\partial t^2} - E \frac{\partial^2 u(x,t)}{\partial x^2} + 2\kappa N D u(x,t) - \kappa H(x) * u(x,t) = 0 \tag{3-16}$$

The corresponding dispersion relation, in the nondimensional form, is:

$$\Omega^2 = K^2 + 2N\chi + \frac{j\chi(1-e^{2jK})}{K} \sum_{h=0}^{N-1} e^{2j(1-2N+4h)K} \tag{3-17}$$

Evidently the above equation reduces to Eq. (3-13) when $N = 1$.

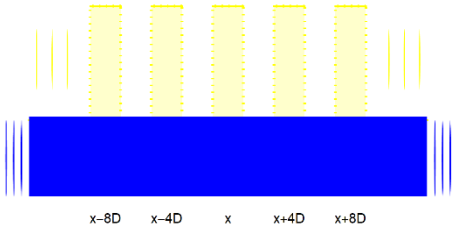


Fig. 3. 17: Long-range waveguide with arbitrary number of rectangular interaction region

To investigate the behaviour of plane waves in systems with arbitrary number of interaction regions, as characterized by Eq. (3-17), Fig. 3. 18 shows the effect of $N$ (number of sub-windows) on the dispersion curves. It is clear the general trend is distorted radically as the number of inclusions $N$ (sub-windows) grows. Notably, even a small subcritical value ($\chi = 1$) for a system with $N = 1$ causes several crest and trough on the curves associated to systems with higher number of interaction regions. Therefore, single/multiple pair of frequencies, depending upon the number of inclusions, are born at which elastic waves stop travelling.

Fig. 3. 18 implicitly suggests the change in the critical value of $\chi$ for systems with different number of sub-windows. To demonstrate this fact, Fig. 3. 19 exhibits the variation of $\log \chi_{cr}$ against the change in number of sub-windows. The figure reveals the larger the $N$, the smaller the $\chi_{cr}$.

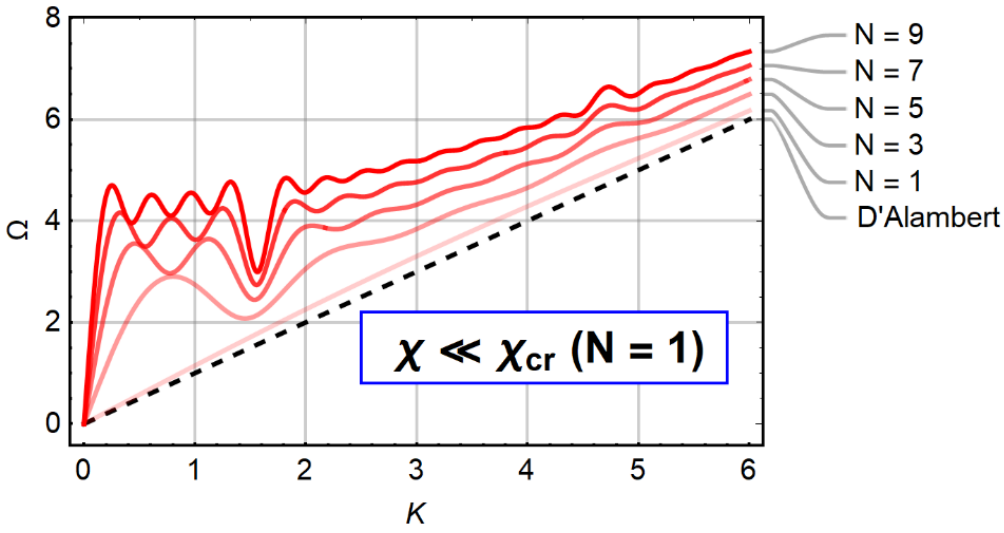


Fig. 3. 18: Dispersion curves corresponding to a long-range with a single sub-window

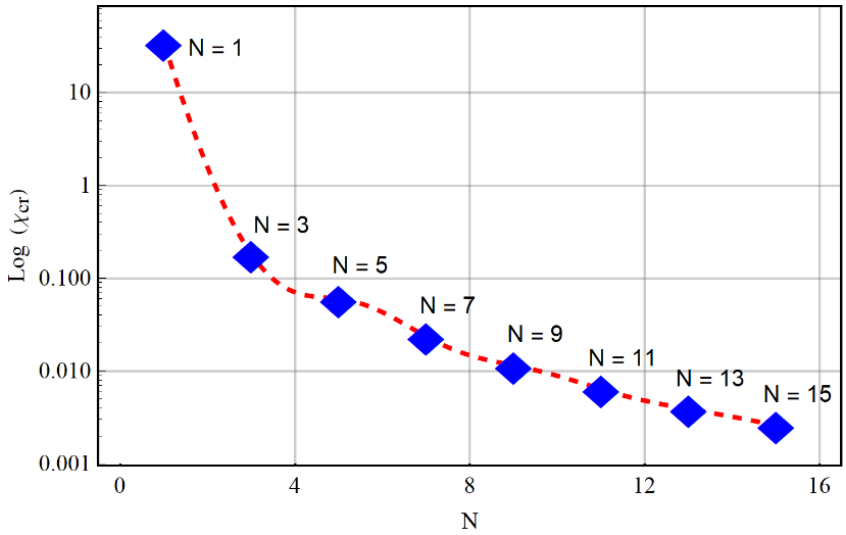


Fig. 3. 19: Change in $\chi_{cr}$ against $N$

However, the value of the critical value drops by two orders of magnitude at the first step, when $N$ varies from one to three, smoother decline in value of $\chi_{cr}$ is observed in further steps. The practical implication of this assessment is the possibility of achieving zero/negative group velocity by far less stiffer connections when more sub-windows are considered. For instance, roughly 200 times smaller $\chi$ is required to have backwards going wave envelopes by adding only two more interaction regions ($N = 3$).

Another feature of such systems is realized by investigating the response of their finite counterpart under external loading. To that end, Eq. (3-11) is discretized by finite difference method (FDM). Courant-Friedrich stability condition with $\sigma^2 = 0.5$ is assumed to guarantee the convergence of the applied method. A long-range bar of length ten, with $D = 1$, $c = 1$, $E/\kappa = 0.01$, $\Delta x = 0.01$ and $\Delta t = \sigma\, \Delta x\, /c$ is considered. A random noise is applied to the system as initial condition. The nondimensional response of the bar as well as the Fast Fourier Transform (FFT) of the displacement signal is shown in Fig. 3. 20. Note that the wave amplitude is nondimensionalized with the respect to the largest amplitude at each associated time step.

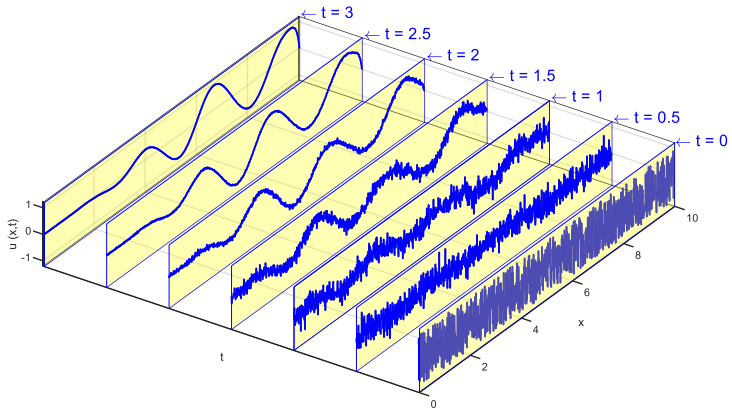


(a)

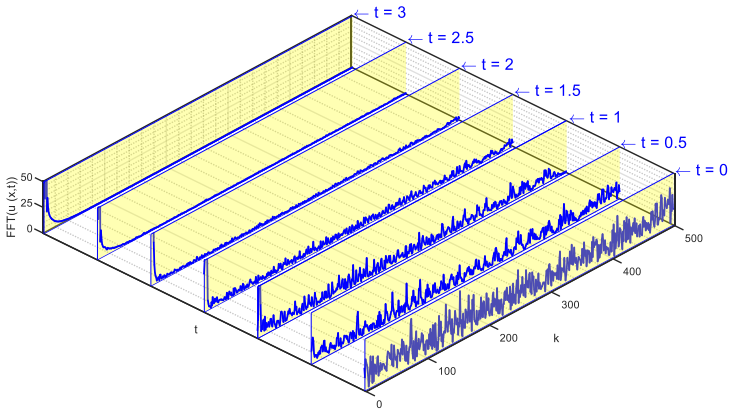


(b)

Fig. 3. 20: a) Nondimensional wave amplitude and b) the corresponding fast Fourier transform for a long-range waveguide ($\chi = 100$)

Fig. 3. 20a shows the variations of nondimensional wave amplitude along the waveguide at different time instants. This figure illustrates the development of localization caused by nonlocal interactions which may be realized a priori by delving into the dispersion relation corresponding to the unbounded counterpart of the system, i.e., Eq. (3-13). In fact, the emergence of *sinc* function in the dispersion relation of the long-range waveguide implies the existence of a specific type of localization phenomenon, namely low pass, which causes the suppression of the energy content of the output signal as time goes by. To gain a better insight, the FFT of the displacement signals at each time steps is computed and depicted in Fig. 3. 20b. The figure highlights the changes in the contributing spatial frequencies through time. It appears that at larger time steps, only smaller wavenumbers are allowed to pass and the bandpass becomes narrower.

### 3.2.2.2. A summation model for long-range waveguides

Here, a simple model is considered in which the nonlocalities are not equally spaced and the interaction distance between the latter extreme of two consecutive spring-like links varies by the factor $L/2^{|i|}$ with $i$ being the indicator corresponding to the second link, unlike to those of the previous section. This leads to confinement of the interaction window of the length $4D$ as the number of nonlocalities tends to infinity. The schematic of such system is shown in Fig. 3. 21.

The dynamic description of the system is follows:

$$\rho\frac{\partial^2 u(x,t)}{\partial t^2} = E\frac{\partial^2 u(x,t)}{\partial x^2} - \sum_{i=-N}^{0}\frac{\kappa}{2^{|i|}}\left[u(x,t) - u\left(x+\frac{1-2^{|i|}}{2^{|i|-1}}D,t\right)\right] - \sum_{i=0}^{N}\frac{\kappa}{2^{|i|}}\left[u(x,t) - u\left(x+\frac{2^{|i|}-1}{2^{|i|-1}}D,t\right)\right] \quad (3\text{-}18)$$

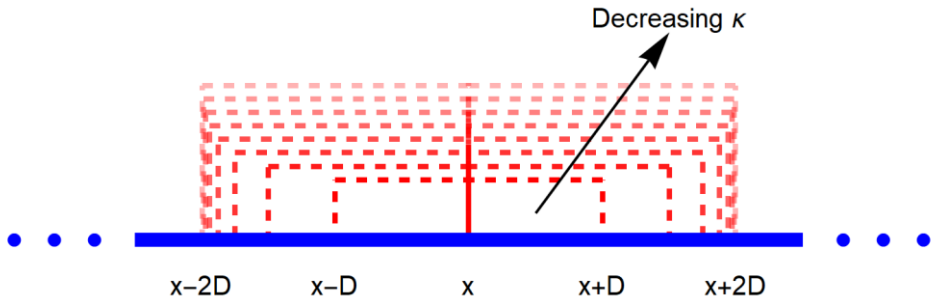


Fig. 3. 21: Waveguide with unequally spaced nonlocalities

Similar to the model shown in Fig. 3. 1, the mutual interactions are assumed to become weaker as the distance between two extremes increases.

The dispersion relation corresponding to Eq. (3-18) is:

$$K^2 - \Omega^2 + \chi\sum_{i=-N}^{0}\frac{\left[1-e^{\frac{jK\left(1-2^{|i|}\right)}{2^{|i|-1}}}\right]}{2^{|i|}} + \chi\sum_{i=0}^{N}\frac{\left[1-e^{\frac{jK\left(2^{|i|}-1\right)}{2^{|i|-1}}}\right]}{2^{|i|}} = 0 \quad (3\text{-}19)$$

and the group velocity curves associated to this case are:

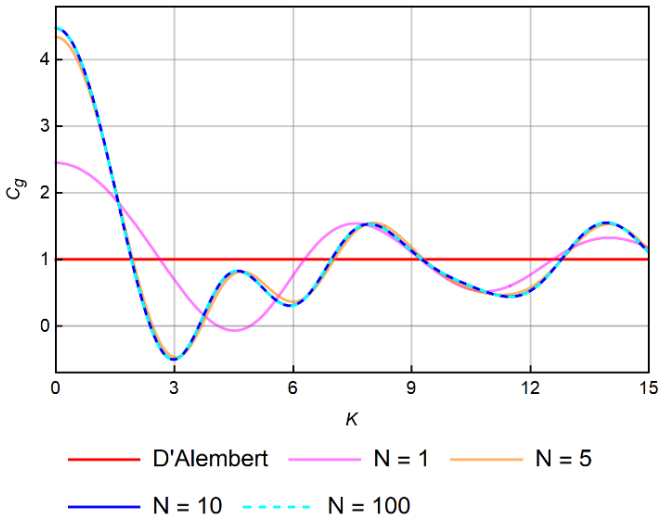


Fig. 3. 22: Group velocity curves for the waveguide with unequally spaced nonlocalities ($\chi = 10$)

Although no explicit formula may not be extracted for the case with $N \to \infty$, the figure demonstrates the convergence of curves to a specific trend as the number of nonlocalities increases. Furthermore, for a supercritical value of $\chi$ (dependent upon $N$), the performance of the system shown in Fig. 3. 21 is similar to the previous cases although the long-range interactions are confined within a restricted region.

## 3.3. Resonator-based long-range homogenous waveguide

Here in this section, we aim to introduce a category of homogenous long-range configurations (see section 2.2. in chapter 2), which provide stopbands unlike the type studied in the previous section. To develop such models, we propose a brand-new class of long-range connectors. The newly selected long-range connectors bring extra degrees-of-freedom (DOF) to the system, analogous to conventional locally resonant acoustic metamaterials (LRAMs). A rather complete analysis of such systems is given in the following subsections. A conventional 1D waveguide is considered as the host structure, coupled with different long-range superstructures, each composed of specific long-range connectors having various degrees-of-freedom. Note that the long-range interactions among non-adjacent points are assumed to take place within a confined window, and thereby the integral model is adopted, similar to that of subsection 3.2.2.1.

### 3.3.1. Generalized mathematical model

Let us consider a comprehensive arrangement for the resonator unit, which can be seen as a generalization for simpler layouts. Two examples of more trivial cases are brought in the next two subsections. Here, the long-range superstructure is composed of identical resonator units, where the unit itself contains an arbitrary number of layers with each layer consisting of fixed numbers of masses and springs, but arbitrary for now. Masses and springs are included in the corresponding composition in each layer, as shown in Fig. 3. 23.

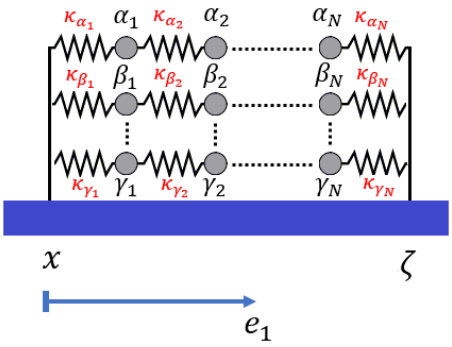


Fig. 3. 23: waveguide with a generalized long-range resonator-based superstructure

In this case, long-range connectors are no longer simple spring-like links unlike those of the previous section, and they are replaced by generalized resonator units. The foremost distinction lies in the contribution of the assumed unit to the overall degrees of freedom of the entire configuration. The long-range connectors employed in the previous section do not add any extra degrees-of-freedom to the system and the dynamic of the system is totally controlled by the already existing ones, provided by the host structure (waveguide). Instead, the constituents of the long-range superstructure i.e., the generalized resonator units bring multiple degrees-of-freedom to the system, as shown in Fig. 3. 23. Note that the masses may move in the axial direction exclusively.

The governing equation of motion for the system is:

$$\rho A \frac{\partial^2 w(x,t)}{\partial t^2} - EA \frac{\partial^2 w(x,t)}{\partial x^2} - \int_{-\infty}^{\infty} N_x(x,\zeta,t)\, Y(x-\zeta) d\zeta = 0 \qquad (3\text{-}20)$$

Here, $N(x,\zeta,t)$ represents the long-range force exerted by composing elements of the long-range superstructure, and $Y(x)$ is an arbitrary kernel responsible for confining the interaction region. From physical point of view, the intensity of interactions typically reduces by some significant orders of magnitude as the distance between the hub point $x$ and the hovering point $\zeta$ increases. Besides, it is essential to put restrictive limits on the interaction region in order to avoid obtaining infinite values from the integral term, which describes the summation of long-range forces induced by the generalized resonator units. Other parameters involved in Eq. (3-20) are identical to those employed in the previous sections.

The long-range force $N(x,\zeta,t)$ is:

$$N(x,\zeta,t) = \underline{T}^T \underline{q} - S\, w(x,t) \qquad (3\text{-}21)$$

where

$$S = \kappa_{\alpha_1} + \kappa_{\beta_1} + \cdots + \kappa_{\gamma_1} \qquad (3\text{-}22a)$$

$$\underline{T}^T = \left[\kappa_{\alpha_1}, 0, \dots, 0, \kappa_{\beta_1}, 0, \dots, 0, \dots, \kappa_{\gamma_1}, 0, \dots, 0\right] \qquad (3\text{-}22b)$$

To extract the only unknown in Eq. (3-21) being $\underline{q}$, the dynamic description of the masses involved in the corresponding configuration is derived as:

$$\underline{\underline{M}}\,\underline{\ddot{q}} + \underline{\underline{K}}\,\underline{q} = \underline{B}_{\alpha_1}\left[w(x,t) - \underline{R}^T_{\alpha_1}\underline{q}\right] + \underline{B}_{\beta_1}\left[w(x,t) - \underline{R}^T_{\beta_1}\underline{q}\right] + \cdots + \underline{B}_{\gamma_1}\left[w(x,t) - \underline{R}^T_{\gamma_1}\underline{q}\right] + \underline{B}_{\alpha_N}\left[w(\zeta,t) - \underline{R}^T_{\alpha_N}\underline{q}\right] + \underline{B}_{\beta_N}\left[w(\zeta,t) - \underline{R}^T_{\beta_N}\underline{q}\right] + \cdots + \underline{B}_{\gamma_N}\left[w(\zeta,t) - \underline{R}^T_{\gamma_N}\underline{q}\right] \quad (3\text{-}23)$$

where $w(x,t)$ is the axial displacement of the waveguide at $x$ and accordingly $w(\zeta,t)$ is the associated displacement at $\zeta$. $\underline{B}$ and $\underline{R}^T$ are vectors with constant entries, and Greek letters with the subscripts "1" and "$N$" are respectively referring to masses located at the back and the front ends of each layer within the unit. $\underline{\underline{M}}$ and $\underline{\underline{K}}$ are the inertial and stiffness matrices of the generalized resonator unit and $\underline{q}$ is the corresponding displacement vector for all masses involved in the unit. Clearly, the dimensions of the presented vectors and matrices are to be determined for any specific unit, which subscribes to the general layout shown in Fig. 3. 23.

The expression for $N(x,\zeta,t)$ in the temporal Fourier domain becomes:

$$\widehat{N}(x,\zeta,\omega) = \underline{T}^T\underline{\hat{q}} - S\,\hat{w}(x,\omega) \quad (3\text{-}24)$$

To obtain $\underline{\hat{q}}$, the temporal Fourier transform is applied to Eq. (3-23), providing:

$$\underline{\hat{q}} = \underline{H_1}\hat{w}(x,\omega) + \underline{H_2}\hat{w}(\zeta,\omega) \quad (3\text{-}25)$$

with

$$\underline{H_1} = \left[-\underline{\underline{M}}\omega^2 + \underline{\underline{K}} + \underline{\underline{U}}\right]^{-1}\underline{B}_{\alpha_1} + \left[-\underline{\underline{M}}\omega^2 + \underline{\underline{K}} + \underline{\underline{U}}\right]^{-1}\underline{B}_{\beta_1} + \cdots + \left[-\underline{\underline{M}}\omega^2 + \underline{\underline{K}} + \underline{\underline{U}}\right]^{-1}\underline{B}_{\gamma_1} \quad (3\text{-}26a)$$

$$\underline{H_2} = \left[-\underline{\underline{M}}\omega^2 + \underline{\underline{K}} + \underline{\underline{U}}\right]^{-1}\underline{B}_{\alpha_N} + \left[-\underline{\underline{M}}\omega^2 + \underline{\underline{K}} + \underline{\underline{U}}\right]^{-1}\underline{B}_{\beta_N} + \cdots + \left[-\underline{\underline{M}}\omega^2 + \underline{\underline{K}} + \underline{\underline{U}}\right]^{-1}\underline{B}_{\gamma_N} \quad (3\text{-}26b)$$

where

$$\underline{\underline{U}} = \underline{B}_{\alpha_1}\underline{R}^T_{\alpha_1} + \underline{B}_{\beta_1}\underline{R}^T_{\beta_1} + \cdots + \underline{B}_{\gamma_1}\underline{R}^T_{\gamma_1} + \underline{B}_{\alpha_N}\underline{R}^T_{\alpha_N} + \underline{B}_{\beta_N}\underline{R}^T_{\beta_N} + \cdots + \underline{B}_{\gamma_N}\underline{R}^T_{\gamma_N} \quad (3\text{-}27)$$

Substituting Eq. (3-25) into Eq. (3-24) as well as use of the temporal Fourier transform of Eq. (3-20) gives:

$$-\rho A\omega^2\hat{w}(x,\omega) = EA\frac{\partial^2\hat{w}(x,\omega)}{\partial x^2} + \int_{-\infty}^{\infty}\{\{\underline{T}^T\underline{H_1} - S\}\hat{w}(x,\omega) + \underline{T}^T\underline{H_2}\hat{w}(\zeta,\omega)\}Y(x-\zeta)d\zeta \quad (3\text{-}28)$$

Introducing $G_0 = \underline{T}^T\underline{H_1} - S$ and $G_1 = \underline{T}^T\underline{H_2}$, Eq. (3-28) takes the form:

$$-\rho A\omega^2\hat{w} = EA\frac{\partial^2\hat{w}}{\partial x^2} + G_0\hat{w}\int_{-\infty}^{\infty}Y(x-\zeta)d\zeta + G_1\hat{w} * Y(x) \quad (3\text{-}29)$$

Defining $Y_0 = \int_{-\infty}^{\infty}Y(x-\zeta)d\zeta$, the dispersion relation, after applying the spatial Fourier transform, is:

$$\rho A\omega^2 - EAk^2 + G_0Y_0 + \hat{G}_1\hat{Y} = 0 \quad (3\text{-}30)$$

Here $\hat{Y}$ denotes the spatial Fourier transform of the kernel $Y(x)$.

In the following subsections, two simple types of resonator units are considered as the constituents of the long-range superstructure. Although the dispersion relations of interest can be extracted based on the presented framework, a direct approach is adopted for the corresponding task. The analyses provide numerical results, helpful for realization of occurring phenomena.

### 3.3.2. Single degree-of-freedom resonator unit

At this point, the long-range connectors are single degree-of-freedom resonator units, as shown in Fig. 3. 24. The kinematic parameter associated with the mass is denoted by $q(\zeta, t)$.

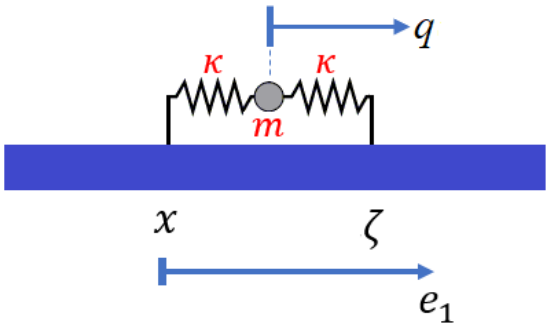


Fig. 3. 24: A simple model for long-range resonator-based waveguides

Each resonator unit is composed of a mass as well as two identical springs of stiffness $\kappa$, and thereby a single degree-of-freedom (SDOF) subsystem. The springs attach the mass to the waveguide at $x$ and $\zeta$.

The governing equation of motion for the system is:

$$\rho A \frac{\partial^2 w(x,t)}{\partial t^2} - EA \frac{\partial^2 w(x,t)}{\partial x^2} - \int_{-\infty}^{\infty} N_x(x,\zeta,t)\, H(x-\zeta) d\zeta = 0 \qquad (3\text{-}31)$$

A similar notation is employed here with respect to the previous subsection; and $H(x)$ is a symmetric rectangular window, identical the window shown in Fig. 3. 12. Unlike $Y(x)$, $H(x)$ is a specific window, which satisfies the required condition regarding the confinement. Note that the present system is a homogenous long-range configuration according to the discussion given in chapter 2.

The long-range force $N_x(x,\zeta,t)$ is proportional to the relative displacement of the resonator's mass with respect to that of the waveguide at $x$ as:

$$N_x(x,\zeta,t) = \kappa\,[q(\zeta,t) - w(x,t)] \qquad (3\text{-}32)$$

The governing equation of motion for the mass is:

$$m\ddot{q}(\zeta,t) + \kappa[q(\zeta,t) - w(x,t)] + \kappa[q(\zeta,t) - w(\zeta,t)] = 0 \qquad (3\text{-}33)$$

Expressing Eq. (3-33) in the temporal Fourier domain and performing a simple mathematical manipulation, one obtains:

$$\hat{q}(\zeta,\omega)=\frac{\kappa[\hat{w}(x,\omega)+\hat{w}(\zeta,\omega)]}{2\kappa-m\omega^2} \tag{3-34}$$

Here, the over-hat indicates the temporal Fourier transform of the associated displacement signal and $\omega$ is the temporal frequency of the structure.

Substituting Eq. (3-34) into the temporal Fourier transform of the long-range force (3-32) provides:

$$\hat{N}_x(x,\zeta,\omega)=\kappa\left[\frac{\kappa[\hat{w}(x,\omega)+\hat{w}(\zeta,\omega)]}{2\kappa-m\omega^2}-\hat{w}(x,\omega)\right] \tag{3-35}$$

In the light of Eq. (3-35), the temporal Fourier transform of Eq. (3-31) takes the form:

$$-\rho A\omega^2\hat{w}(x,\omega)=EA\frac{\partial^2\hat{w}(x,\omega)}{\partial x^2}+2D\kappa\left\{\frac{\kappa\,\hat{w}(x,\omega)}{2\kappa-m\,\omega^2}-\hat{w}(x,\omega)\right\}+\frac{\kappa^2\,\hat{w}(x,\omega)}{2\kappa-m\,\omega^2}*H(x) \tag{3-36}$$

where $*$ denotes the convolution operation and $2D$ is the active length of the window $H(x)$. The dispersion relation is obtained by applying the spatial Fourier transform to Eq. (3-36) as:

$$\rho A\omega^2=EAk^2-2\kappa D\left\{\frac{\omega_0^2}{2\omega_0^2-\omega^2}-1\right\}-2\kappa\frac{\omega_0^2}{2\omega_0^2-\omega^2}\frac{\sin(kD)}{k} \tag{3-37}$$

Note that the dispersion relations (3-37) can be directly extracted using the generalized mathematical model presented in the previous subsection. In the above equation, $\omega_0=\sqrt{\kappa/m}$ is a natural frequency parameter and $k$ is the wavenumber.

Introducing the nondimensional parameters $K=kD$, $\Omega=\omega D\sqrt{\rho/E}$, $\Omega_0=\omega_0 D\sqrt{\rho/E}$ and $\chi=\kappa D^3/EA$, the dispersion relation becomes:

$$\Omega^2=K^2+2\chi\left\{1-\frac{\Omega_0^2}{2\Omega_0^2-\Omega^2}\left[1+\frac{\sin(K)}{K}\right]\right\} \tag{3-38}$$

As evident, the dispersion behavior of the systems is controlled by the nondimensional natural frequency parameter $\Omega_0$ and the nondimensional characterizing parameter $\chi$, which roughly specifies the intensity of long-range forces.

The dispersion behaviour of the long-range waveguide with long-range SDOF resonator units (see Fig. 3. 24) is displayed in Fig. 3. 25. Owing to the special mathematical form of the dispersion relation in terms of frequency, it provides two separate dispersion branches, namely acoustic branch (AB) and optical branch (OB). In the optical mode, the particular movement of the resonator's mass with respect to $w(x,t)$ allows the structure to interact with existing electromagnetic fields, if present. Therefore, the optical mode can be activated by some electromagnetic emissions such as infrared radiation. Evidently, a complete stopband can emerge between the branches, dependent upon the adopted value for the frequency parameter $\Omega_0$. The term "stopband" refers to a range of frequencies within which propagation of acoustic and optical phonons is forbidden. stopbands are exhibited by red shaded regions. Based on the figures, width of the generated gap varies by $\Omega_0$, and it shrinks as the natural frequency $\Omega_0$ rises, for a fixed value for $\chi$; and it eventually fades away.

In order to evaluate the effect of $\chi$ on characteristics of the stopband, the dispersion curves are provided for two different values of $\chi$ in Fig. 3. 26 for $\Omega_0^2 = 100$. The figure suggests that the corresponding gap of $\chi = 50$ is distinguishably wider with respect to that of the system with $\chi = 10$. One may intuitively perceive this conclusion from Eq. (3-38), where the magnitude of the second term on the right-hand side of the equation, the contribution of long-range forces, is largely managed by the value of $\chi$, and since the associated term includes $\Omega^2$, the placement of one branch varies by a change in $\chi$ on $\Omega - K$ map.

Therefore, considering Fig. 3. 25 and Fig. 3. 26, the width of the generated stopband can be tuned by manipulating both parameters $\Omega_0$ and $\chi$. One crucial point to be understood is the possibility of achieving complete stopbands in such configurations unlike the systems described in the previous section. Again, the replacement of simple springs by resonator units brings extra degrees-of-freedom to long-range systems, laying the foundation for the born of stopbands by the identical mechanism observed in LRAMs.

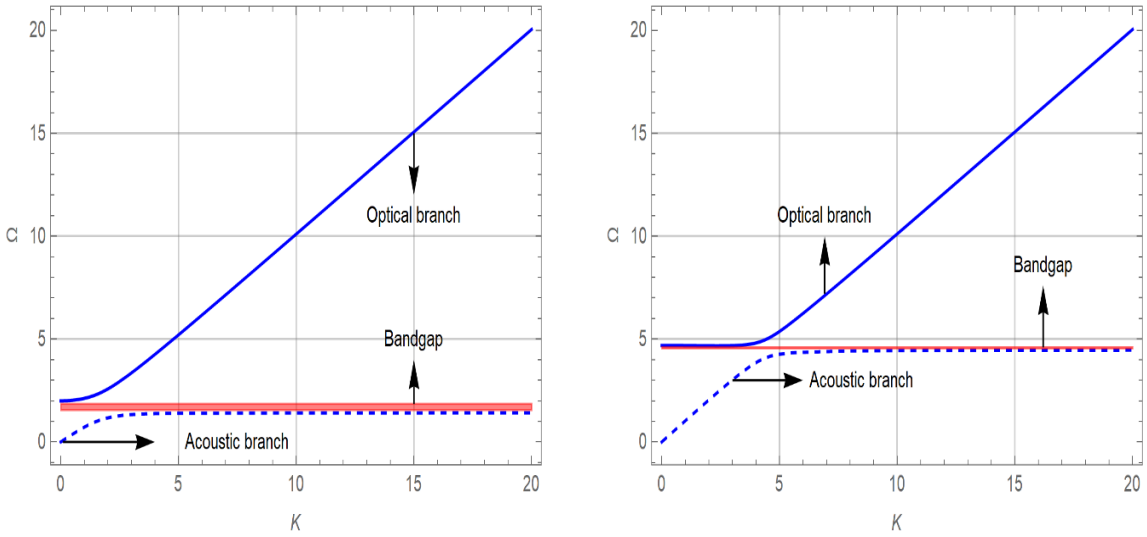


(a) $\Omega_0^2 = 1$ (b) $\Omega_0^2 = 10$

Fig. 3. 25: Representation band structure of a resonator-based long-range waveguide (SDOF) ($\chi = 1$)

What makes this study interesting is the existence of some ripples along the curve path of the acoustic branch unlike conventional locally resonant acoustic metamaterials. In fact, the speed of acoustic phonons in the long wavelength limit is impacted by the long-range nature of the system, and thereby a system with conceived potentials for presenting intriguing effects. As shown in Fig. 3. 27, the group velocity associated with the acoustic branch is plotted against the nondimensional wavenumber $K$. One to one correspondence of speed of acoustic phonons and the corresponding group velocity allows to reach a clear idea about the velocity of acoustic phonons. The figure indicates the possibility of occurrence of a situation in which the acoustic phonons are forced to stop travelling in the vicinity of some individual wavenumber(s)/frequency(ies) as well as propagating backwardly. From the figure, such phenomena do not occur unless $\chi$ exceeds a certain threshold. For instance, the curve corresponding to the system with $\chi = 1$ neither touches nor crosses the horizontal axis,

implying no unusual behaviour, whereas the curve associated with $\chi = 100$ crosses the axis for twice, i.e., wave-stopping and the speed of acoustic phonons becomes negative within the bands bounded by the wave-stopping wavenumbers. As earlier mentioned, these characteristics are unique to the long-range configurations as distinct from LARMs. Eventually, the speed of acoustic phonons tends to zero for small wavelengths.

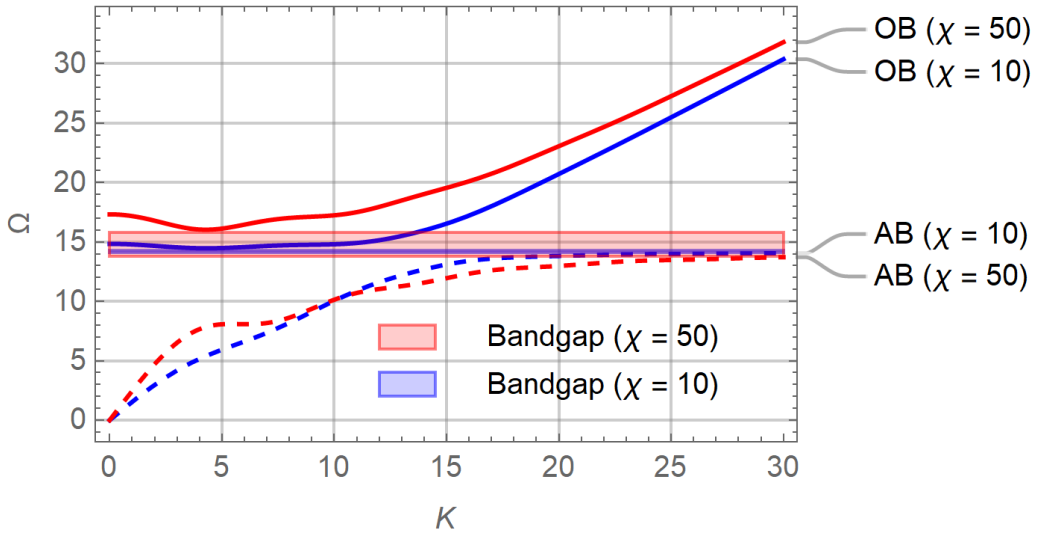


Fig. 3. 26: Band structure of a resonator-based long-range waveguide ($\Omega_0^2 = 10^2$)

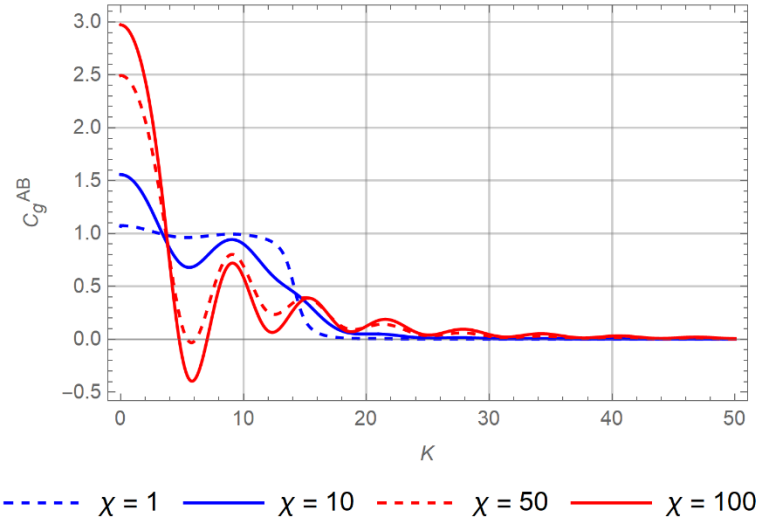


Fig. 3. 27: Group velocity curves corresponding to the acoustic branch for different value of $\chi$ ($\Omega_0^2 = 10^2$)

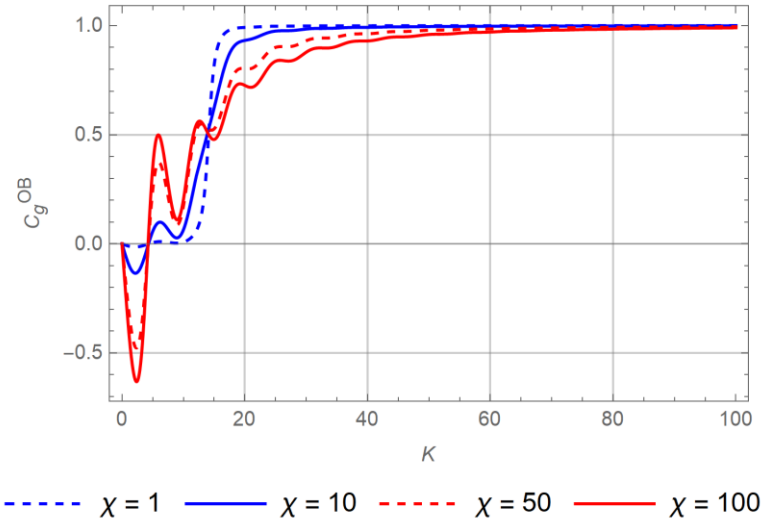


Fig. 3. 28: Group velocity curves corresponding to the optical branch for different value of $\chi$ $(\Omega_0^2 = 10^2)$

On the other hand, the optical dispersion branch contains attractive information about the propagation of optical phonons including the speed of travelling optical phonons. Analogous to the previous comment, the group velocity response corresponding to the optical branch is correlated with the speed of optical phonons. Curiously enough, all the curves shown in Fig. 3. 28 start from zero moving towards negative values, implying backward propagation of optical phonons in a specific long-wavelength band, and hence the occurrence of the zero/negative speed for the optical phonons is guaranteed for the adopted value of $\chi$. This once more demonstrates the intriguing potential of the long-range property, absent in conventional LRAMs.

In brief, the existence of distant communication among points produces certain intriguing phenomena, detectable from the group velocity response of both principal branches, namely acoustic and optical. The chance of steering acoustic and optical phonons in the backward direction is provided by the modified dynamics owing to the inclusion of the long-range superstructure.

### 3.3.3. Double degrees-of-freedom resonator unit

The present case considers a double degrees-of-freedom resonator unit as the long-range connector, allowing for distant communication between the hub point $x$ and the hovering point $\zeta$ (see Fig. 3. 29). The unit contains two masses, $m_1$ and $m_2$ and three identical springs of the stiffness $\kappa$. The axial displacement of masses is represented by $q_1(\zeta, t)$ and $q_2(\zeta, t)$, respectively.

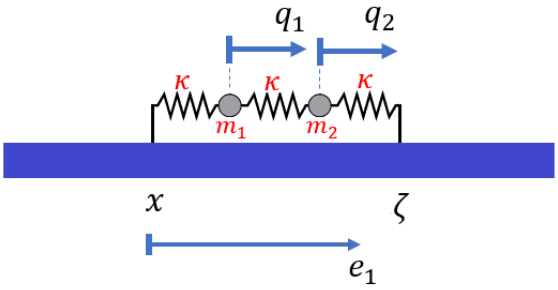


Fig. 3. 29: Long-range waveguide with a rectangular interaction region

Similar to the previous case, all points within the rectangular window $H(x)$ of length $2D$ interact nonlocally with $x$ via long-range connectors, here double degrees-of-freedom resonator units, as shown in Fig. 3. 29.

Although the general equation of motion for the above system is identical to that given in Eq. (3-31), the mathematical expression for long-range force $N_x(x,\zeta,t)$ takes the following form:

$$N_x(x,\zeta,t) = \kappa[q_1(\zeta,t) - w(x,t)] \tag{3-39}$$

The governing equations of motion for the masses are:

$$m_1\ddot{q}_1(\zeta,t) + \kappa[q_1(\zeta,t) - w(x,t)] + \kappa(q_1(\zeta,t) - q_2(\zeta,t)) = 0 \tag{3-40a}$$

$$m_2\ddot{q}_2(\zeta,t) + \kappa[q_2(\zeta,t) - w(\zeta,t)] + \kappa[q_2(\zeta,t) - q_1(\zeta,t)] = 0 \tag{3-40b}$$

Through the instrumentality of temporal Fourier transform and some mathematical operations, the expression for $q_1(\zeta,t)$, in the temporal Fourier domain, is:

$$\hat{q}_1(\zeta,\omega) = \frac{\hat{w}(\zeta,\omega)+(2-\omega^2/\omega_2^2)\hat{w}(x,\omega)}{3-2\omega^2(1/\omega_1^2+1/\omega_2^2)+\omega^4/\omega_2^2\omega_1^2} \tag{3-41}$$

Following the similar procedure adopted in the previous subsection, the counterpart of Eq. (3-36) is:

$$\rho A\omega^2\hat{w}(x,\omega) = EA\frac{\partial^2\hat{w}(x,\omega)}{\partial x^2} - 2\kappa L\left(\frac{2-\frac{\omega^2}{\omega_2^2}}{3-2\omega^2\left(\frac{1}{\omega_1^2}+\frac{1}{\omega_2^2}\right)+\frac{\omega^4}{\omega_2^2\omega_1^2}} - 1\right)\hat{w}(x,\omega) - \frac{\kappa}{3-2\omega^2(1/\omega_1^2+1/\omega_2^2)+\omega^4/\omega_2^2\omega_1^2}\hat{w}(x,\omega) * H(x) \tag{3-42}$$

where $\omega_1 = \sqrt{\kappa/m_1}$ and $\omega_2 = \sqrt{\kappa/m_2}$ are two frequency parameters. The dispersion relation corresponding to the above equation, in the nondimensional form, is:

$$\Omega^2 = K^2 + 2\chi\left\{1 - \frac{1}{3-2\left(\frac{\Omega^2}{\Omega_1^2}+\frac{\Omega^2}{\Omega_2^2}\right)+\frac{\Omega^4}{\Omega_2^2\Omega_1^2}}\left[2 - \frac{\Omega^2}{\Omega_2^2} + \frac{\sin(K)}{K}\right]\right\} \tag{3-43}$$

with

$$K = kD \tag{3-44a}$$

$$\Omega = \omega D\sqrt{\rho/E} \tag{3-44b}$$

$$\Omega_1 = \omega_1 D\sqrt{\rho/E} \quad (3\text{-}44c)$$

$$\Omega_2 = \omega_2 D\sqrt{\rho/E} \quad (3\text{-}44d)$$

$$\chi = \kappa D^3/EA \quad (3\text{-}44e)$$

To realize the dispersion characteristics of the current configuration, the dispersion curves are provided in Fig. 3. 30 for two different sets of $(\Omega_1, \Omega_2)$. Since the special mathematical form of the dispersion relation (3-43) is sixth order in terms of frequency Ω, it is composed of three separate branches. The low-frequency branch is the acoustic one and the one on the top is the optical branch. The one in middle is a mixed mode. Due to the existence of three branches, the band structure can contain at most two complete stopbands, placing between every two consecutive branches. High sensitivity of the band structure to the value of $(\Omega_1, \Omega_2)$ is realized by comparing Fig. 3. 30a and Fig. 3. 30b, where a rise in $\Omega_2$ leads to the closure of upper gap. Clearly, adopting resonator units with higher degrees-of-freedom is associated with the generation of a larger number of stopbands in the corresponding band structure.

Regarding the effect of the nondimensional parameter $\chi$ on the dispersion characteristics, Fig. 3. 31 suggests the possibility of widening the lower gap by considering larger χ, similar to what concluded for Fig. 3. 26. Besides, it is shown that the upper gap does not emerge for the adopted parameters $\chi$, $\Omega_1$ and $\Omega_2$, which confirms the hypothesis raised in the previous comment. This gives us an instrument to manipulate the gaps in a desired manner.

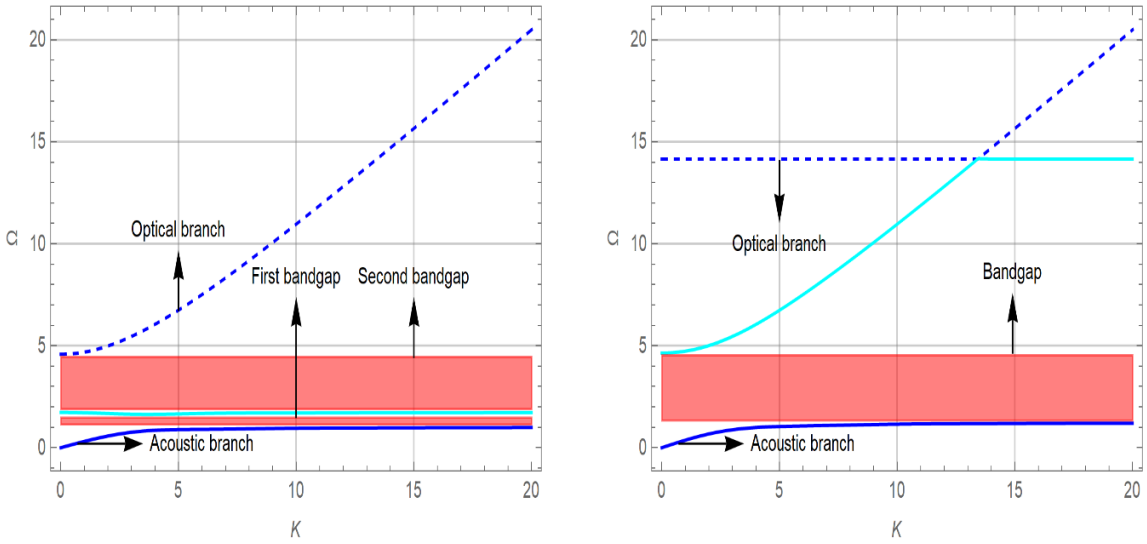


(a) $\Omega_1^2 = 1$ & $\Omega_2^2 = 1$ (b) $\Omega_1^2 = 1$ & $\Omega_2^2 = 10^2$

Fig. 3. 30: Representation band structure of a resonator-based long-range waveguide (2DOF) $(\chi = 10)$

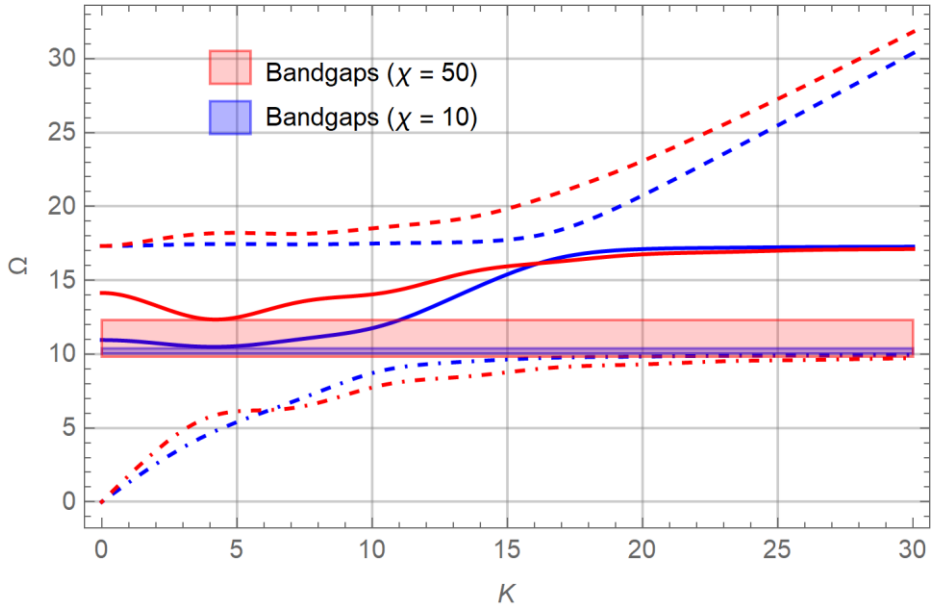


Fig. 3. 31: Band structure of a resonator-based long-range waveguide
($\Omega_1^2 = 10^2$ & $\Omega_2^2 = 10^2$)

Fig. 3. 32 is devoted to investigating the speed of acoustic phonons while travelling across the system. Again, unusual behaviours such as zero/negative group velocity are seen in the group velocity response, exclusively when the long-range system is characterized by either the critical or supercritical values of $\chi$, as displayed in Fig. 3. 32. Clearly, the critical value $\chi_{cr}$ depends on other involved parameters, $\Omega_1$ and $\Omega_2$.

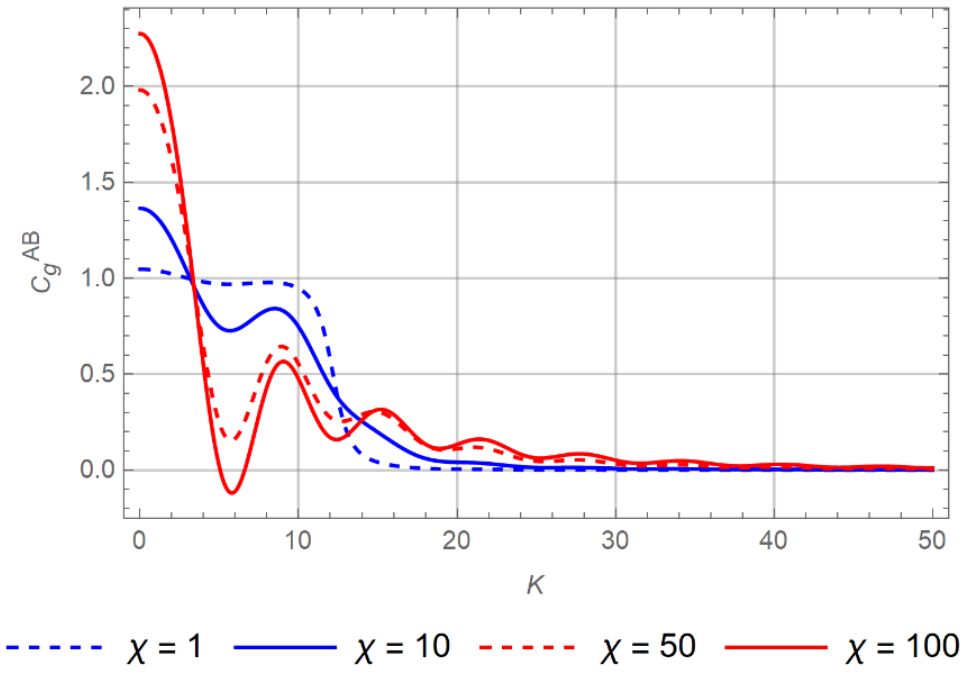


Fig. 3. 32: Group velocity curves corresponding to the acoustic branch for different values of $\chi$
($\Omega_1^2 = 10^2$ & $\Omega_2^2 = 10^4$)

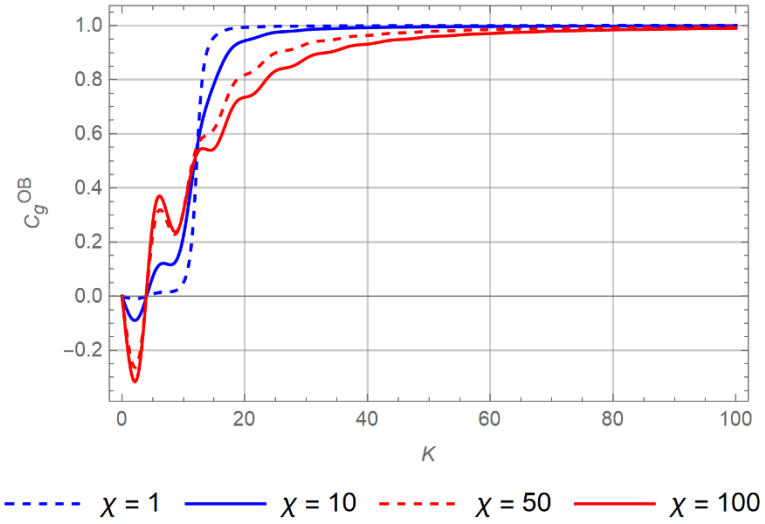


Fig. 3. 33: Group velocity curves corresponding to the optical branch for different values of $\chi$ ($\Omega_1^2 = 10^2$ & $\Omega_2^2 = 10^4$)

The last assessment in this part examines the influence of long-range property on the speed of optical phonons. Here, curves demonstrate the relation between the wavenumber $K$ and the group velocity curves connected with optical dispersion branch, as displayed in Fig. 3. 33. Evidently, the long-range nature of the system alters the curve paths, generating significant fluctuations in the long-wavelength range. Such fluctuations produce zero/negative values of $C_g^{OB}$ within a particular wavenumber/frequency band. Similar trends have been observed in the previous case, as exhibited in Fig. 3. 28.

## 3.4. Long-range homogenous membrane

This section is an attempt to study the effects of long-range forces when introduced to a simple two-dimensional domain. The spring-like links run the interactions among non-adjacent particles. Note that the results of the following analysis was already published and reported in Ref. [107,111].

To begin with, the dynamic discerption of a classical membrane is:

$$\rho \frac{\partial^2 u(x,y,t)}{\partial t^2} - T\,\nabla^2 u(x,y,t) = 0 \qquad (3\text{-}45)$$

where $\nabla^2$ represents the Laplacian operator. Also, $u(x,y,t)$, $\rho$ and $T$ are the deflection, mass per unit area, and the tension per unit length, respectively. This equation is typical of a structure, which exclusively considers the elastic connections between a point and the immediate neighbours. New advances in additive manufacturing open the chance to assume connections among distant points as well. Their presence is regarded by allocating an integral term, analogous to that in Eq. (3-10), to the equation of motion as:

$$T\,\nabla^2 u - \rho \frac{\partial^2 u}{\partial t^2} - \kappa \iint_{-\infty}^{\infty} [u(x,y,t) - u(\xi,\eta,t)] H(x-\xi, y-\eta) d\xi d\eta = 0 \qquad (3\text{-}46)$$

where $\kappa$ represents the spatial stiffness modulation of the spring-like links. The mathematical model carries two distinct elastic behaviours: the long-range interactions described by the integral term $\iint_{-\infty}^{\infty} \kappa\,[u(x,y)-u(\xi,\eta)]H(x-\xi,y-\eta)d\xi d\eta$, and the short-range interactions described by the differential term $\nabla^2 W$. The integral term mechanically resembles simple springs, connecting two points. The axisymmetric cylindrical window $H(r)=H\left(\sqrt{x^2+y^2}\right)$ is chosen as (see Fig. 3. 34)

$$H(r)=\begin{cases}1, & |r|\le a\\ 0, & |r|>a\end{cases} \tag{3-47}$$

where $a$ is a positive number representing the interaction radius. Using the convolution theorem, equation (3-46) reads into:

$$T\,\nabla^2 u(x,y,t)-\rho\frac{\partial^2 u(x,y,t)}{\partial t^2}-\kappa\,S\,u(x,y,t)+k\,H(x,y)*u(x,y,t)=0 \tag{3-48}$$

where $S$ is the area of the region of interaction and $*$ denotes the convolution operation. In this case, both the tree-periodicity and the leaf-periodicity are not present, and the investigated system is simply long-range homogeneous.

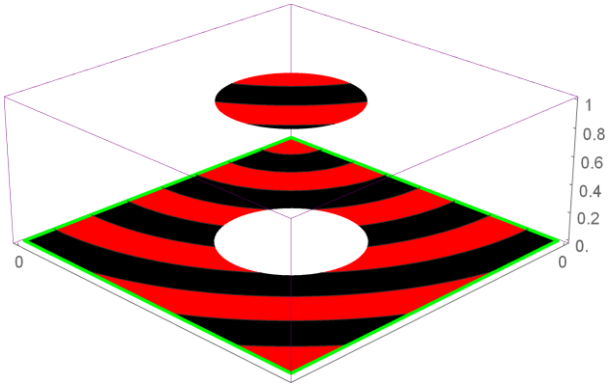


Fig. 3. 34: Representation of a cylindrical window

Assuming plane wave solution, the dispersion relation is obtained as:

$$\rho\omega^2=T(k_1^2+k_2^2)+\kappa\,S-\kappa\,aJ_1\left(a\sqrt{k_1^2+k_2^2}\right)/\sqrt{k_1^2+k_2^2} \tag{3-49}$$

$J_1$ is the Bessel function of first kind. The term $\kappa(aJ_1(ak_1^2+k_2^2)/\sqrt{k_1^2+k_2^2}-S)$ corresponding to nonlocal interactions may give birth to new propagation scenarios.

Eq. (3-49) is rewritten in nondimensional form as follows:

$$\Omega^2=(K_1^2+K_2^2)+\chi\left[\pi-J_1\left(\sqrt{K_1^2+K_2^2}\right)/\sqrt{K_1^2+K_2^2}\right] \tag{3-50}$$

with

$$\Omega=a\sqrt{\rho/T}\,\omega \tag{3-51a}$$

$$K_{1,2}=a\,k_{1,2} \tag{3-51b}$$

$$\chi = \kappa\, a^4/T \tag{3-51c}$$

According to Eq. (3-51c) and similarly to the one-dimensional cases, $\chi$ is a ratio comparing roughly the strength of long-range and the short-range forces. Eq. (3-50) discloses that the system presents specific phenomena such as wave-stopping and negative group velocity given a large enough $\chi$. This is shown in Fig. 3. 35a and Fig. 3. 35b, where the dispersion surfaces corresponding to the long-range membrane with subcritical and supercritical $\chi$ are plotted. Since the slope of the tangents to the dispersion surfaces is directly associated to the group velocity, these surfaces provide some information about the potential phenomena in system. As for the one-dimensional cases, wave-stopping and negative group velocity emerge when the nondimensional parameter $\chi$ exceeds a threshold and subsequently severe wrinkles are embedded into the texture of the surface (see Fig. 3. 35b).

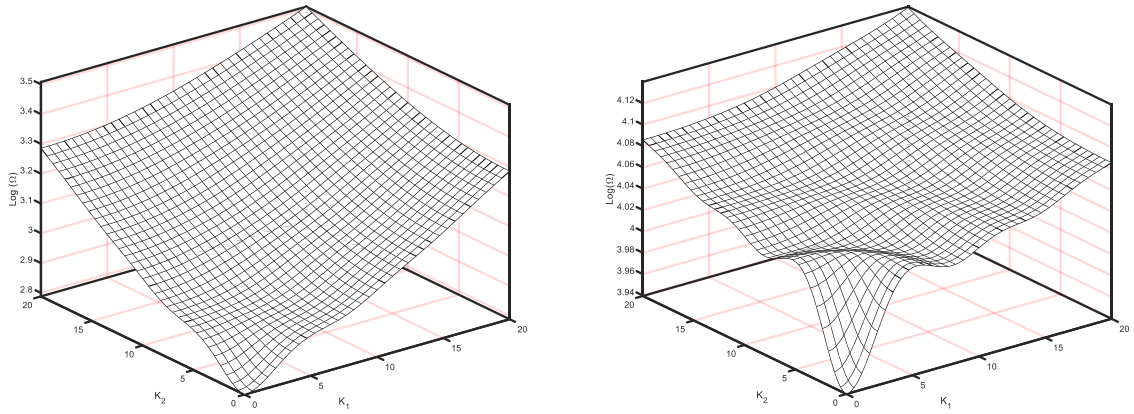


(a) (b)

Fig. 3. 35: Dispersion surfaces for long-range membrane a) $\chi = 100$ b) $\chi = 1000$

The phase and group velocities are as follows:

$$\boldsymbol{C}_p = \widehat{\boldsymbol{K}}\ \Omega/|\boldsymbol{K}| \tag{3-52a}$$

$$\boldsymbol{C}_g = \vec{\nabla}_{\boldsymbol{K}}\Omega \tag{3-52b}$$

where $\vec{\nabla}$ denotes the gradient of the nondimensional frequency $\Omega$ and $\widehat{\boldsymbol{K}}$ is the unit vector in $\boldsymbol{K}$-direction.

Fig. 3. 36 exhibits the vector plot corresponding to the phase velocity vector $\boldsymbol{C}_p$ of a long-range membrane with $\chi = 1000$. The figure shows considerably high magnitude phase velocity vectors (red) when the wavenumber vector $\boldsymbol{K}$ approaches zero due to the presence of the expression $\widetilde{K} = \sqrt{K_1^2 + K_2^2}$ in the denominator of $\boldsymbol{C}_p$'s components. From the direction of stream vectors (blue), no irregularity in the phase velocity behavior is perceived and similar trends are observed for any arbitrary value of $\chi$.

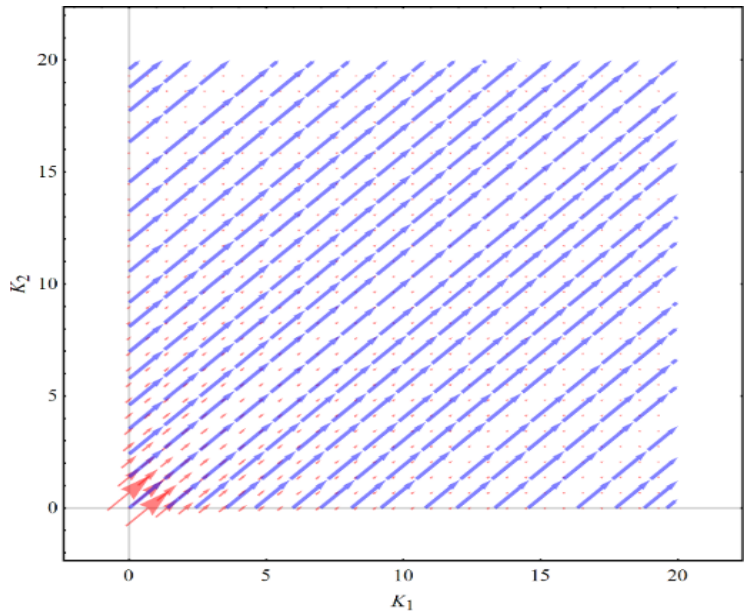


Fig. 3. 36: Vector plot of phase velocity for long-range membrane ($\chi = 1000$)

Fig. 3. 37 depict the changes in the group velocity of the long-range membrane. According to the vector plot provided for the system with $\chi = 100$, the typical stream vectors, similar to those of the classical system ($\chi = 0$), is preserved though considerable decrease in magnitude of velocity vectors (red) is observed in some regions. On the other hand, unlike the previous case, one distinguishes both inwards and outwards streamlines for the system with $\chi = 1000$, implying the emergence of negative group velocity within a sectorial region in $K_1 - K_2$ plane. Accordingly, the modal density $\mathrm{n}(\Omega)$ is mathematically singular at frequencies generated by any ordered pair $(K_1, K_2)$ placed on the borders of the sectorial region.

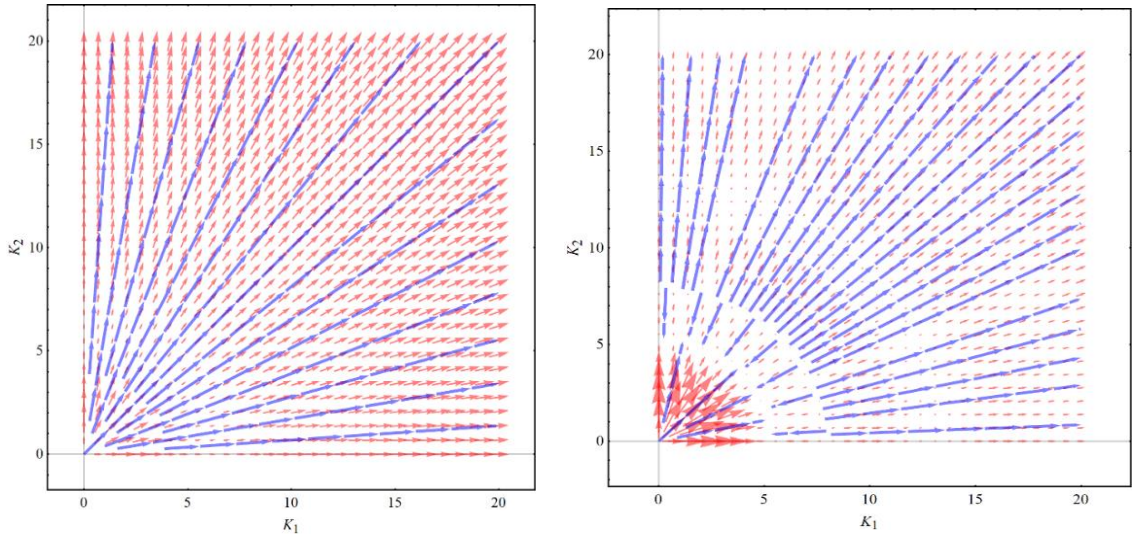


ss(a) (b)

Fig. 3. 37: Vector plot of group velocity for long-range membrane
a) $\chi = 100$ b) $\chi = 1000$

Eventually, as with the one-dimensional case, the dispersion relation corresponding to the long-range membrane contains a term that plays a key role in removing large spatial frequency components. In fact, some aspects of the output signal alter due to the introduction of the additional expression, which includes the Bessel function, usually identified as a low-pass filter. Note that there is no need for external device as a controller to block the energy contents with small wavelengths and the intrinsic property of the structure takes the charge automatically.

## 3.4. Final remarks

The nature of conventional systems subject to profound change, when integrated with external links responsible for long-range interactions. This chapter intends to shed a light on the alteration took place due to this integration, majorly in terms of wave propagation behaviour. Towards that end, various combinations of connectivity templates and long-range connector types have been defined for a long-range one-dimensional waveguide, and a complementary example has been provided to show the ingenuity of the long-range interaction concept, when associated to a higher dimension domain, i.e., membrane. Application of plane wave solution to the dynamic description of each case yields an analytical dispersion relation, revealing the very essence of the systems under investigation. Uncommon effects such as zero/negative group velocity, redistribution of modes across the frequency domain, and stopbands are demonstrated by the virtue of the obtained analytical wavenumber-frequency relations.

# Chapter 4: Nonlinear long-range homogenous waveguide

## 4.1. Introduction

Nonlinearity is the source of many interesting phenomena in systems. It generally refers to the nonlinear terms in the strain-displacement relation. Although such terms are usually disregarded, they regain their importance once the large displacements are predominant. Nonlinearity is the common link among a variety of mechanical systems, which ties the resonances to the amplitude of oscillations, unlike linear systems. Other intrinsic characteristics of nonlinear systems is the occurrence of resonances that are the modulation of the excitation frequency, namely subharmonic and superharmonic resonances.

Both long-range connectors and the host structure were assumed to behave linearly in the cases investigated in the previous chapter; nevertheless, deep influences on the performance of systems in terms of waves was realized. This chapter tries to reach an understanding of changes made in behaviour of genuine long-range systems, in particular a long-range waveguide, when the structure happens to capture the nonlinear characteristics.

The analysis studies a bounded nonlinear host structure with embedded linear long-range connectors under random excitation. Considering the first vibrational mode, the system is linearized with the aid of statistical linearization. Due to the presence of an integral term in the resulting dispersion relation, a specific feature of the system is understood via Fredholm theorem. Then the effect of nonlinearity and noise on the plane wave characteristics of the system is estimated by homogenising the dispersion relation.

## 4.2. Randomly excited nonlinear long-range waveguide

A nonlinear waveguide under random excitation with linear spatial nonlocalities is the centre of attention in this section. The stochastic excitation brings out the nonlinear characteristics, which are only present in large displacement regime. A couple of simplifying assumption are raised to treat the sophisticated dynamics.

### 4.2.1. General formulation and linearization procedure (random excitation)

A waveguide subjected to an external longitudinal random force is considered. infinitesimal strain-displacement relation cannot be employed when the system undergoes large strains. The displacement at each point is the difference between the deformed and undeformed position:

$$u = X - x \tag{4-1}$$

where $x$ is the position of a particle in the reference configuration and $X$ represents the spatial coordinate of the same particle in the deformed configuration. The Piola-Kirchhoff stress is:

$$\sigma_{11} = E_0 \epsilon_{11} = E_0 \left(1 + \frac{1}{2}\frac{\partial u}{\partial x}\right)\frac{\partial u}{\partial x} \tag{4-2}$$

Here, $E_0$ is the Young's modulus and $\epsilon_{ij}$ represents the Lagrangian strain tensor, which may be obtained as:

$$\epsilon_{ij} = \frac{1}{2}\left(\frac{\partial u_i}{\partial x_j} + \frac{\partial u_j}{\partial x_j} + \frac{\partial u_k}{\partial x_i}\frac{\partial u_k}{\partial x_j}\right) \tag{4-3}$$

Applying Hamilton's principle, the nonlinear equation of motion reads:

$$\rho \frac{\partial^2 u(x,t)}{\partial t^2} - E_0 \frac{\partial^2 u(x,t)}{\partial x^2}\{1 + 3\frac{\partial u(x,t)}{\partial x} + \frac{3}{2}\left[\frac{\partial u(x,t)}{\partial x}\right]^2\} = F(x,t) \tag{4-4}$$

Here the term $F(x,t)$ denotes the random excitation stimulating the nonlinear characteristics. This equation is yet to be integrated with another term, which would explain the presence of long-range effects via external spring-like links. The interactions are assumed to take place within a rectangular window, analogous to the case studies in the previous chapter. Since the system of interest assumes the same connectivity template suggested in subsection 3.2.2.1, the configuration is a simple long-range homogenous one.

Thus, the governing equation for the new configuration is:

$$\rho \frac{\partial^2 u(x,t)}{\partial t^2} - E_0 \frac{\partial^2 u(x,t)}{\partial x^2}\left\{1 + 3\frac{\partial u(x,t)}{\partial x} + \frac{3}{2}\left[\frac{\partial u(x,t)}{\partial x}\right]^2\right\} + \kappa \int_{-\infty}^{\infty}[u(x,t) - u(\xi,t)]\, H(x-\xi)d\xi = F(x,t) \tag{4-5}$$

where $H(x)$ represents the interaction region, and $\kappa$ is the characteristic stiffness of the links. This equation involves linear and nonlinear differential terms as well as an integral contribution, governing the dynamic behaviour of the system. To treat this nonlinear integral-differential equations, statistical linearization (SL) [119] is employed to approach the problem as an effective method. To reach an understanding of how the method works, let us consider the general form of a nonlinear equation as:

$$\underline{\underline{D}}_L(\underline{u}) + \underline{\underline{D}}_{NL}(\underline{u}) = \underline{F}(\underline{x},t) \tag{4-6}$$

where $\underline{\underline{D}}_L$ and $\underline{\underline{D}}_{NL}$ are, respectively, the linear and nonlinear integral-differential connectors acting on a displacement vector. The SL method suggests replacing the nonlinear connectors by a set of arbitrary linear ones, say $\underline{\underline{\bar{D}}}_L\left(\underline{u},\underline{p}\right)$, as:

$$\underline{\underline{D}}_L(\underline{u}) + \underline{\underline{\bar{D}}}_L\left(\underline{u},\underline{p}\right) = \underline{F}(\underline{x},t) \tag{4-7}$$

Here, $\underline{\underline{\bar{D}}}_L$ denotes the arbitrary equivalent linear connectors, and $\underline{p}$ is an array of parameters which works as weighting functions. These parameters are to be learned accurately for the resulting linear system to mimic the behaviour of the nonlinear configuration. Here a second

order derivative differential operator is adopted for producing a linearized dynamic description. Thus, the equivalent linearized form is:

$$\rho \frac{\partial^2 u(x,t)}{\partial t^2} - E_0(1+\check{p}) \frac{\partial^2 u(x,t)}{\partial x^2} + \kappa \int_{-\infty}^{\infty} [u(x,t) - u(\xi,t)]\, H(x-\xi) d\xi = F(x,t) \quad (4\text{-}8)$$

The term $\hat{p} \frac{\partial^2 u(x,t)}{\partial x^2}$ is employed as the equivalent linear term. Comparing Eq. (4-6) and Eq. (4-7), it is immediate to evaluate the function error as:

$$\underline{e}\left(\underline{u}, \underline{p}\right) = \underline{\underline{D}}_{NL}(\underline{u}) - \underline{\underline{D}}_{NL}(\underline{u}) \quad (4\text{-}9)$$

Based on the considered model, the function error is:

$$e = \frac{\partial^2 u}{\partial x^2}\left\{3\frac{\partial u}{\partial x} + \frac{3}{2}\left(\frac{\partial u}{\partial x}\right)^2\right\} - \check{p}\frac{\partial^2 u}{\partial x^2} \quad (4\text{-}10)$$

where $\check{p}$ is an unknown parameter to be determined via the minimization condition. The SL approach necessitates to minimize of the expected value of $\underline{e}$ with respect to the entries of $\underline{p}$:

$$\frac{\partial \mathbb{E}\{\underline{e}^T(\underline{p})\, \underline{e}(\underline{p})\}}{\partial \underline{p}} = 0 \quad (4\text{-}11)$$

Thus, the optimal the vector $\underline{p}^*$, obtained by the condition (11), enables to proceed with the linear equation $\underline{\underline{D}}_L(\underline{u}) + \underline{\underline{\bar{D}}}_L\left(\underline{u}, \underline{p}^*\right) = \underline{F}(\underline{x}, t)$ rather than a comparatively complex nonlinear one. Expressing the displacement in terms of the first normal mode $u(x,t) = \phi(x)q(t)$ with the temporal parts of the displacement signal $q(t)$ to be stationary random processes, Eq. (4-10) and Eq. (4-11) provide:

$$\check{p} = \frac{3}{2}\left(\frac{\partial \phi}{\partial x}\right)^2 \mathbb{E}\{q^2\} + 3\frac{\partial \phi}{\partial x}\mathbb{E}\{q\} \quad (4\text{-}12)$$

Note that, for the sake of simplicity, only the first mode is considered in this study. In fact, while studying the system in low frequency range, it is reasonable to define the correction factor $\check{p}$ in terms of the fundamental mode only. Provided that the random variable is equipped with Gaussian probability density function, a reasonably simplified expression for $\check{p}$ is derived as:

$$\check{p} = \frac{9}{2}\left(\frac{\partial \phi}{\partial x}\right)^2 \hat{\sigma}_q^2 \quad (4\text{-}13)$$

Here $\hat{\sigma}_q^2$ is the variance associated to the random variables $q$. The governing equation of motion in the modal form for a specific index is:

$$\rho\phi \frac{\partial^2 q}{\partial t^2} - E_0\left(1 + \frac{9}{2}\left(\frac{\partial \phi}{\partial x}\right)^2 \hat{\sigma}_q^2\right)\frac{\partial^2 \phi}{\partial x^2} q + \kappa q \int_{-\infty}^{\infty} [\phi(x) - \phi(\xi)] H(x-\xi) d\xi = F(x,t) \quad (4\text{-}14)$$

Note that the equivalent linear term simply serves as a correction factor for the coefficient of the conventional second order spatial derivative. The parameters $\hat{\sigma}_q^2$ in this equation are yet

determined. For that purpose, the above equation is multiplied by the orthogonal eigenfunction $\bar{\phi}$ and integrated over the domain, yielding:

$$\rho \frac{\partial^2 q}{\partial t^2} \int_0^l \phi \bar{\phi}\, dx - E_0 q \int_0^l \left(1 + \frac{9}{2}\left(\frac{\partial \phi}{\partial x}\right)^2 \hat{\sigma}_q^2\right) \frac{\partial^2 \phi}{\partial x^2} \bar{\phi}\, dx + \kappa q \int_0^l \bar{\phi}\ [\int_{-\infty}^{\infty} [\phi(x) - \phi(\xi)] H(x - \xi) d\xi] dx = \int_0^l F(x,t) \bar{\phi}\, dx \quad (4\text{-}15)$$

To further proceed with analysis, specific definitions for the orthogonal basis $\phi$ is vital. Using the orthogonal property of the basis $\phi$, the above equation simplifies as:

$$\frac{\partial^2 q}{\partial t^2} + R^2 q = \tilde{F}(t) \quad (4\text{-}16)$$

where $R^2$ is the unique coefficient for each type of boundary conditions, and:

$$\tilde{F}(t) = \int_0^l F(x,t) \phi\, dx \quad (4\text{-}17)$$

Using Duhamel's integral, the solution to Eq. (4-16) is:

$$q(t) = \frac{1}{R} \int_0^t \tilde{F}(\tau) \sin[R(t-\tau)]\, d\tau \quad (4\text{-}18)$$

To capture the statistical properties of the output signal $u$, covariance calculations should be done. Assuming $F(x,t) = \psi(x) f(t)$, after doing several mathematical manipulations, $\hat{\sigma}_q^2$ can be evaluated from:

$$\hat{\sigma}_q^2 = \frac{1}{2\pi} [\int_0^l \phi^2\, dx\, ][\int_0^l \psi\, \phi\, dx]^2\ [\int_{-\infty}^{+\infty} \left|\hat{q}\left(\omega, \hat{\sigma}_q^2\right)\right|^2 S_f\, d\omega] \quad (4\text{-}19)$$

where $S_f$ is the power spectral density of the random noise $f(t)$. This equation suggests a random noise with high intensity generates greater values of the variance $\hat{\sigma}_q^2$, affording significant changes in the response of system due to the larger value of the correction factor. Having $\hat{\sigma}_q^2$ determined, the motion of the system can be described by Eq. (4-14).

## 4.2.2. Periodically modulated coefficient and instability

The emergence of instability in systems governed by partial differential equations with periodic coefficients has been observed, giving rise to stopbands in the band structure of the system. In particular, the Mathieu's differential equation, which includes a spatially varying periodic coefficient can present such behaviour in certain frequency ranges. Since the linearization procedure brought above influences the differential part and eventually generate an equation in nodding acquaintance with the form of Mathieu's equation, it is important to examine the stability of the resulting differential part. From Eq. (4-14), the non-integral contributions of the linearized equation of motion is:

$$\rho \frac{\partial^2 u}{\partial t^2} - E\left(1 + \frac{9}{2} \phi'^2 \hat{\sigma}_q^2\right) \frac{\partial^2 u}{\partial x^2} = F(x,t) \quad (4\text{-}20)$$

Since the eigenmode $\phi$ is uniquely defined for any specific boundary condition, each case should be investigated separately. Assuming $u(x,t) = U(x)e^{-j\omega t}$, the above equation, for a clamped waveguide, for which $\phi = \sin(\omega_0 x)$ takes the form:

$$\rho\omega^2 U + E\left(1 + \frac{9\pi^2\hat{\sigma}_q^2}{2L^2}\cos\left(\frac{\pi x}{L}\right)^2\right)\frac{d^2U}{dx^2} = -F(x,t) \quad (4\text{-}21)$$

Assuming a substantially lengthy rod, the contribution of the term $\frac{9\pi^2\hat{\sigma}_q^2}{2L^2}$ is very small so that it can be considered as a perturbation $\epsilon$. To realize the status of stability in such a system, multiple scale method is selected as an efficient method to construct a valid approximate solution for the problems. Defining the dependence of $x$ on different length scales $X_0, X_1, X_2, \dots, X_N$, where:

$$X_n = \epsilon^n x \quad (4\text{-}22)$$

Therefore, the displacement $\hat{u}$ may be expressed as [120]:

$$U(x;\epsilon) = \sum_{n=0}^{N-1}\epsilon^n U_n(X_0, X_1, X_2, \dots, X_N) + O(\epsilon X_N) \quad (4\text{-}23)$$

where $N$ defines the number of scales. Considering $N = 2$, the following equations corresponding to $X_0$, $X_1$ and $X_2$ are obtained:

$$\epsilon^0 : \frac{\partial^2 U_0}{\partial X_0^2} + \rho\omega^2 U_0 = 0 \quad (4\text{-}24a)$$

$$\epsilon^1 : \frac{\partial^2 U_1}{\partial X_0^2} + \rho\omega^2 U_1 + 2\frac{\partial^2 U_0}{\partial X_0 X_1} + \cos\left(\frac{\pi X_0}{L}\right)^2\frac{\partial^2 U_0}{\partial X_0^2} = 0 \quad (4\text{-}24b)$$

The general solution of Eq. (4-24a) is:

$$U_0(X_0, X_1) = B_1(X_1)\ \sin(\omega X_0) + B_2(X_1)\ \cos(\omega X_0) \quad (4\text{-}25)$$

Where $B_1(X_1)$ and $B_2(X_1)$ are unknown coefficients. Substitution of Eq. (4-25) in Eq. (4-24b) gives

$$\frac{\partial^2 U_1}{\partial X_0^2} + \omega^2 U_1 = \left(\frac{\rho\omega^2}{2}B_2 - 2\omega\sqrt{\rho}\frac{\partial B_1}{\partial X_1}\right)\cos\left(\omega\sqrt{\rho}X_0\right) + \left(\frac{\rho\omega^2}{2}B_1 + 2\omega\sqrt{\rho}\frac{\partial B_2}{\partial X_1}\right)\sin\left(\omega\sqrt{\rho}X_0\right) + \frac{\rho\omega^2 B_2}{4}\left(\cos\left(\left[\sqrt{\rho}\omega - \frac{2\pi}{L}\right]X_0\right) + \cos\left(\left[\sqrt{\rho}\omega + \frac{2\pi}{L}\right]X_0\right)\right) + \frac{\rho\omega^2 C_1}{4}\left(\sin\left(\left[\sqrt{\rho}\omega - \frac{2\pi}{L}\right]X_0\right) + \sin\left(\left[\sqrt{\rho}\omega + \frac{2\pi}{L}\right]X_0\right)\right) = 0 \quad (4\text{-}26)$$

To ensure no exponentially growing terms in $\tilde{\hat{u}}_1$, the resonant terms are forced to be zero as:

$$\frac{\rho\omega^2}{2}B_2 - 2\omega\sqrt{\rho}\frac{\partial B_1}{\partial X_1} = 0 \quad (4\text{-}27a)$$

$$\frac{\rho\omega^2}{2}B_1 + 2\omega\sqrt{\rho}\frac{\partial B_2}{\partial X_1} \quad (4\text{-}27b)$$

Expressing one coefficient in terms of the other one gives:

$$\frac{\partial^2 B_1}{\partial X_1^2} + \frac{\rho\omega^2}{8}B_1 = 0 \quad (4\text{-}28)$$

The solution to the above equations implies no exponential growth, and thereby no instability. On the other hand, this analysis is only valid, when $\omega\sqrt{\rho}$ is far away from $\frac{\pi}{L}$. To investigate the stability in the vicinity of this value, the frequency is expanded as $\rho\omega^2 + \epsilon\delta$. In this case, Eq. (4-24b) modifies as:

$$\frac{\partial^2 U_1}{\partial X_0^2} + \rho\omega^2 U_1 + 2\frac{\partial^2 U_0}{\partial X_0 X_1} + \cos\left(\frac{\pi X_0}{L}\right)^2 \frac{\partial^2 U_0}{\partial X_0^2} + \delta U_0 = 0 \tag{4-29}$$

Then the secular term, counterpart of Eq. (4-28) becomes:

$$\frac{\partial^2 C_1}{\partial X_1^2} + \frac{\left(2\delta L^2 - \pi^2\right)^2}{16L^2\pi^2} C_1 = 0 \tag{4-30}$$

Based on this equation, a pointwise instability takes place at $\delta = \pi^2/2L^2$, where a stopband of zero width is generated. Thus, over the entire frequency domain, no broadband instability is created due to the introduction of nonlinearity in the system.

### 4.2.3. Fredholm's integral and entangled wavenumbers

To investigate of the intrinsic dynamic features of the system, it is necessary to realize the corresponding dispersion behaviour. To start with, as mentioned earlier, a rectangular window $H(x)$ is considered:

$$H(x) = \begin{cases} 1, & |x| \le D \\ 0, & |x| > D \end{cases} \tag{4-31}$$

with $D$ being the real positive quantity determining the length of the window. In the light of (31), the linearized governing equation motion is of the form

$$\rho\frac{\partial^2 u(x,t)}{\partial t^2} - E_0\left(1 + \frac{9}{2}\left(\frac{\partial\phi}{\partial x}\right)^2 \hat{\sigma}_q^2\right)\frac{\partial^2 u(x,t)}{\partial x^2} + 2D\kappa\, u - \kappa\, H * u = F(x,t) \tag{4-32}$$

with $*$ denoting the convolution operation. Assuming $\Phi(x) = \left(\frac{\partial\phi}{\partial x}\right)^2$, performing the spatiotemporal Fourier transform on the homogeneous form of Eq. (4-32) gives:

$$\rho\omega^2\hat{\hat{u}} - E_0 k^2\hat{\hat{u}} - \frac{9}{2}E_0\hat{\sigma}_q^2\Phi(x) * k^2\hat{\hat{u}} - 2\kappa D(1 - \operatorname{sinc} kD)\hat{\hat{u}} = 0 \tag{4-33}$$

Employing the definition of the convolution integral, Eq. (4-33) takes the form

$$[\rho\omega^2 - E_0 k^2 - 2\kappa D(1 - sinc\, kD)]\hat{\hat{u}} = \frac{9}{2}E\int_{-\infty}^{\infty}\hat{\sigma}_q^2\Phi\left(k - \bar{k}\right)\bar{k}^2\hat{\hat{u}}\left(\bar{k}\right)d\bar{k} \tag{4-34}$$

This evidently represents an inhomogeneous Fredholm's integral equation. Expressing Eq. (4-34) in discrete domain, one obtains:

$$\underline{\underline{A}}\,\underline{\hat{\hat{u}}} = 0 \tag{4-35}$$

with

$$\left[\underline{\underline{A}}\right]_{m\times n} = \frac{9}{2}\hat{\sigma}_q^2\Phi(k_m - k_n)k_n^2\Delta k - \left(\rho\omega^2 - E_0 k_m^2 - 2\,\kappa\, D(1 - \operatorname{sinc} k_m D)\right)\delta_{mn}$$

$$\left[\underline{\hat{u}}\right]_{n\times 1} = \left[\hat{u}(k_1), \hat{u}(k_2), \dots, \hat{u}(k_n)\right]^T \tag{4-36}$$

The discretized form can be regarded as a homogenous matrix equation. Provided that the system has a singular matrix, where the determinant of $\underline{A}$ vanishes, a solution is found. The above relation refers to an intricate underlying state giving birth to entanglement of wavenumbers, which is not the typical of conventional linear systems, implying that the exciting a frequency range is not necessarily correlated with the excitation of a particular spatial frequency band. This, presence of nonlinearity causes deep changes in propagation characteristics of the system. In fact, not a unique wavenumber can be associated to a specific $\omega$ and numerous combinations of discrete wavenumber $k_i$ $(i = 1, 2, \dots, N)$ with $N$ tending to infinity, are available to produce that frequency.

### 4.2.4. Approximate dispersion analysis

To have a rough idea of the dispersion behaviour of the system, Eq. (4-32) is rewritten as:

$$\rho \frac{\partial^2 u(x,t)}{\partial t^2} - \tilde{E}\left(x, \hat{\sigma}_q^2\right) \frac{\partial^2 u(x,t)}{\partial x^2} + 2D\kappa\, u - \kappa\, H * u = F(x,t) \tag{4-37}$$

Here, the term $\tilde{E}(x, \hat{\sigma}_q^2)$ is the equivalent stiffness, which is a spatially varying parameter modulated by the intensity of the noise. For a clamped long-range rod, the variation of this parameter along the axis, in its generic form, is shown in Fig. 4. 1. To eliminate the problem of treating a parametric equation, $\tilde{E}(x, \hat{\sigma}_q^2)$ is expressed in terms of an average value $\bar{E}$. This provides the opportunity to achieve a rough understanding the status of the plane waves within the medium.

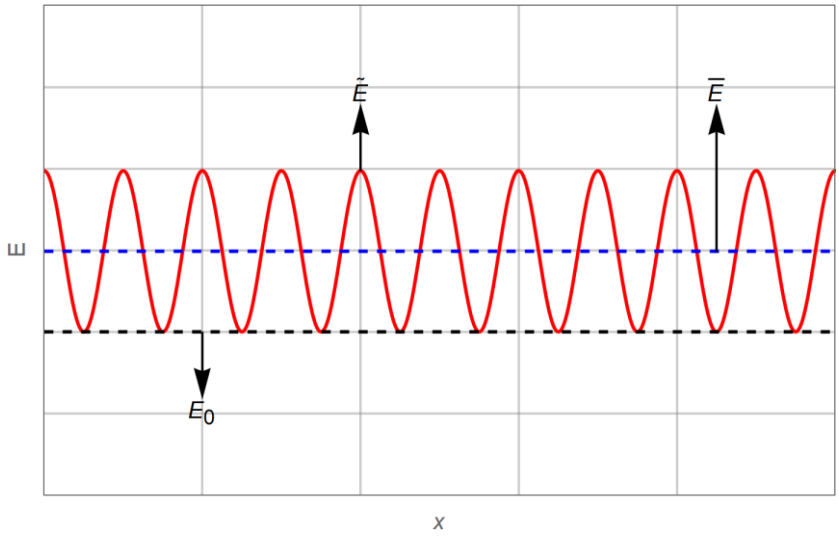


Fig. 4. 1: Variation of the equivalent stiffness along the axis

The dispersion relation corresponding to the homogenised problem, in the nondimensional form, is:

$$\Omega^2 = K^2 + 2\chi(1 - sincK) \tag{4-38}$$

with the following nondimensional parameters

$$\chi = \kappa D^3/\bar{E} \tag{4-39a}$$

$$\Omega = \omega D\sqrt{\rho/\bar{E}} \tag{4-39b}$$

$$K = kD \tag{4-39c}$$

To realize the implication of this mathematical scheme, an exaggerated hypothetical example is made, where the level of noise massively modulates the value of $\bar{E}$, leading to considerable change in the value of $\chi$. Fig. 4. 2 reports the variation of group velocity $C_g = d\Omega/dK$ for different values of the nondimensional parameter $\chi$, when all geometrical and physical parameters of the systems are fixed but the intensity of noise. The figure explains the emergence of zero/negative group velocity in systems with $\chi$ exceeding a critical value (more information about the similar system is given in chapter 3). Furthermore, the system moves away from disclosing unconventional behaviour as the level of noise increases. Indeed, higher level of noise is accompanied by higher average stiffness $\bar{E}$ and decrease in the value of $\chi$, and consequently farther from the irregular propagation regimes.

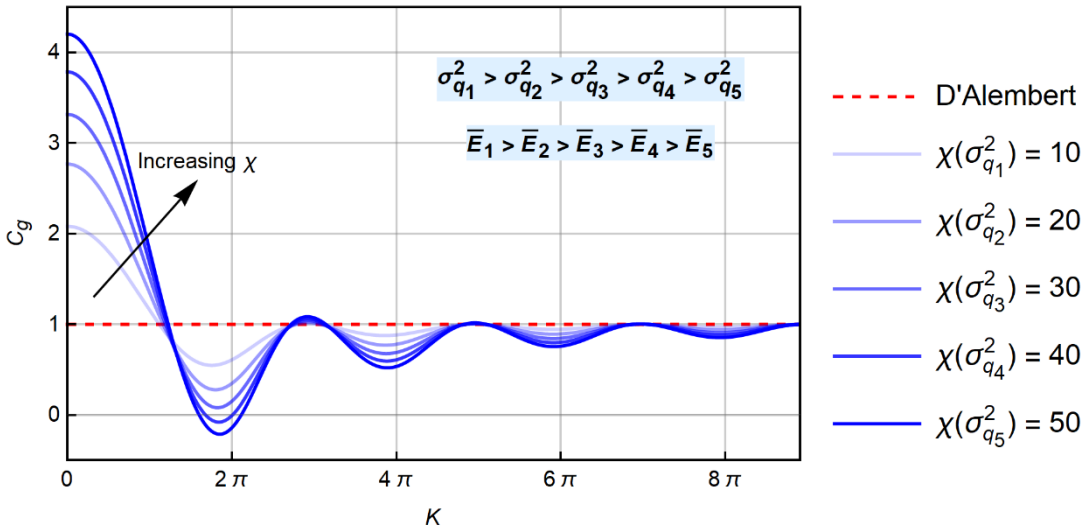


Fig. 4. 2: Nondimensional dispersion relation

The result presented are not sufficient to fully characterize the wave propagation behaviour within the system since nonlinearities give rise to a parametric integral-differential equation, taking away the opportunity to obtain an explicit dispersion relation. However, the approximate solution given above, at the minimum, provides a dim understanding regarding the status of travelling waves.

## 4.3. Nonlinear long-range connectors

As shown previously, nonlinearity makes additional influences including the coupling of the wavenumbers; however, the scenario might be hugely impacted in case of nonlinear

interaction. To give a general idea of this case, nonlinear spring-like connections are considered, wherefore the spring force satisfies:

$$F_{LR} = \kappa \sum_i \vartheta_i [u(x,t)]^i \quad \& \quad \vartheta_1 = 1 \tag{4-40}$$

where $\vartheta_i$ is the corresponding nonlinearity parameter. Assuming first and second order terms, the governing equation for a long-range waveguide with rectangular interaction region is found as:

$$\rho \frac{\partial^2 u(x,t)}{\partial t^2} - E \frac{\partial^2 u(x,t)}{\partial x^2} - \kappa\{2Lu - u * H(x) + 2L\vartheta_2 u^2 + \vartheta_2 u^2 * H(x) - 2L\vartheta_2 u[u * H(x)]\} = 0 \tag{4-41}$$

To gain an insight in behaviour of the system in terms of waves, Fourier transform both in time and space has been applied, and one can arrive at:

$$\rho\omega^2 \hat{u}(k,\omega) - Ek^2 \hat{u}(k,\omega) + \kappa\{2a\hat{u}(k,\omega) - \hat{\hat{H}}(k)\hat{u}(k,\omega) + 2a\vartheta_2[\hat{u}(k,\omega) ** \hat{u}(k,\omega)] + \vartheta_2 \hat{\hat{H}}(k)[\hat{u}(k,\omega) ** \hat{u}(k,\omega)] - 2a\vartheta_2 \hat{u}(k,\omega) ** \left[\hat{\hat{H}}(k)\hat{u}(k,\omega)\right]\} = 0 \tag{4-42}$$

Assuming the solution in terms of normal functions $\phi_r$ as:

$$u(x,t) = \sum_r \phi_r(x)\, q_r(t) \tag{4-43}$$

with

$$\hat{u}(k,\omega) = \sum_r \hat{\phi}_r(k)\, \hat{q}_r(\omega) \tag{4-44}$$

and employing the similar approach as of the one in subsection 4.2.3., the dispersion relation, for a given $r = R$, may be expressed as follow

$$T_{ijmn} \underline{\hat{\phi}}_{R_{m\times 1}} \underline{\hat{q}}_{R_{1\times n}} = 0 \tag{4-45}$$

with

$$T_{ijmn} = \left[\rho\omega_n^2 - Ek_m^2 + \kappa 2a - \kappa\hat{\hat{H}}(k_m)\right]\delta_{im}\delta_{jn} + \kappa\left\{2a\vartheta_2\left[\hat{\phi}_R(k_i - k_m)\hat{\phi}_R(k_m)\Delta k\right]\left[\hat{q}_R(\omega_j - \omega_n)\hat{q}_R(\omega_n)\Delta\omega\right] + \vartheta_2\hat{\hat{H}}(k_i)\left[\hat{\phi}_R(k_i - k_m)\hat{\phi}_R(k_m)\Delta k\right]\left[\hat{q}_R(\omega_j - \omega_n)\hat{q}_R(\omega_n)\Delta\omega\right] - 2a\vartheta_2\left[\hat{\phi}_R(k_i - k_m)\hat{\phi}_R(k_m)\hat{\hat{H}}(k_m)\Delta k\right]\left[\hat{\hat{H}}(k_m)\hat{q}_R(\omega_j - \omega_n)\hat{q}_R(\omega_n)\Delta\omega\right]\right\} = 0 \tag{4-46a}$$

$$\left[\underline{\hat{\phi}}_R\right]_{m\times 1} = \left[\hat{\phi}_R(k_1), \dots, \hat{\phi}_R(k_m)\right]^T \tag{4-46b}$$

$$\left[\underline{\hat{q}}_R\right]_{1\times n} = \left[\hat{q}_R(\omega_1), \dots, \hat{q}_R(\omega_n)\right] \tag{4-46c}$$

As seen, $T_{ijmn}$ is a multidimensional array with four dimensions. To characterize the behaviour of such a system, we utilize the notion of hyperdeterminant which is practical for multidimensional arrays. Hyperdeterminant $Det(T)$ is a polynomial and describes the underlying field of the multi-dimensional vector spaces. One concludes each temporal and spatial frequency is entangled intricately with other counterparts within the introduced

discretized domain. Clearly, this complexity is originated from the introduction of nonlinearity to the forcing integral term, and it sets conditions which were not present before.

## 4.4. Final remarks

Nonlinearities usually trigger a new spectrum of phenomena to systems due to the higher level of complexity they introduce to the dynamics. This chapter is devoted to understanding the effects induced by nonlinearities in long-range systems, majorly in an implicit way. Unlike the spring-like links, the host structure (waveguide) is assumed to capture the nonlinear characteristics, and dynamics is linearized to facilitate the study by statistical linearization approach. This made possible by considering the imposition of a random excitation on the system responsible for making the effect of nonlinearities apparent. Homogenisation of the linearized dynamics suggests the occurrence postponement of the unusual effects discussed in the last chapter including the wave-stopping and negative group velocity. Independently, another case is concisely studied, highlighting how the integration of nonlinear long-range connectors to a conventional linear waveguide results in entanglement of frequencies and wavenumber, analogous to the coupling of wavenumbers in the previous case.

# Chapter 5: Long-range non-homogeneous periodic configurations: tree-periodicity

## 5.1. Introduction

Several studies have revealed that periodic structures bring eccentric characteristics to the band structure of systems, dissimilar to that of conventional domains. This could stem from simple mechanical components such as mass-spring units, attached to a host structure, absorbing the travelling energy at their resonance frequencies, and consequently prohibiting the energy to propagate within certain frequency ranges. On the other hand, Bragg's scattering is another mechanism, which enables the generation of such frequency bandwidth. In fact, due to the impedance mismatch among the constructing elements of the periodic array, the wavefronts try to adjust their speed while entering the neighbouring element with different acoustic properties, and the status of success in this attempt determines the band structure.

This chapter is devoted to developing periodic structures by means of long-range connectors, i.e., nonlocalities. Although the utilized nonlocalities are simple spring-like springs, their unique distribution provide the chance to get periodic configurations. As a matter of fact, rather than the cases studied in chapters three and four, the adopted connectivity template here does not involve all particles inside the domain. In this fashion, the structure accommodates in the category of long-range non-homogenous periodic configurations according to the concept of graph-periodicity introduced in chapter 2. Here, long-range connectors serve as essential components for creating a genuine periodic arrangement as opposed to the classical metamaterials, where the specific sequence of impedance mismatched elements is responsible for the task.

A comprehensive analysis is conducted on a periodic waveguide when the periodicity is induced by the long-range connectors. Floquet method is utilized to identify the band structure of the system, and the underlying mechanism in charge of generating the stopbands is realized by comparing the energy transmission across the new channel, i.e., the nonlocalities and the conventional path being the waveguide. Then this idea is implemented on a conventional elastic compound rod and the joint effects induced by impedance mismatch and nonlocalities is studied. Eventually, the possibility of blocking travelling waves by these extensional connections is demonstrated for an axisymmetric cylindrical shell, where the coupled flexural and longitudinal modes contribute in transporting the energy.

## 5.2. Waveguide with periodic nonlocalities

This section is concerned with the performance of a periodic waveguide, where the periodicity is promoted by long-range connectors. First, a simple model of propagation of plane waves

travelling across the domain is realized with the help of Floquet theorem. Then, other analyses are performed on the harmonically excited semi-infinite counterpart of the system to understand other characteristics of the system including the working mechanism responsible for forming the associated band structure.

### 5.2.1. Band structure identification

The simplest way to gain insights into the behaviour of systems with periodic nonlocalities (PN) is described in this section. The stopband structure of a conventional rod embedded with external links, forming a periodic structure, as shown in Fig. 5. 1, is investigated. A unit cell of the periodic structure is composed of two identical bar segments as well as of two springs. In the graph-periodicity classification, this can be seen as a tree-periodic structure of period $L$ and leaf-periodic with same period, with only two leaves each tree ($N = 2$).

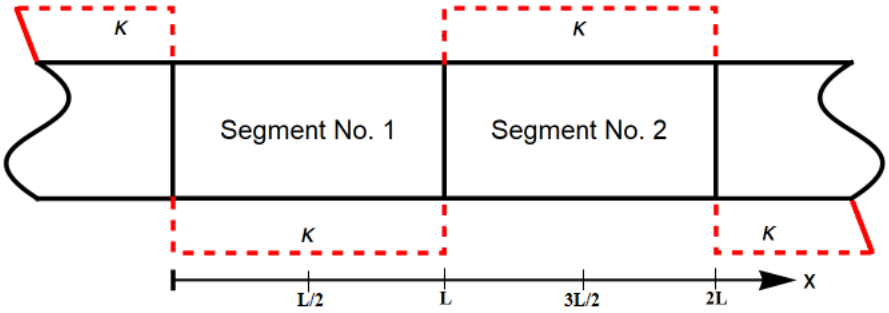


Fig. 5. 1: A unit cell of a uniform rod with nonlocalities

As already mentioned, the functionality of the spring elements in this structure differs from the classical periodic configurations, where springs are assembled in various configurations with discrete masses to compose a waveguide [113,114,121–124] or resonators attached to a unit-cell [27–29]. Note that the structure shown in Fig. 5. 1 is non-homogenous, which is true for all the configurations taken into account throughout the current chapter.

The unit cell of the periodic array shown in Fig. 5. 1 features instantaneous transmission of force across itself, in parallel with conventional elastic wave propagation. The periodic nature of the system entails the presence of periodic coefficients in the corresponding governing equation of motion. Since the domain of interest is periodic, Floquet theorem provides a framework for finding the solution by considering a bounded portion of the system, i.e., the unit cell. To perform the Floquet analysis, obtaining the equation of motion and the matching conditions are required, and, for that purpose, the variational principle is adopted.

To apply Hamilton's principle $\delta H = 0$, the action integral should be formulated as:

$$H = \int_{t_1}^{t_2} (T - U)\, dt \qquad (5\text{-}1)$$

The total elastic energy $U$ stored in the deformable body (see Fig. 5. 1) and the kinetic energy $T$ are given by:

$$U = \frac{1}{2}\left[\int_0^L EA\left(\frac{\partial u_1}{\partial x}\right)^2 dx + \int_L^{2L} EA\left(\frac{\partial u_2}{\partial x}\right)^2 dx\right] + \frac{1}{2}\kappa[(u_1(L,t) - u_1(0,t))^2 + (u_2(2L,t) - u_2(L,t))^2] \quad (5\text{-}2a)$$

$$T = \frac{1}{2}\left[\int_0^L \rho A\left(\frac{\partial u_1}{\partial t}\right)^2 dx + \int_L^{2L} \rho A\left(\frac{\partial u_2}{\partial t}\right)^2 dx\right] \quad (5\text{-}2b)$$

Here, $E$, $\rho$, $A$ and $L$ are the Young's modulus, the mass density, the cross-section and the length corresponding to the segments, in the order given; and distant points on the rod interact nonlocally via springs with the stiffness $\kappa$.

The governing equation of motion for longitudinal waves for each segment, based on the Hamilton's principle, is:

$$\frac{\partial^2 u_i(x,t)}{\partial t^2} = \frac{1}{c^2}\frac{\partial^2 u_i(x,t)}{\partial x^2} \quad , \quad i = 1,2 \quad (5\text{-}3)$$

Here, $c^2 = E/\rho$ is the speed of the sound. The Hamilton's principle yields the matching conditions, extracted using stationary conditions for the action integral (5-1), as:

$$u_1\rfloor_L - u_2\rfloor_L = 0 \quad (5\text{-}4a)$$

$$EA\frac{\partial u_1}{\partial x}\Big|_L - EA\frac{\partial u_2}{\partial x}\Big|_L + \kappa[u_1(L,t) - u_1(0,t)] + k[u_2(L,t) - u_2(2L,t)] = 0 \quad (5\text{-}4b)$$

Eventually, the Floquet-Bloch periodicity conditions are

$$u_1\rfloor_{L/2} - \Lambda\, u_2\rfloor_{3L/2} = 0 \quad (5\text{-}5a)$$

$$\frac{\partial u_1}{\partial x}\Big|_{L/2} - \Lambda\,\frac{\partial u_2}{\partial x}\Big|_{3L/2} = 0 \quad (5\text{-}5b)$$

where $\Lambda$ is a nondimensional parameter function of the Bloch parameter $K_B$ [125]. Indeed, $\Lambda = e^{iK_B}$ is a conventional notation for periodic structures, which enables a more straightforward discussion of the results than by interpreting them in terms of $K_B$. It will be discussed how for $|\Lambda| = 1$, a full wave transmission is observed. Instead, for any value such that $|\Lambda| \neq 1$, stopbands occur in the dynamic response of the structure. One may note that the Floquet-Bloch periodicity conditions are chosen at the mid-span of the segments. It stems from the choice of symmetric periodicity cell. In order to reduce the number of involved parameters in this problem, the system of equations (4) and (5) is written in the nondimensional format as:

$$\hat{u}_1\rfloor_1 - \hat{u}_2\rfloor_1 = 0 \quad (5\text{-}6a)$$

$$\frac{\partial \hat{u}_1}{\partial X}\Big|_1 - \frac{\partial \hat{u}_2}{\partial X}\Big|_1 + \widehat{K}[\hat{u}_1(1,t) - \hat{u}_1(0,t)] + \widehat{K}[\hat{u}_2(1,t) - \hat{u}_2(2,t)] = 0 \quad (5\text{-}6b)$$

$$\hat{u}_1\rfloor_{1/2} - \Lambda\,\hat{u}_2\rfloor_{3/2} = 0 \quad (5\text{-}6c)$$

$$\frac{\partial \hat{u}_1}{\partial X}\Big|_{1/2} - \Lambda\,\frac{\partial \hat{u}_2}{\partial X}\Big|_{3/2} = 0 \quad (5\text{-}6d)$$

where $X = x/L$ and $\hat{u}_i = u_i/L$ $(i = 1, 2)$ and the nondimensional stiffness is $\hat{K} = \kappa L/EA$. For each segment of the periodic rod, the displacement field $\hat{u}_j(X, t)$, the general solution of Eq. (5-3), has the canonical form:

$$\hat{u}_j(X, t) = \varphi_j e^{i\omega X - i\omega t} + \psi_j e^{-i\omega X - i\omega t} \tag{5-7}$$

Here, $\omega = \Omega L/c$. Substituting the above equation in the system of Eqs. (6) yields a system of four linear homogeneous algebraic equations function of the amplitudes of the right- and left-going waves in each segment and independent with respect to time. The nontrivial solution of the above system of equations is

$$\Lambda^2 + q(\omega)\Lambda + 1 = 0 \tag{5-8}$$

with

$$q(\omega) = \frac{-2\,[\omega\cos(\omega) + \hat{K}\,\sin(\omega)]}{\omega + \hat{K}\sin(\omega)} \tag{5-9}$$

The discriminant function ($DF$) of the quadratic equation (8) is given by:

$$DF = -\frac{4\,\omega\sin(\omega)(2\hat{K}(1-\cos(\omega)) + \omega\sin(\omega))}{(\omega + \hat{K}\sin(\omega))^2} \tag{5-10}$$

If this function is positive, the roots of equation (5-8) are real-valued and the frequency $\omega$ falls into a stopband. If this function is negative, roots are complex conjugate and the frequency $\omega$ belongs to a pass band. This discriminant, function of nondimensional stiffness and frequency, is depicted in Fig. 5. 2 with marked stopband borders. The areas shown in red are those associated with stopbands and the light brown domain corresponds to the pass bands. The borders between these two regions are defined by the condition $\mathrm{DF} = 0$. To meet the preceding condition, three different solutions for Eq. (5-10) are available and clearly, the trivial solution, shown in yellow, is not of interest. The second set of solutions requires $sin(\omega)$ to be zero, yielding $\omega = n\pi$, with $n$ being a natural number, which are distinctly shown in the figure with black solid lines. Eventually, the blue curves are associated with the third solution $\hat{K} = -\omega\cot(\omega/2)/2$.

The analysis of the eigenfrequencies of a unit periodicity cell shown in Fig. 5. 1 with free ends yields eigenfrequencies defined by the third solution and by the condition $\cos(\omega) = 1$. The second solution $\omega = n\pi$ perfectly matches the eigenfrequencies of the same unit cell with both ends fixed. Obviously, the set of eigenfrequencies $\omega = 2n\pi$ is shared by the unit cells with fixed-fixed and free-free boundary conditions. Therefore, these frequencies define the gaps of the zero width [23].

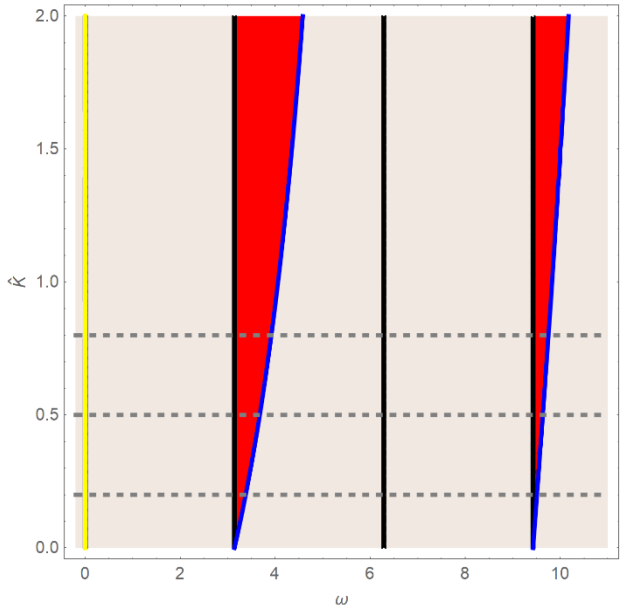


Fig. 5. 2: Stiffness-frequency diagram

The frequency dependence of the roots of the characteristic equation (5-9) is shown in Fig. 5. 3, for three values of the stiffness parameter. Two different regimes are clearly seen: a flat line, i.e., $|\Lambda| = 1$, represents pass band, and the elliptic-like curves, result of distinct real roots of the characteristic equation, represent stopbands. The frequency, at which the stopband emerges, remains unchanged for different values of $\hat{K}$, as reported earlier by Fig. 5. 2. Finally, as shown, stiffer external links promotes wider gaps. It is worthwhile to note that the width and the location of the stopbands perfectly match the data already presented in Fig. 5. 2.

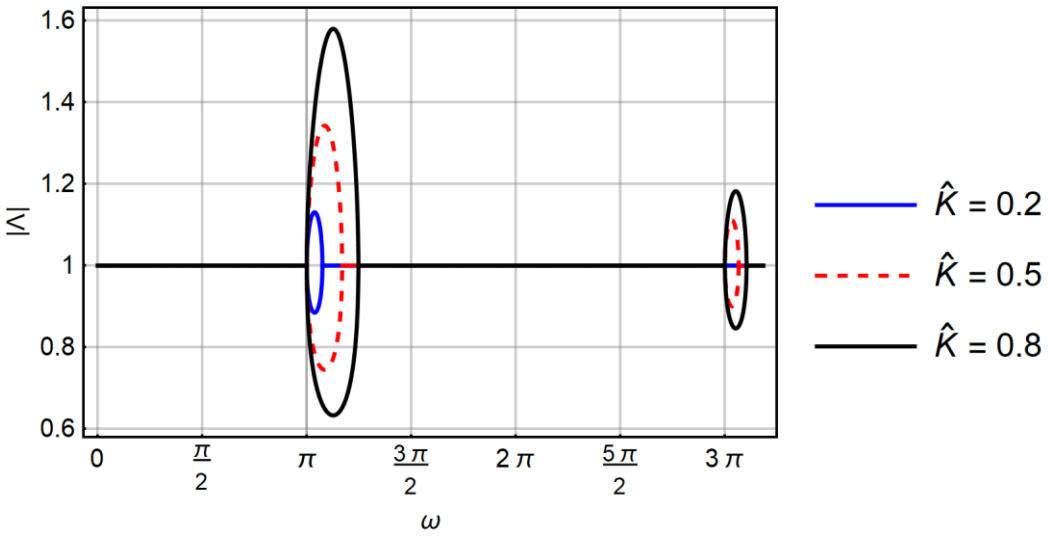


Fig. 5. 3: Band structure for uniform waveguide with nonlocalities

Inspection of Eq. (5-10) suggests $DF$ becomes singular when its denominator vanishes, producing:

$$\hat{K} = -\frac{\omega}{\sin(\omega)} \tag{5-11}$$

This implies that one root of Eq. (5-8) diverges and the other tends to zero. This indicates the birth of stopbands with infinitely large attenuation, a desirable effect for vibro-isolation purposes. Note that this effect is characteristic of the periodic nonlocality since it specifically depends on $\widehat{K}$. In the absence of external springs, the denominator of $DF$ simply collapses into $\omega$, and no similar effect emerges.

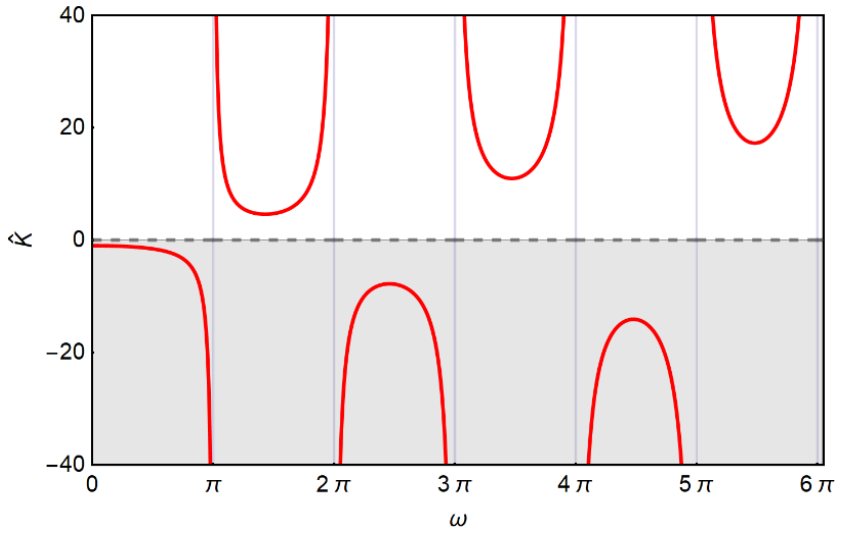


Fig. 5. 4: Critical stiffness as a function of frequency

Fig. 5. 4 shows the plot of $\widehat{K}$ yielded by Eq. (5-11), provided over a wide range of $\widehat{K}$. Note that the case of negative stiffness will be addressed in the next section. The infinite attenuation effect appears within regularly separated bandwidths. At lower frequencies, this 'complete', or 'ideal' attenuation may be obtained by deploying springs of relatively small stiffness, while this effect is more difficult to reach when the frequency increases, requiring higher spring stiffness. The minimum stiffness, which delivers infinite attenuation, is easily found by equating the first derivative of denominator of Eq. (5-11) to zero giving $\tan(\omega_0) = \omega_0$. The first root is $\omega_0 = 4.721$ with the corresponding nondimensional stiffness $\widehat{K} = 4.721$.

On balance, it is concluded that disruption of the energy transfer may be achieved using the instantaneous long-range forces between a priori selected fixed stations in a waveguide. Unlike the case considered in the previous section, the underlying physical mechanism employed here is the Bragg's destructive interference of waves, the 'trademark' of periodic waveguides.

## 5.2.2. Negative stiffness and low frequency stopbands

The desirable influence of nonlocalities on the stopbands in terms of broadening and stronger attenuation, especially in the low frequency band, has been demonstrated in the previous section. However, the principal demand to pull the first stopband to the lowest possible frequencies has not been met neither using impedance mismatch nor using the long-range interactions. Hence, here a radical change in the physics of the system is assumed to accomplish this very highly demanding task. So far, the analysis has been limited to the physically meaningful positive values of the stiffness of the springs. Here, the stiffness $\widehat{K}$ in Eq. (5-10) is

allowed to attain negative values: that is, the forces exerted by the external links act in the opposite direction with respect to configuration described in section 3. For $-1.5 \leq \widehat{K} \leq 0.2$, the analysis of the discriminant equation shows the possibility of pulling the stopbands to arbitrary low frequencies given a proper negative value for stiffness (see Fig. 5. 5).

Although the negative values are not compatible with real-life springs, the equivalent force, exerted by the hypothetical springs with negative $\widehat{K}$, can plausibly be generated by devices exhibiting such a behaviour, which are well known and broadly used in vibration control, with a magnet being a simple example. However, another possibility is an active control system, in which piezo elements are used to generate forces proportional to the instant difference in displacements of control points and acting in the requested direction. Note that technicalities of practical implementation of this concept are not dwelled here and in what follows just demonstrate the effect, which can be obtained by these means.

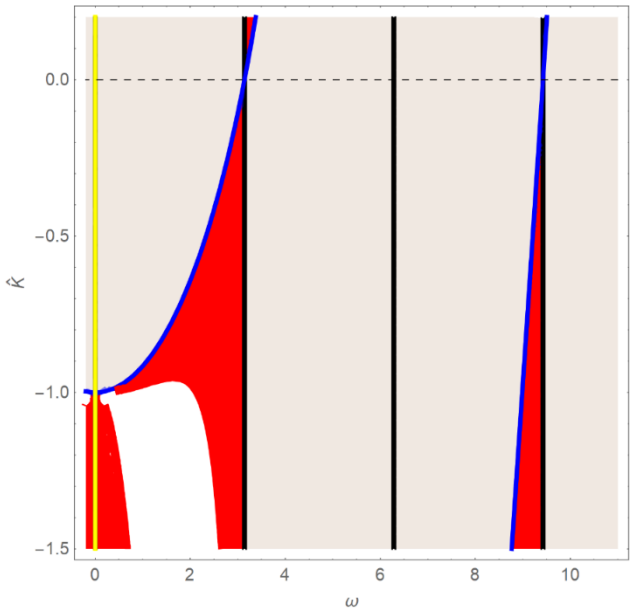


Fig. 5. 5: Stiffness-frequency diagram

### 5.2.3. Virtual experiment by insertion loss analysis

So far, the analysis has been confined to solution of problems in free wave propagation for infinite periodic waveguides with periodic nonlocalities. Further insights into their behaviour come from solutions of the forcing problem. Its standard formulation is associated with calculations of Insertion Losses (IL).

The insertion loss in dB is given by [126]:

$$IL = 10 \log_{10} E_0/E_s \tag{5-12}$$

Here, $E_0$ is the energy flux (EF) in a semi-infinite uniform D'Alembert waveguide (i.e., with the springs removed) and $E_s$ denotes the EF in the same semi-infinite waveguide equipped with

an insert (i.e., with the non-local connectors) in the same excitation conditions, as illustrated in Fig. 5. 6. The EF averaged over a period of motion for a dilatation time-harmonic wave in a one-dimensional waveguide is [127]:

$$E(x) = -\frac{1}{2} Re[N_x(x)\underline{V}(x)] \tag{5-13}$$

where $N_x(x)$ and $\underline{V}(x)$ are the axial force and the conjugate of the axial velocity, respectively.

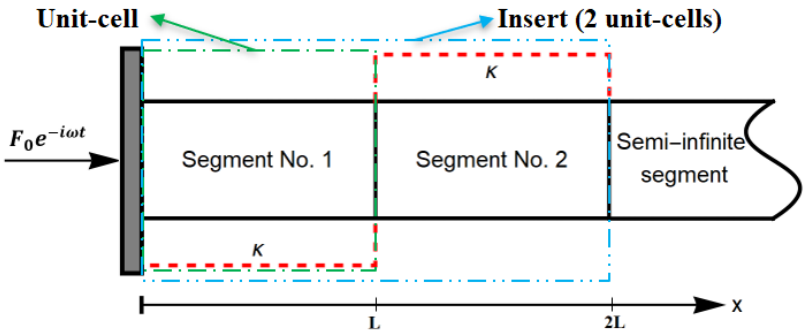


Fig. 5. 6: Semi-infinite uniform rod with nonlocalities with two inclusions

Let us first consider a semi-infinite uniform waveguide with two long-range connectors as shown in Fig. 5. 6. Then the semi-infinite segment obeys Sommerfeld radiation condition and supports outgoing travelling wave, while pairs of direct and reflected waves are generated in segments 1 and 2. The amplitudes of these five waves are determined by using the following conditions:

$$\hat{F} - \frac{\partial \hat{u}_1}{\partial X}\rfloor_0 + \hat{K}[\hat{u}_1\rfloor_0 - \hat{u}_1\rfloor_1] = 0 \tag{5-14a}$$

$$\hat{u}_1\rfloor_1 - \hat{u}_2\rfloor_1 = 0 \tag{5-14b}$$

$$\frac{\partial \hat{u}_1}{\partial X}\rfloor_1 - \frac{\partial \hat{u}_2}{\partial X}\rfloor_1 + \hat{K}[\hat{u}_1\rfloor_1 - \hat{u}_1\rfloor_0] + \hat{K}[\hat{u}_2\rfloor_1 - \hat{u}_2\rfloor_2] = 0 \tag{5-14c}$$

$$\hat{u}_2\rfloor_2 - \hat{u}_3\rfloor_2 = 0 \tag{5-14d}$$

$$\frac{\partial \hat{u}_2}{\partial X}\rfloor_2 - \frac{\partial \hat{u}_3}{\partial X}\rfloor_2 + \hat{K}[\hat{u}_2\rfloor_2 - \hat{u}_2\rfloor_1] = 0 \tag{5-14e}$$

Here, $\hat{F} = F/EA$. Solving the above system fully characterizes the wave motion in the system. As already shown by various studies [22,23], insertion loss $IL$ at the frequencies inside the stopbands is significantly higher with respect to those within pass bands. In fact, insertion loss is a mean to distinguish passbands from the stopbands, and its increase corresponds to the magnitude of $\Lambda$ within stopbands.

Fig. 5. 7 compares the insertion loss for three different cases, i.e. two, three and four unit-cells. Based on the figure, the peaks are located around stopbands already predicted by the Floquet analysis. Indeed, the loss at stopband frequencies is notably large, which virtually verifies the performance of the infinite structure presented beforehand (see Fig. 5. 3). Furthermore, it is apparent how the higher the number of unit-cells, the larger the amplitude of peaks around the

stopband frequencies. It is worth mentioning that for a limited number of unit-cells, the bandwidth of the peaks does not precisely determine the bandwidth of the associated stopbands. Eventually, the plot suggests the existence of points at which the insertion loss becomes null for all the curves. These points have been defined as shared points. Furthermore, each curve presents other points of null insertion loss, but those are strictly related to the number of the unit-cells in the insert. The discussion that follows is devoted to the physical interpretation of all these points of zero insertion loss.

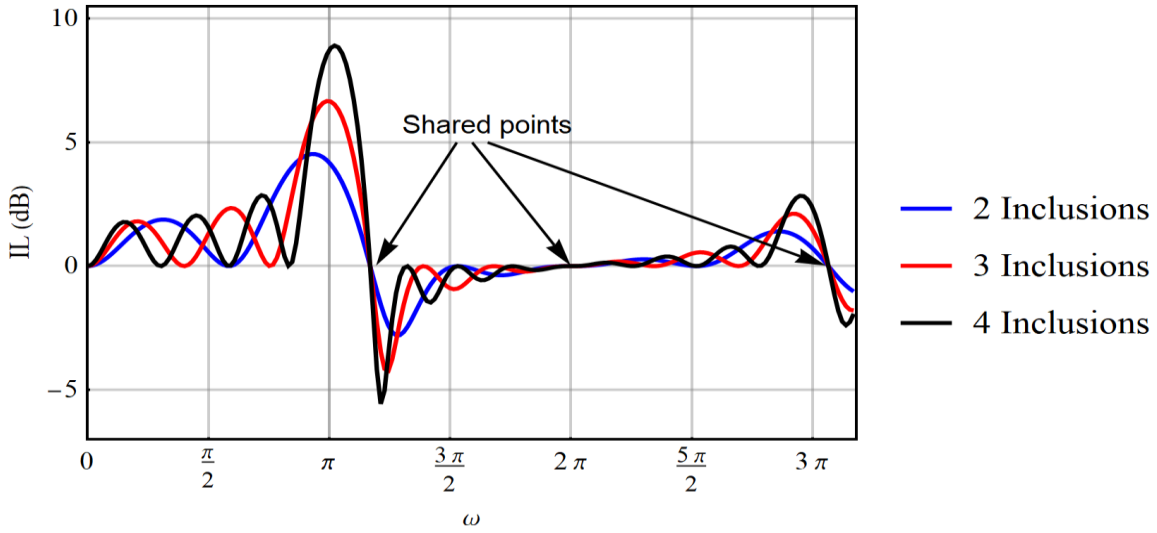


Fig. 5. 7: Insertion loss for a semi-infinite uniform waveguide with nonlocalities ($\widehat{K} = 0.5$)

In the above figure, regardless of the number of unit-cells in the insert, there are shared points at which the insert is fully transparent, i.e., $IL = 0$. In Ref. [24], it is shown how the eigenfrequencies associated to the free-free unit-cell of a periodic structure are related to borders of stopbands. The eigenfrequency equations of the associated stopband are $\cos(\omega) = 1$ and $\widehat{K} + \omega \cot(\omega/2)/2 = 0$. Since the shared points occur exactly at these eigenfrequencies, it is clear how there is a one-to-one correspondence between shared points and borders of these stopbands. In addition to the shared points, there are other points on each curve, where $IL = 0$. These zeros correspond to eigenfrequencies of the corresponding insert with both ends free.

To further explain the correspondence between shared points and stopbands, Fig. 5. 8 reports the single case of three unit-cells. Fig. 5. 8 presents the case of a semi-infinite structure with an insert composed of three unit-cells to highlight the above comments. The global behaviour is partially determined by the collective characteristics of the insert, and by the intrinsic properties of the single unit-cell (see Fig. 5. 6). Indeed, the figure shows, more than the trend of the insertion loss $IL$ (red solid curve), the eigenfrequencies of the insert, green dashed curves, and the eigenfrequencies of the unit-cell, magenta dot-dashed curves, all with respect to the nondimensional frequency. The behaviour of the insert is expressed by two separate equations, namely $\widehat{K} + 2\omega \cot(\omega) - \omega/\sin(\omega) = 0$ and $\widehat{K} + 2\omega \cot(\omega)/3 + \omega/3 \sin(\omega) = 0$: the green curves and; since the insert changes according to the number of unit-cells, it carries the

information regarding the zeros related to the specific structure. These zeros belong to the pass band frequencies, since they fall outside the major peaks, as shown in Fig. 5. 7. It is worth mentioning that the zeros corresponding to the magenta curve are the shared points, identical to those exhibited in Fig. 5. 7, due to the presence of the unit-cell in each insert.

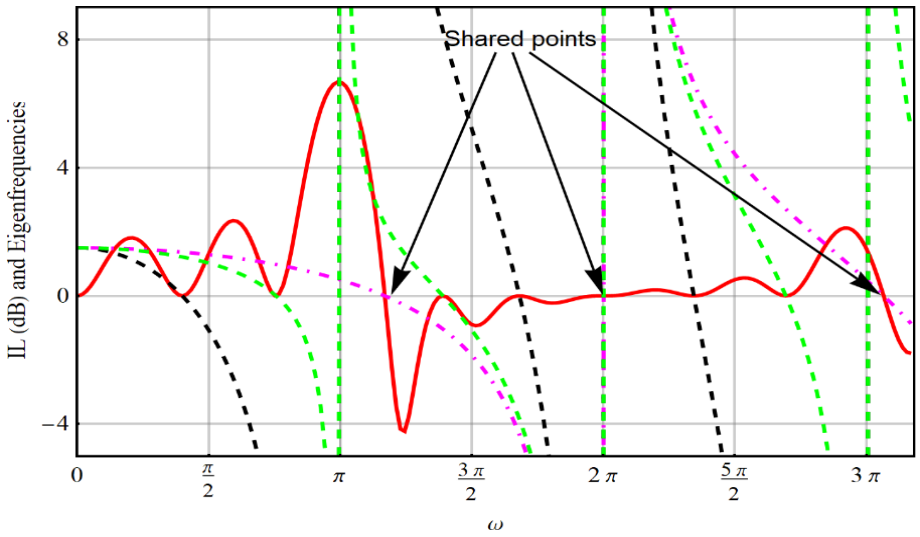


Fig. 5. 8: Insertion loss and related eigenfrequency curves for a three-component semi-infinite rod: Red curve: insertion losses ($\widehat{K} = 0.5$), Magenta lines: Eigenfrequency equation of the free-free unit cell, Green curves: Eigenfrequency equations associated with the free-free insert

It is worth to notice how a same system with spring elements, characterized by negative effective stiffness, the stopbands are pushed leftwards. For a fixed value of stiffness, Fig. 5. 9 highlights strong attenuation in the low frequency band, an attractive occurrence, which is in close agreement with what already demonstrated in Fig. 5. 5. Besides, the amplification of peaks is observed at low frequency range as the number of unit-cells in the insert increases, akin to cases displayed in Fig. 5. 7.

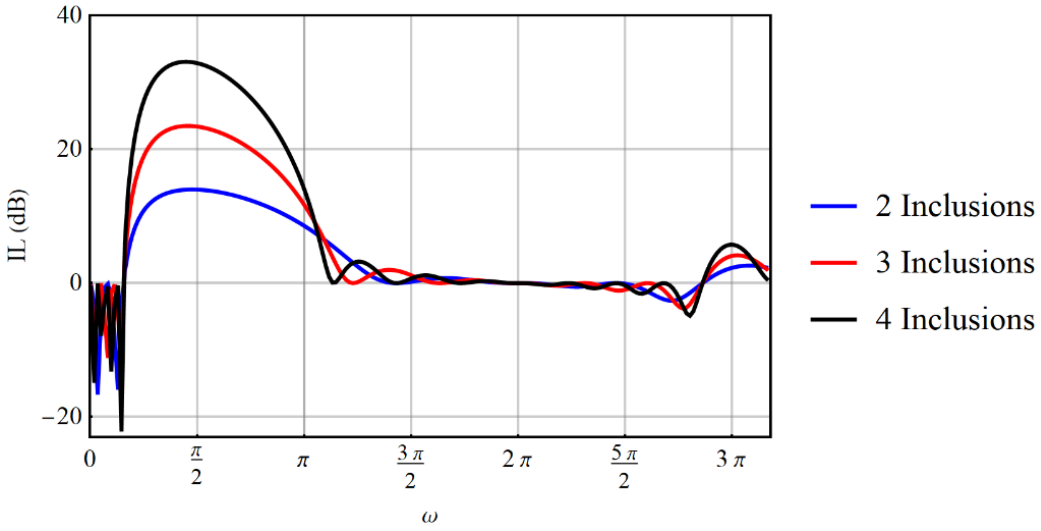


Fig. 5. 9: Insertion loss for a uniform rod with nonlocalities ($\widehat{K} = -0.98$)

Fig. 5. 10 shows the variation of the insertion loss for a selected number of unit-cells and for different negative values of $\hat{K}$. It is evident how the more the stiffness turns into critical, the more the stopband is moved leftwards, in compliance with Fig. 5. 5. Again, the significant amplification of peaks is apparent in the low frequency band by an increase in $\hat{K}$.

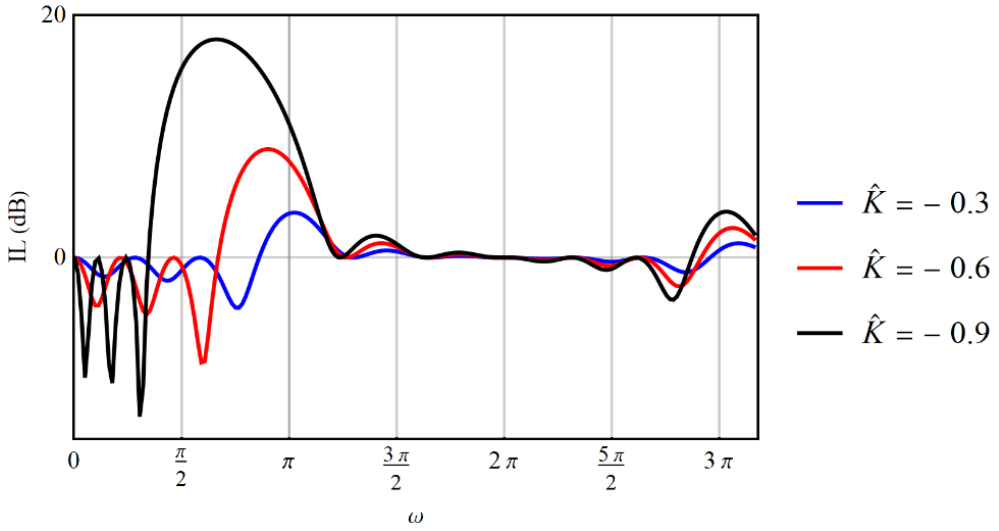


Fig. 5. 10: Effect of stiffness on insertion loss for a uniform rod with nonlocalities (three inclusions)

## 5.2.4. Working mechanism and energy flow partition

As pointed out in the previous subsection the distinctive feature of a periodic waveguide with periodic nonlocalities is the co-existence of the energy transport in its conventional 'continuous' path and the instantaneous energy transfer by non-inertial long-range connectors. This intriguing issue is addressed in this section. As seen from equation (5-14a), the driving force $\hat{F}$ at $x = 0$ is balanced by two components: a force in the segment 1 and a nonlocal force in the spring. This is illustrated in Fig. 5. 6 and now in Fig. 5. 11 as a textbook setup 'springs in parallel'. However, since we consider an open system with the energy leakage to the far field, the division of the external force to two components entails similar energy partition, as sketched in Fig. 5. 11.

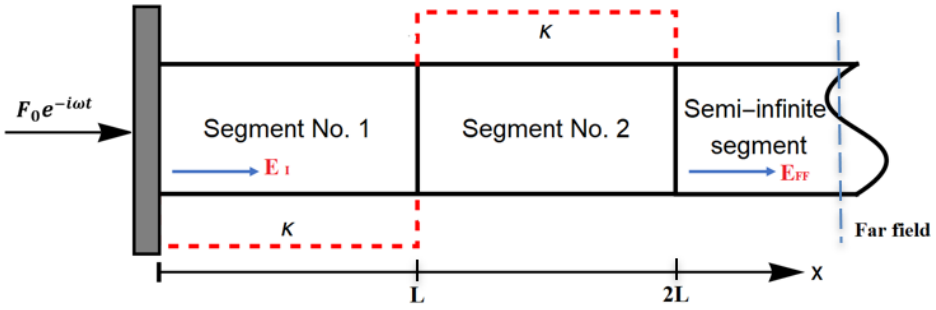


Fig. 5. 11: Semi-infinite uniform rod with nonlocalities with two inclusions

The force acquired by the segment 1 at $x = 0$ generates the conventional energy transmission across the segments by a travelling wave at the finite speed $c$ in the amount $E_I$, see Fig. 15. Since the material losses are excluded, this energy is conveyed in full to the end of insert. This is the action of a primary source, well known in acoustics. The non-inertial springs transmit their part of a driving force instantaneously to the right end of the first cell, so do all the other springs till the end of last cell. Then the instantaneous "spring-borne" force acts at the right end of the insert as a secondary source. Naturally, the interaction between these sources may be either constructive or destructive. Such a secondary source cannot exist in the conventional periodic compound rods, and it induces appreciable changes in the energy flux. Indeed, while in conventional periodic structures with no material losses energy flux does not depend upon the distance $x$, here it experiences a jump at the interface between the insert and the semi-infinite segment (see Fig. 5. 11). In Ref. [122], the similar effect is called 'tunnelling power flow'., which is also customarily understood in a different sense [128]. To assess the interaction between the primary and the secondary source, the energy flux $E_I$ injected into the rod at $x = 0$, where the external force is applied, and the energy flux $E_{FF}$ (i.e., in the far field) in the semi-infinite segment are compared:

$$EFP = 10 \log_{10} E_I / E_{FF} \tag{5-15}$$

where EFP, in dB, stands for energy flux partition. It is straightforward, using the mathematical induction method, to prove that, in contrast to insertion losses, this characteristic is independent upon the number of unit-cells in the periodic insert and is defined by the elementary formula:

$$EFP = 10 \log_{10} \frac{\omega}{\omega + \hat{K} \sin(\omega)} \tag{5-16}$$

This function is plotted in Fig. 5. 12. As long as $\omega < \pi$, the constructive interference takes place as the secondary source cooperates with the primary source and adds to the energy flowing through the rod from x=0. Indeed, negative values of EFP are produced whenever $E_I < E_{FF}$. At the frequency $\omega = \pi$, $EFP = 0$, implying no energy injection produced by the force transmitted via springs and a constant energy flux along the whole structure. Recalling Eq. (5-13), this condition occurs, when the spring force is shifted by $\pi/2$ with respect to the complex conjugate of the velocity. When $\omega$ becomes larger than $\pi$, the inequality sign swaps: $E_I > E_{FF}$ (see Fig. 5. 12). Thus, positive values of $EFP$ imply that the secondary source opposes the energy transmission to the far field, i.e., destructive interference takes place. Transitions between constructive and destructive interference occur every $\pi$ and at each 'switching frequency' $\omega = n\pi$ $(n = 2, 3, 4, \dots, N)$, with $N$ being a positive integer, the force imposed by the end spring does not contribute to the energy flux.

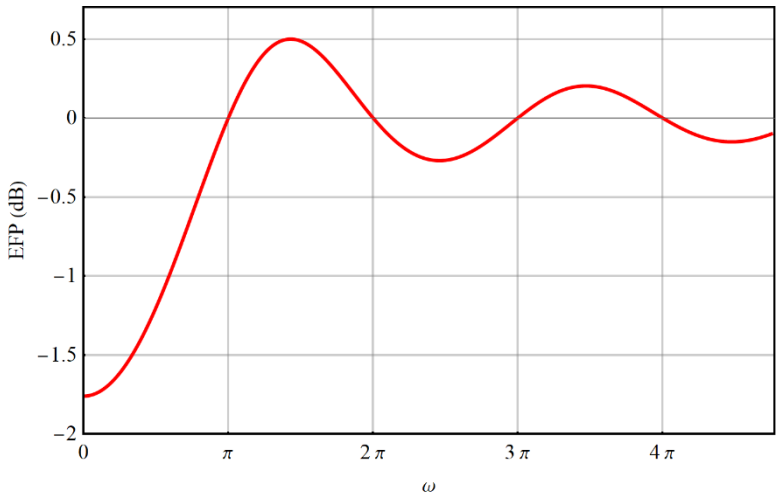


Fig. 5. 12: Energy flow partition

For clarity, it should be emphasised that quantity Energy Flux Partition introduced and analysed in this section is completely different from the insertion losses dealt with in the previous subsection, despite that both involve the energy flux in a far field for a waveguide with an insert. In IL, this energy flux is referred to the energy flux in a uniform waveguide, so that IL strongly depend upon the number of periodicity cells. In EFP the reference is the amount of energy which travels with the conventional speed c in the rod from the point $x = 0$, where the external force is applied, to the end on the periodic insert. This quantity does not depend upon the number of periodicity cells in an insert.

## 5.3. Elastic compound waveguide with periodic nonlocalities

This section explains the changes made in wave propagation properties of a conventional periodic elastic compound rod when integrated with nonlocalities. This implies the existence of two separate source for generation of stopbands in the band structure of the system. The studies put forward in the following section is provided in a concise format since most of the employed concepts and methods are indeed identical to those presented in the previous section.

### 5.3.1. Band structure identification

To generalize the posed problem given in last section, a unit cell of a periodic elastic compound rod with periodic nonlocality (PECRPN), which is composed of two different types of segments as well as of two springs, is taken into account (see Fig. 5. 13). $E_i$, $\rho_i$, $A_i$ and $L_i$ $(i = 1, 2)$ are the Young's modulus, the mass density, the cross-section and the length corresponding to each segment, respectively.

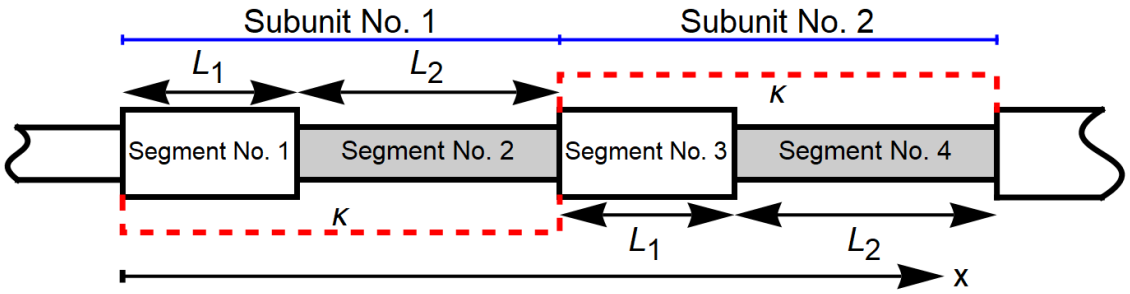


Fig. 5. 13: A unit cell with nonlocalities and impedance mismatch

Following the Hamilton's principle as shown in the previous sections, the matching conditions, in the nondimensional form, are:

$$\tilde{u}_1\rfloor_1 - \tilde{u}_2\rfloor_1 = 0 \tag{5-17a}$$

$$\frac{\partial \tilde{u}_1}{\partial X}\Big|_1 - \frac{Z}{c_{12}}\frac{\partial \tilde{u}_2}{\partial X}\Big|_1 = 0 \tag{5-17b}$$

$$\tilde{u}_2\rfloor_{1+\gamma} - \tilde{u}_3\rfloor_{1+\gamma} = 0 \tag{5-17c}$$

$$\frac{Z}{c_{12}}\frac{\partial \tilde{u}_2}{\partial X}\Big|_{1+\gamma} - \frac{\partial \tilde{u}_3}{\partial X}\Big|_{1+\gamma} + \tilde{K}[\tilde{u}_2(1+\gamma,t) - \tilde{u}_1(0,t)] + \tilde{K}[\tilde{u}_3(1+\gamma,t) - \tilde{u}_4(2+2\gamma,t)] = 0 \tag{5-17d}$$

$$\tilde{u}_3\rfloor_{2+\gamma} - \tilde{u}_4\rfloor_{2+\gamma} = 0 \tag{5-17e}$$

$$\frac{\partial \tilde{u}_3}{\partial X}\Big|_{2+\gamma} - \frac{Z}{c_{12}}\frac{\partial \tilde{u}_4}{\partial X}\Big|_{2+\gamma} = 0 \tag{5-17f}$$

where $X = x/L_1, \gamma = L_2/L_1$ and $\tilde{u}_i = u_i/L_1$ $(i = 1, 2, 3, 4)$ are the nondimensional coordinate, the nondimensional length parameter and nondimensional displacement associated to each segment, respectively. In addition, $Z = \rho_2 c_2 A_2/\rho_1 c_1 A_1$ denotes the impedance mismatch parameter, which is a ratio between the acoustic impedance of the segments, $\tilde{K} = \kappa L_1/E_1 A_1$ is the nondimensional spring stiffness and finally, $c_{12} = c_1/c_2$ symbolizes the sound speed ratio. It is already known by literature how impedance mismatch in periodic configurations is vehicle of stopbands in the dynamic response of a system [23]. Based on what earlier discussed, proper choice of periodicity conditions is necessary. To ensure that, the periodicity conditions are assumed as:

$$\tilde{u}_2\rfloor_{1+\gamma/2} - \Lambda\,\tilde{u}_4\rfloor_{2+3\gamma/2} = 0 \tag{5-18a}$$

$$\frac{\partial \tilde{u}_2}{\partial X}\Big|_{1+\gamma/2} - \Lambda\,\frac{\partial \tilde{u}_4}{\partial X}\Big|_{2+3\gamma/2} = 0 \tag{5-18b}$$

Following the procedure outlined in the previous section, it is straightforward to obtain a characteristic equation corresponding to Eq. (5-8):

$$q(\omega) = \frac{-2\,Z\cos(\tau\omega)(\omega\cos(\omega)+\tilde{K}\sin(\omega))+\sin(\tau\omega)(-2\,\tilde{K}\cos(\omega)+(1+Z^2)\,\omega\cos(\omega))}{Z\,\omega+Z\,\tilde{K}\cos(\tau\omega)\,\sin(\omega)+\tilde{K}\cos(\omega)\,\sin(\tau\omega)} \tag{5-19}$$

Here, $\tau = c_{12}\gamma$ is the ratio of propagation times and it is defined at the outset that $\tau \leq 1$ [23].

The discriminant function is

$$DF = \frac{\omega(2Z-2Z\cos(\tau\omega)\cos(\omega)+(1+Z^2)\sin(\tau\omega)\sin(\omega))(-2Z\omega-2Z\cos(\tau\omega)(\omega\cos(\omega)+2\tilde{K}\sin(\omega))}{Z\,\omega+Z\,\tilde{K}\cos(\tau\omega)\,\sin(\omega)+\tilde{K}\cos(\omega)\,\sin(\tau\omega)} + \frac{(-4\tilde{K}\cos(\omega)+(1+Z^2)\,\omega\sin(\omega))\sin(\tau\omega))}{Z\,\omega+Z\,\tilde{K}\cos(\tau\omega)\,\sin(\omega)+\tilde{K}\cos(\omega)\,\sin(\tau\omega)} \quad (5\text{-}20)$$

As explained in the previous section, positive/negative values of DF correspond to the stop/pass bands. As shown in the previous section, the long-range interaction is a novel promising tool to introduce periodicity in an otherwise uniform waveguide and to control location and width of stopbands. Given the mathematical framework in section 5.2., it is natural to explore possibilities to enhance the standard 'impedance mismatch' attenuation in periodic structures using non-locality.

Considering Eq. (5-8) and Eq. (5-19), the variation of $|\Lambda|$ against the frequency is demonstrated in Fig. 5. 14. It compares the response of a periodic elastic compound rod integrated with nonlocalities (PECRPN) and its counterpart without external elastic links (PECR). Additionally, the case of a uniform waveguide with nonlocalities is represented (PN). The numerical results are obtained for $Z = 0.6$, $c_{12} = 0.4$ and $\gamma = 2$. The periodic structure (Red line, PECR) generates five stopbands at frequencies around 1.7, 3.5, 5.2, 7 and 8.7. The uniform rod integrated with periodic long-range links (PN) with $\tilde{K} = 0.5$ (Blue lines) introduce three distinct stopbands that, in the low-frequency range, are close to the red ones. While at low frequencies, the two configurations PECR and PN produce overlapping stopbands, at higher frequencies the configuration with nonlocalities generates smaller number of stopbands in the considered frequency range. Finally, the spring inclusions (Black dot dashed lines, PECRPN) have effects only over odd-numbered stopbands, while a perfect overlapping of the even-numbered stopbands for PECR and PECRPN is observed. The odd-numbered ones appear slightly rightward moved, in a wider frequency bandwidth and with a larger amplitude as a consequence of the increased $|\Lambda|$, which further produces a sharper wave decay.

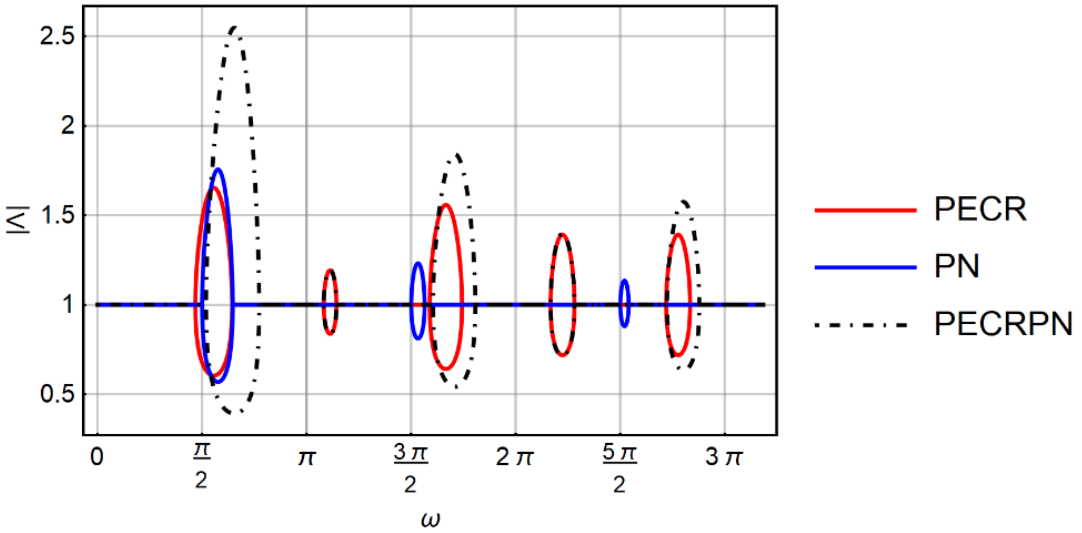


Fig. 5. 14: Comparison between three different cases

The mathematical framework presented in this section allows gaining insight into band structure of a periodic elastic compound rod integrated with external links. These external links bring new feature to the classical periodic system due to their long-range exertion of force, which may be put into practice via various means. The impedance mismatch provides a larger number of gaps with respect to a uniform waveguide with nonlocalities. Since the broadening and the attenuation effect on the first gap is striking, for acoustic isolation purposes it is reasonable to combine an elastic compound rod with nonlocalities. For other applications, as whenever it is required to avoid specific resonances, the contribution of nonlocalities becomes less relevant. Accordingly, in the higher frequency ranges, sticking to the systems with only impedance mismatch seems justifiable.

The results presented in Fig. 5. 14 are obtained for a priori chosen value of the geometrical and physical properties. One may think at the inverse problem by setting the value of the desired frequencies at which the stopbands should occur and consequently tailor the design of the system, as in real problems. As the interest is here on PN systems, this problem translates into identifying the stiffness of springs for the PN structure to mimic the behaviour of a conventional periodic system (PECR). The interest would be the magnification of all the existing stopbands in terms of amplitude and bandwidth. This is ideally achievable by a constructive combination of impedance mismatch and nonlocalities, as they both contribute in forming the final band structure of the system (see Fig. 5. 13), even though as shown in Fig. 5. 14, their coupling can only affect the odd-numbered ones. This is related to the adopted configuration given in Fig. 5. 13. As the springs connect neighbouring subunits, they miss the connection between the segments within a subunit, which is instead the case of the system PN in Fig. 5. 1, for the uniform cross section and material properties. However, a possible strategy can be easily outlined: the frequencies at which the stopbands emerge can be obtained by the $DF$ for the elastic compound rod with no nonlocalities [23] for given geometrical and mechanical properties; the introduction of this value of frequency into Eq. (5-9), which holds for PN system, returns the required value of stiffness for the spring-like connections.

Unlike what is represented Fig. 5. 3, the seeds of the gaps, which are influenced by the nonlocalities, are not fixed anymore. This fact may be simply illustrated from a mathematical point of view. As indicated earlier, the boundaries between the pass and stopbands is defined by Eq. (5-9). Considering a simple compound elastic rod with no springs, $q(\omega)$ simplifies as [23]:

$$q(\omega) = (Z + 1/Z)\sin(\tau\omega)\sin(\omega) - 2\cos(\tau\omega)\cos(\omega) \tag{5-21}$$

Given the transcendental nature of Eq. (5-21), one may straightforwardly obtain the transition frequencies $\omega = \omega_0$ between the stop and pass bands once the impedance mismatch and the ratio of propagation times are fixed. Perturbing the stiffness by small quantity, i.e., $\widetilde{K} = \epsilon$, the frequency becomes:

$$\omega = \omega_0 + \epsilon\omega_1 \tag{5-22}$$

Expanding $DF$ around $\epsilon = 0$ and considering the contribution of the first order term only, one obtains:

$$\omega_1 = -\frac{\partial DF}{\partial \bar{K}} \Big/ \frac{\partial DF}{\partial \omega}\Big|_{\substack{\epsilon = 0 \\ \omega = \omega_0}} \tag{5-23}$$

Given Eq. (5-23) and the values of $\tau$ and $Z$ as assumed, the first four critical frequencies are evaluated as a result of the change in the value of the stiffness. The exact values are obtained numerically and together with the approximated frequencies, i.e., $\omega = \omega_0 + \epsilon\omega_1$, are represented in Fig. 5. 15. As it appears, no change is observed for the frequencies which correspond to the stopbands of zero width at $\omega = 0$ and $\omega = \pi$, which is in close correspondence to what already shown in Fig. 5. 2 and Fig. 5. 3. Evidently, the discrepancies become significant as $\epsilon$ diverges more from zero. Note that the value at the frequencies associated with non-zero width stopbands slightly increase as nonlocalities are introduced to the system.

Although gaps widening and pushing them to lower bands is of value, the figure suggests that the latter is not satisfied. This can be achieved with the help of systems with negative stiffness as described earlier in subsection 5.2.2.

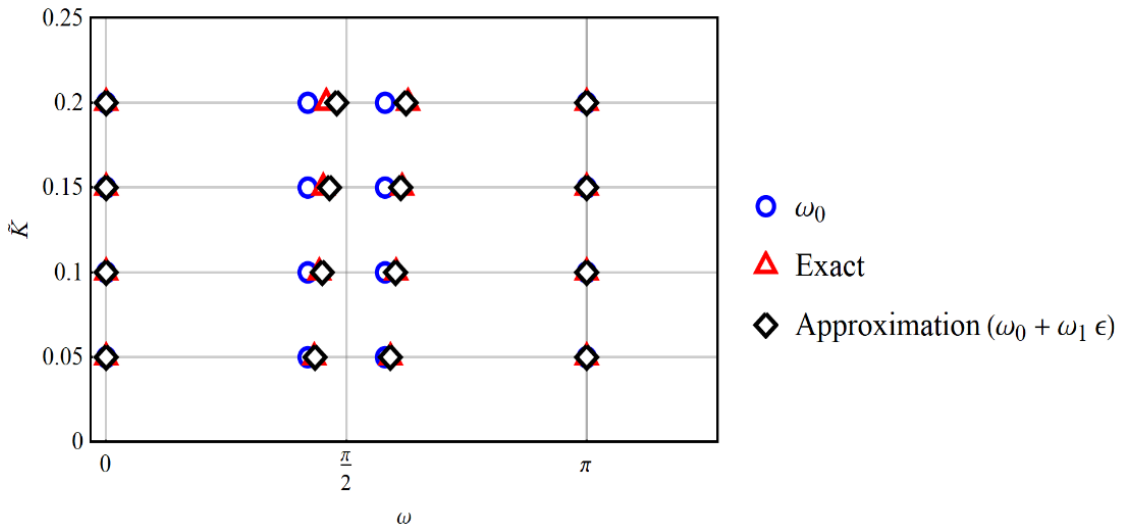


Fig. 5. 15: Change in critical frequencies due to the introduction of nonlocalities ($Z = 0.6, \tau = 1$)

## 5.3.2. Insertion loss analysis

The investigation about the $IL$ is completed by considering the case a semi-infinite rod characterized by nonlocalities and impedance mismatch. Fig. 5. 16 highlights the key role played by impedance mismatch in attenuating the wave energy and unveils two effects: 1) in agreement with the other structure, the higher the number of inclusions, the larger the magnitude of the peaks, to the limit of infinite magnitudes for an infinite number of inclusions; 2) the comparison with uniform waveguide in Fig. 5. 7 reveals larger amplitude of the peaks due to impedance mismatch.

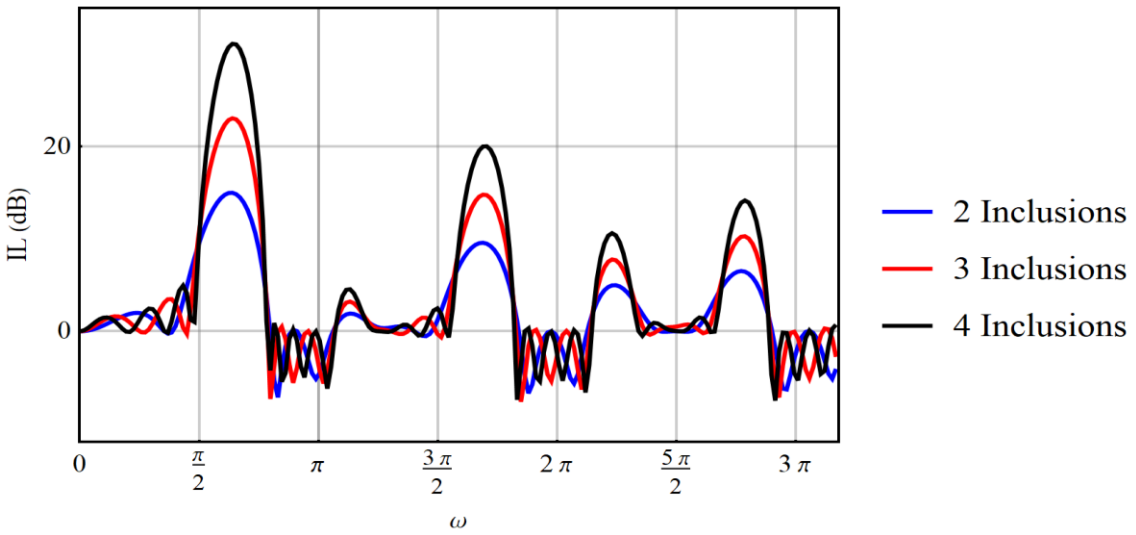


Fig. 5. 16: Insertion loss for an elastic compound rod with nonlocalities
($Z = 0.6$, $c_{12} = 0.4$, $\gamma = 2$, $\widetilde{K} = 0.5$)

## 5.4. Axisymmetric cylinder with periodic nonlocalities

This section is an attempt to extend the concept of periodic nonlocalities to higher dimension domains in order to examine the possibility of blocking the energy within certain frequency ranges by employing solely longitudinal links, when coupled transverse and extensional modes are in charge of carrying energy. The system of interest, as in Fig. 5. 17, is composed of an infinite axisymmetric cylindrical shell. Besides, spring-like links let distant points interacting with each other. The inclusion of the periodically allocated axial connections generates new dynamic effects in the dynamic performance. The global dynamic response, by the displacements $\bar{u}(x,t)$ and $\bar{w}(x,t)$ along the axis and along the transverse direction, respectively, is associated by the following coupled differential equations:

$$\frac{Eh}{1-\nu^2}\left(\frac{d^2\bar{u}}{dx^2}+\frac{\nu}{R}\frac{d\bar{w}}{dx}\right)=\rho\frac{d^2\bar{u}}{dt^2} \tag{5-24a}$$

$$\frac{Eh}{1-\nu^2}\left(\frac{h^2}{12}\frac{d^4\bar{w}}{dx^4}+\frac{\bar{w}}{R^2}+\frac{\nu}{R}\frac{d\bar{u}}{dx}\right)=\rho\frac{d^2\bar{w}}{dt^2} \tag{5-24b}$$

with $\rho$, $E$, $R$, $h$, and $\nu$ being the mass density, Young's modulus, radius, thickness and Poisson's ratio, respectively. The nondimensional forms become:

$$\frac{d^2u}{dX^2}+\Omega^2u-\nu\frac{dw}{dX}=0 \tag{5-25a}$$

$$\nu\frac{du}{dX}+w+\frac{h^2}{12R^2}\frac{d^4w}{dX^4}-\Omega^2w=0 \tag{5-25b}$$

$X=x/R$ denoting the nondimensional axial coordinate, $u=\bar{u}/R$ and $w=\bar{w}/R$ the nondimensional axial and bending displacements, are introduced. $\Omega=\sqrt{(1-\nu^2)\rho R^2\omega^2/E}$ is the nondimensional frequency. In the correspondent structure, the energy is carried out via

coupled modes due to the coupling between the axial and bending terms in the equations of motion. This may be perceived by inspecting Eqs. (5-25) where both $u$ and $w$ are present in both equations indicating the link between the extensional and flexural modes.

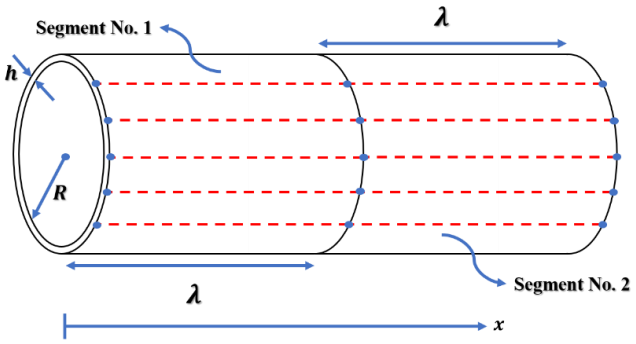


Fig. 5. 17: A periodicity cell of a cylindrical shell with periodic nonlocalities

Using modal coefficients $\tau_i$, the general solution for the system of equations (5-25) is:

$$w = \sum_{i=1}^{6} \overline{w}_i \, e^{jk_i x} \tag{5-26a}$$

$$u = \sum_{i=1}^{6} \tau_i \, \overline{w}_i \, e^{jk_i x} \tag{5-27b}$$

$k_i$ $(i = 1, 2, \dots, 6)$ are the roots of the dispersion relation for a homogenous and isotropic axisymmetric cylindrical shell. Given the above expressions for the displacements $u$ and $w$, twenty-four equations, in total, are necessary to fully characterize the kinematics of both segments. However, only twelve of them are self-sufficient and the rest are indeed connected to the independent ones by the modal coefficients. The modal coefficients are:

$$\tau_i = \frac{j\nu k_i}{k_i^2 - \Omega^2} = j\,\frac{1 + \frac{h^2 k_i^4}{12R^2} - \Omega^2}{\nu k_i} \tag{5-27}$$

where $j$ is the imaginary unit. Considering a unit cell of the system, which contains two equivalent shell segments coupled with periodic nonlocalities of stiffness $\kappa$, the interface conditions between the neighbouring segments 1 and 2, in the nondimensional form, are:

$$w_1\rfloor_{X=\lambda} = w_2\rfloor_{X=\lambda} \tag{5-28a}$$

$$\left.\frac{dw_1}{dX}\right|_{X=\lambda} = \left.\frac{dw_2}{dX}\right|_{X=\lambda} \tag{5-28b}$$

$$\left.\frac{d^2w_1}{dX^2}\right|_{X=\lambda} = \left.\frac{d^2w_2}{dX^2}\right|_{X=\lambda} \tag{5-28c}$$

$$\left.\frac{d^3w_1}{dX^3}\right|_{X=\lambda} = \left.\frac{d^3w_2}{dX^3}\right|_{X=\lambda} \tag{5-28d}$$

$$u_1\rfloor_{X=\lambda} = u_2\rfloor_{X=\lambda} \tag{5-28e}$$

$$\left.\frac{du_1}{dX}\right|_{X=\lambda} + \nu w_1\rfloor_{X=\lambda} = \left.\frac{du_2}{dX}\right|_{X=\lambda} + \nu w_2\rfloor_{X=\lambda} + \widehat{K}\left[u_1\rfloor_{X=\lambda} + u_2\rfloor_{X=\lambda} - \left(u_1\rfloor_{X=0} + u_2\rfloor_{X=(1+\gamma)\lambda}\right)\right] \tag{5-28f}$$

where $\hat{k} = \kappa R(1-\nu^2)/E$ denotes the nondimensional spring stiffness. $\lambda = L_1/R$ and $\gamma = L_2/L_1$ are nondimensional length parameters. Note that the parameter $\gamma$ is kept as a variable in the above formulas for the sake of generality but it is set to one throughout this study. The above conditions are referring to the continuity of axial and bending displacements, the slopes $dw/dX$, the flexural moments $d^2w/dX^2$ and bending forces $d^3w/dX^3$ at the interface. Besides, the condition regarding the continuity of the axial force i.e. Eq. (5-28f), is modified by an additional term $\widehat{K}[u_1]_{X=\lambda} + u_2]_{X=\lambda} - \big(u_1]_{X=0} + u_2]_{X=(1+\gamma)\lambda}\big)]$, which brings into the system the effects induced by nonlocalities. To proceed with the analysis, six more equation are required, which are obtained by considering the Floquet-Bloch periodicity conditions, as:

$$w_1]_{X=\lambda/2} = \Lambda\, w_2]_{X=(1+\gamma/2)\lambda} \tag{5-29a}$$

$$\frac{dw_1}{dX}\Big|_{X=\lambda/2} = \Lambda \frac{dw_2}{dX}\Big|_{X=(1+\gamma/2)\lambda} \tag{5-29b}$$

$$\frac{d^2w_1}{dX^2}\Big|_{X=\lambda/2} = \Lambda \frac{d^2w_2}{dX^2}\Big|_{X=(1+\gamma/2)\lambda} \tag{5-29c}$$

$$\frac{d^3w_1}{dX^3}\Big|_{X=\lambda/2} = \Lambda \frac{d^3w_2}{dX^3}\Big|_{X=(1+\gamma/2)\lambda} \tag{5-29d}$$

$$u_1]_{X=\lambda/2} = \Lambda\, u_2]_{X=(1+\gamma/2)\lambda} \tag{5-29e}$$

$$\frac{du_1}{dx}\Big|_{X=\lambda/2} + \nu w_1]_{X=\lambda/2} = \Lambda\Big(\frac{du_2}{dx}\Big|_{X=(1+\gamma/2)\lambda} + \nu w_2]_{X=(1+\gamma/2)\lambda}\Big) \tag{5-29f}$$

Again, $\Lambda$ is the standard parameter describing the phase shift in a periodic array. The relations (5-29) compare the state vector of neighbouring segments. It is apparent how the state vector gets modified from one cell to the next by the parameter $\Lambda$. Considering $\Lambda = e^{jK_B}$ with $K_B$ being the Bloch parameter, two possibility for its value may be imagined: real-valued $K_B$, hence $|\Lambda| = 1$, suggests the propagation is allowed in the structure, complex valued $K_B$, inducing $|\Lambda| \neq 1$, disclosed the impossibility to project the state vector of one segment on the neighbouring, implying the existence of stopband frequencies. Note that, once $\Gamma$ is defined, its value is constant for any selected periodicity cell. A sixth-order transcendent equation associated with the described system is of the form:

$$\Lambda^6 + A_1\big(\Omega, \widehat{K}\big)\,\Lambda^5 + A_2\big(\Omega, \widehat{K}\big)\,\Lambda^4 + A_3\big(\Omega, \widehat{K}\big)\,\Lambda^3 + A_4\big(\Omega, \widehat{K}\big)\,\Lambda^2 + A_5\big(\Omega, \widehat{K}\big)\,\Lambda + 1 = 0 \tag{5-30}$$

The above polynomial is the nontrivial solution of a system of equations obtained from the combination of Eqs. (5-28) and Eqs. (5-29). Eq. (5-30) proclaims the existence of three pair of roots possibly determining the energy transmission across the domain. Note that, the coefficients in the preceding equation may not be explicitly extracted and values of $\Gamma$ are individually calculated for a given frequency $\Omega$.

This part is devoted to investigating the band structure of an unbounded axisymmetric cylindrical shell in the presence of periodic nonlocalities governed by the nondimensional stiffness $\widehat{K}$. The analysis of the trend of $\Lambda$ with respect to the nondimensional frequency $\Omega$

unveils the existence of several stopbands induced by the introduction of periodic nonlocalities, occurring whenever $|\Lambda| \neq 1$, spread along the entire frequency domain. Since the stopbands usually get smaller, the higher the frequency, only the first two stopbands are here illustrated in Fig. 5. 18a and Fig. 5. 18b. In fact, energy transmission is not permitted about $\Omega = 0.96$ (see Fig. 5. 18a) and $\Omega = 1.23$ (see Fig. 5. 18b), where $|\Lambda|$ may adopt any value but unity.

Evidently, the first gap is significantly broader with respect to the second one of the widths 0.006. The figure implicitly points to the fact that the long-range interactions are conveniently beneficial for blocking the energy paths no matter it is being carried by extensional or bending modes. According to Eq. (5-25), the response of the system is dependent upon the thickness-radius ratio $\eta = h/R$; therefore, the effect of this parameter may sensibly influence the location and the width of the gaps dramatically. Considering other parameters to be fixed as $\nu = 0.3$, $\gamma = 1, \lambda = 1$ and $\widehat{K} = 0.5$, for four different values of $\eta$, the location of the stopbands is given in Table 5. 1.

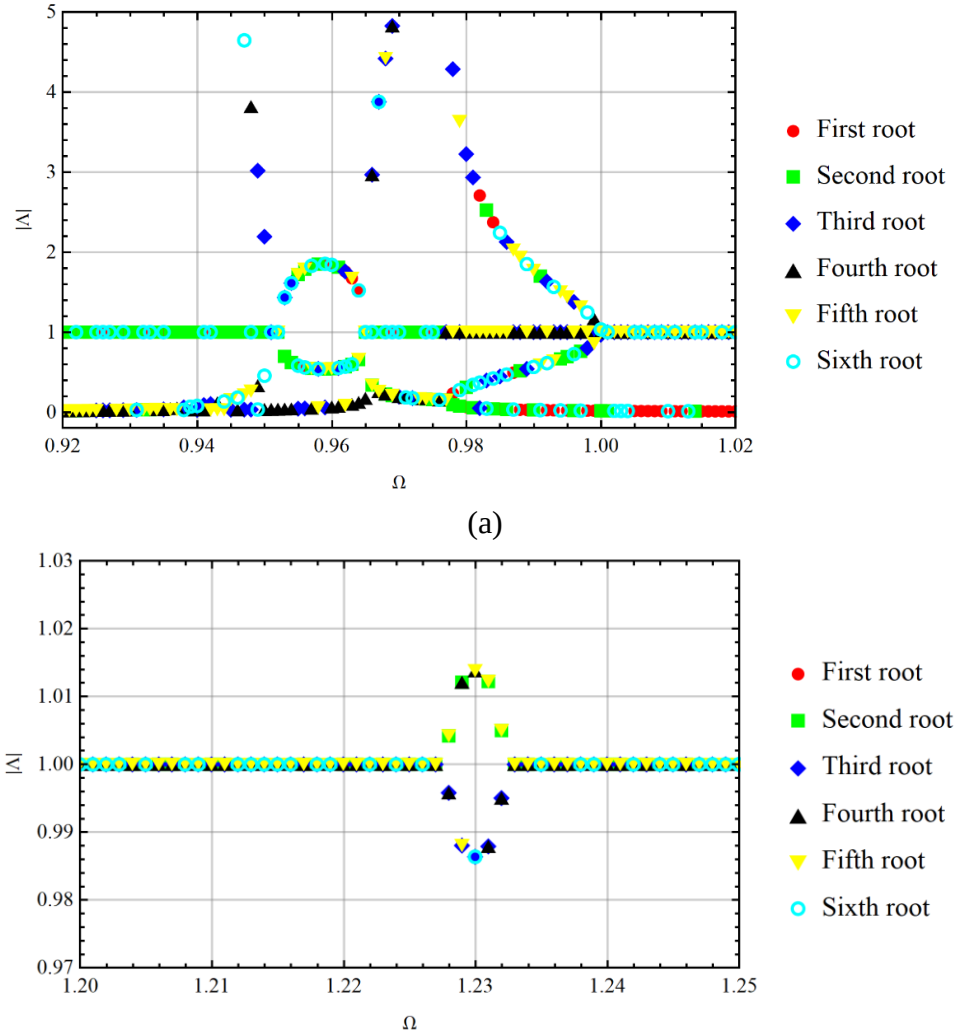


(a)

(b)

Fig. 5. 18: Band structure of an axisymmetric cylindrical shell with periodic nonlocalities ($\widehat{K} = 0.5,\ \eta = 0.02$) a) First gap b) Second gap

Table 5. 1: The low-frequency stopbands in an axisymmetric cylindrical shell with periodic nonlocalities

| $\eta$ | First gap | Second gap |
|---|---|---|
| 0.005 | $0.94895 < \Omega < 0.95495$ | $0.96295 < \Omega < 0.96895$ |
| 0.01 | $0.94895 < \Omega < 0.95795$ | $0.98695 < \Omega < 0.98995$ |
| 0.015 | $0.94995 < \Omega < 0.96195$ | $1.12195 < \Omega < 1.12595$ |
| 0.02 | $0.95195 < \Omega < 0.96495$ | $1.22695 < \Omega < 1.23295$ |

To extract what is brought in the table, a narrow band $\Omega < 1.5$ is taken into account. Although the change in $\eta$ roughly influences the width of the gaps, for the case of first stopband, a quite wider gap is met as this ratio increases. In fact, the left border of both gaps is pulled towards higher frequencies as the thickness-length ratio rises. Obviously, the origin of these gaps may be simply explained by the decoupling of the flexural and longitudinal modes, which are integrated because of the Poisson's ratio and the further discussion is held for the future works.

The frequency dependence of $|\Lambda|$ is demonstrated in Fig. 5. 19, for two values of the nondimensional stiffness, namely $\widehat{K} = 0.2$ shown in black and $\widehat{K} = 0.5$ in red. Two distinct patterns are observed: those points which resemble non-flat curves are originated from the real roots of Eq. (5-30), and the roots constructing the flat lines i.e., $|\Lambda| = 1$, are referring to pass band frequencies. Based on the figure, the right border of the stopband, the frequency at which the stopband vanishes, moves towards higher frequencies for higher values of $\widehat{K}$. The emerging frequency (seed of the stopband) picks a slightly higher value with respect to the frequency associated with the system having less stiff external links. Given the circumstances, a wider gap is attained.

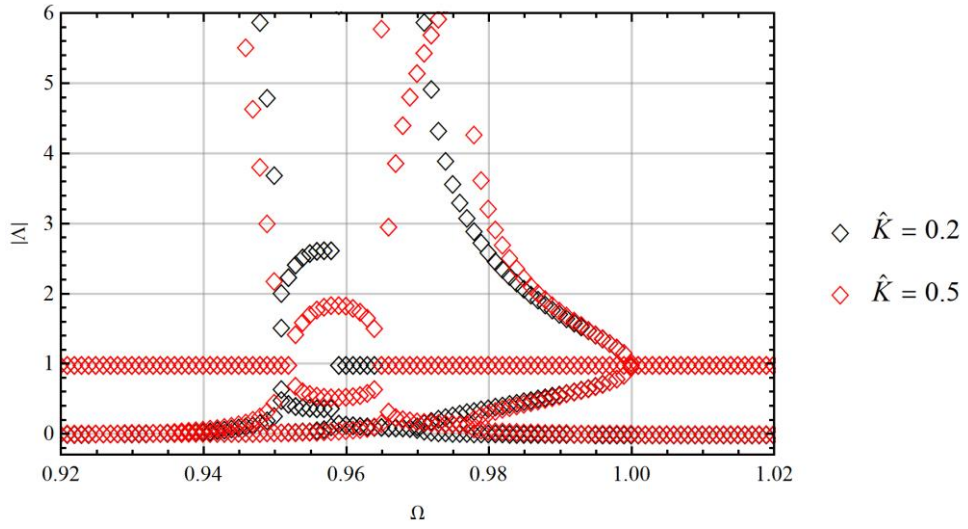


Fig. 5. 19: Band structure of an axisymmetric cylindrical shell with periodic nonlocalities for two different values of nondimensional stiffness $\widehat{K}$ ($\eta = 0.02$)

## 5.5. Final remarks

Development of periodic structures by using long-range connectors is the core idea behind the studies of this chapter. Indeed, long-range communications among selected points of specific domains, based on a periodic pattern, generate arrays capable of mimicking the signature behaviours of conventional periodic configuration. Primarily, propagation of plane waves across a very simple structure with embedded periodic nonlocalities, namely rod, is realized to demonstrate the competence of the idea. Separate study on the energy flow across the system revealed the underlying mechanism for the alterations took place in the associated band structure. The same idea then exercised for other elastic structures such as compound rods and cylindrical shells to prove its beneficial performance and dexterity. The results imply the generation of stopbands in the band structure of the system. Parametric studies reveal the possibility of tuning the gaps' location and their width by altering softer/stiffer nonlocalities.

# Chapter 6: Concluding remarks

This work is an inquiry to examine and identify the arising wave propagation phenomena in macro scaled structures with long-range interactions. Here, long-range models are developed by imposing a long-range superstructure on a conventional host structure, where the superstructure is responsible for establishing communication among non-adjacent parts of the system. The major objective of this study is to manipulate the travelling waves across the domain, which is approached by considering superstructures composed of well-known mechanical entities. In most cases presented along the way, simple spring-like links are considered as long-range connectors, enabling instantaneous transmission of force between non-adjacent points of the domain. A second type of external connectors, namely resonator units are also employed for the case of long-range homogenous systems to examine the emergence of other potential wave effects.

From a certain point view, long-range systems are a special kind of metamaterials since they are artificial arrangements, which are designed for certain purposes. In fact, the essential idea behind this work is to borrow the common concepts proposed in nonlocal elasticity for the sake of engineering novel configurations capable of manipulating waves, which are referred to as *elastic metamaterials*.

Throughout the thesis, several configurations are considered to underline the possibility of achieving various wave effects by the virtue of long-range interactions and periodicity. Due to the abundance of systems investigated in different chapters, the second chapter is devoted to providing a general overview of the contents to avoid any potential confusion for the readers. For that matter, systems under studying are categorized into two main classes, namely long-range homogenous and non-homogenous configurations based the concept of graph-periodicity, given in chapter 2. The key distinction between these two classes is related to the features of connectivity templates adopted for developing long-range models. Provided that the template is identical for all points of the domain, a homogenous configuration is met. On the contrary, contribution of selected groups of points of the domain in distant communication gives rise to long-range non-homogenous system. It is noteworthy that that structures with non-homogenous periodicity are genuinely periodic (tree-periodic); however, long-range homogenous structures may capture the leaf-periodicity property depending upon the connectivity template.

To reach a broad view of the characteristics of wave propagation in long-range systems, conventional thin-walled components such as rods, membrane, and cylindrical shells are selected as the host structure. Simultaneously, the corresponding long-range superstructure is defined so that the existence of analytical solution for the entire configuration is guaranteed. Mathematical details associated with dynamic model for each example is discussed, and then the results are extracted by applying a proper solution method to the developed model.

The corresponding cases of linear long-range homogenous systems are brought in chapter 3, and closed form dispersion relations are obtained by utilising a plane wave solution. Emerging phenomena are hinged on a unique nondimensional parameter $\chi$, providing a measure for the intensity of long-range forces. Based on the analysis, the following propagation effects are realised:

- Zero group velocity, i.e., wave-stopping phenomenon emerges, when the parameter $\chi$ exceeds a certain threshold and meets a critical value $\chi_{cr}$. For $\chi \geq \chi_{\mathrm{cr}}$, the wave envelope, responsible for carrying energy across the domain stops travelling around particular frequencies.
- Negative group velocity is noticed for linear long-range homogenous configuration with $\chi > \chi_{\mathrm{cr}}$, implying backward flow of wave envelopes.
- Redistribution of eigenstates across the frequency domain is realised for systems characterised by $\chi < \chi_{\mathrm{cr}}$ though the group velocity remains positive over the entire frequency band.

Along with $\chi$, nondimensional frequency parameter(s) concerned with the locally resonating mass(es) are in charge of determining the behaviour of resonator-based long-range homogenous configurations. In this case, the following conclusions are drawn:

- Generation of stopbands is observed in the dispersion map of the system, when the constructing elements of long-range superstructure are resonator units instead of simple spring-like links.
- Occurrence of zero/negative group velocity is demonstrated for the acoustic and optical dispersion branches for resonator-based long-range homogenous configurations.
- Dependence of the response characteristics including stopband width and group velocity behaviour to the nondimensional parameter $\chi$ and nondimensional frequency parameter(s) is revealed.

In chapter 4, some analyses are presented for long-range homogenous one-dimensional configuration with a nonlinear host structure under random excitation. The dynamic description is linearized by statistical linearization approach, and some characteristics of systems are identified qualitatively via different mathematical method. Eventually, an approximate dispersion relation is found by homogenizing the linearized equation of motion. The chief results are:

- Wavenumber entanglement as a result of presence of nonlinearity.
- Possibility of altering propagation behaviours by adjusting the level of noise.
- Undesirable impact of noise for driving the system towards disclosing uncommon wave effects such as wave-stopping and negative group velocity.

Long-range non-homogenous periodic systems are the main focus of the second half of the thesis, as given in chapter 5. In the chapter, only special variety of such non-homogenous systems is investigated, where the implementation of the long-range superstructure generates conventional periodic configurations. The associated results are ontained using Floquet theorem to identify the systems' band structure. Subsequently, an insertion loss analysis is

performed to virtually verify the results of Floquet analysis, yielding a broader insight into the characteristics of such systems along with the intended objective. The key findings are:

- Stopbands are present in the band structure of all studied configurations, a signature property of periodic arrangements.
- Possibility of generating stopbands with Bragg's destructive interference mechanism is demonstrated in absence of impedance mismatch in the system.
- Prediction of ultra-low-frequency stopbands, which may even emerge from zero, for systems with spring-like links of negative stiffness.
- Possibility of disrupting the energy transfer carried by coupled modes of different nature for the case of periodic cylindrical shell.

The presented studies were conducted to demonstrate the capacities of conventional systems, when integrated with long-range inclusions. However, to gain insight into the behaviour of bounded counterparts of studied configurations, comprehensive numerical investigations are required, especially for monitoring their response in real-time. Furthermore, launching broad experimental campaigns would be a great asset to both verify the submitted conclusions, and realise the design and manufacturing limitations.

# Appendix A: On systems with temporal long-range effects

## A.1. Introduction

Domains with long-range interactions, as those examined in the previous chapters, possess some interesting features, nominating themselves as qualified options for designing devices requiring such kinds of characteristics. Thus, one may speculate this fertile idea could be the source for beneficial changes in the behaviour of system if extended to the temporal domain. In fact, all the studies presented up to this point of the thesis consider the existence of some physical entities providing spatial interaction among non-adjacent particles, thereby the enrichment of the dynamics. In this chapter, on the other hand, the dynamics is modified by introducing a force, which explains the dependence of the response on its time-history, i.e. temporal interaction.

This topic has been the centre of attention is some fields, where the state of systems is not precisely identified by common formulations at each time step. In some cases [], temporal memory provides assistance for achieving a more realistic response. Bringing this concept to the context of elasticity could be highly beneficial to model several systems such as those for which the structures are in constant interaction with fluid. For instance, moving objectives travelling through a fluid generate vortices and their effect is perceived with certain delay by the body, giving rise to a retarded memory effect, i.e., temporal long-range interaction.

This appendix provides a preliminary analysis to realize the behaviour of the systems with memory effect embedded. To begin with, a very simple continuous configuration, namely rod, is considered and the corresponding dynamics is altered by adding a new term explaining the dependence of displacement output signal on the its history based on certain interaction law. Then the challenges facing this hypothetical system is realized by the straightforward plane analysis. Note that the study carried out in this appendix is not the main focus of this thesis, and the topic is approached as an impulsive response to our curiosity. The following analysis [129] provides an early understanding of such systems though their behaviour is yet to be investigated broadly in the future.

## A.2. Plane waves

An infinite waveguide with a memory effect is considered here. In such systems, the structural response is not only dependent on the instant displacement, velocity, and acceleration, but also upon the changes of the structural response along its time-history. We assume, as a reference, the governing equation for longitudinal vibration and for a linear homogeneous rod can be expressed as:

$$\rho\ddot{u} - Eu'' + \mu \int_{-\infty}^{t} P(t-\tau)\, u(x,t)\, d\tau = 0 \qquad \text{(A.1-1)}$$

where prime denotes space derivation. The additional term $\int_{-\infty}^{t} P(t-\tau)\, u(x,t)\, d\tau$ brings into the equation the memory effect through the kernel $P(t)$. For $P(t) = e^{-\alpha t}\, H(t)$, $H(t)$ being the Heaviside step, and $1/\alpha$ the memory persistency time, applying spatiotemporal Fourier transform, the dispersion relation is obtained as:

$$\rho\omega^2 = Ek^2 + \frac{\mu}{\alpha + j\omega} \qquad \text{(A.1-2)}$$

where the memory delay $\alpha$ is a positive real number and $j$ is the imaginary unit. This is a complex equation with complex roots, which proclaims the fact that the low frequency propagation of waves in such systems is distorted with respect to the standard D'Alembert equation. At higher frequency the memory distortion term $\frac{\mu}{\alpha+j\omega}$ tends to vanish. To obtain a generic nondimensional form of the dispersion relation, the following nondimensional parameters are conveniently considered

$$\Omega = \omega/\alpha \qquad \text{(A.1-3a)}$$

$$K = k\sqrt{E/\rho\alpha^2} \qquad \text{(A.1-3b)}$$

$$\Gamma = \mu/\rho\alpha^3 \qquad \text{(A.1-3c)}$$

In view of these parameter, Eq. (A.1-2) changes as follow:

$$\Omega^2 = K^2 + \frac{\Gamma}{1+\Omega^2} - j\frac{\Gamma\Omega}{1+\Omega^2} \qquad \text{(A.1-4)}$$

Here, Γ is a nondimensional parameter, which distinctly characterizes the system's response with respect to the classical one. The roots of this equation are found as

$$K(\Omega) = \pm\frac{\sqrt{-(1+j\Omega)(\Gamma-\Omega^2-j\Omega^3)}}{1+j\Omega} \qquad \text{(A.1-5)}$$

And the associated waveform is

$$u = A\, e^{\mp K_i x}\, e^{i(\pm K_r x - \omega t)} \qquad \text{(A.1-6)}$$

where $K_r(\Omega)$ and $K_i(\Omega)$ are the real and imaginary components of the wavenumber $K(\Omega)$. This implies the response corresponding to an infinite waveguide with memory shows an exponentially decaying trend governed by $e^{\mp K_i x}$ of the travelling disturbance $e^{i(\pm K_r x - \omega t)}$.

## A.3. Frequency response analysis

The problem under investigation is the forced vibration of a finite waveguide of length $l$. The origin load is at the centre of the rod, and both ends ($x = \pm l/2$) are clamped. The system equation is

$$\rho\ddot{u} - Eu'' + \mu P * u = q(t) \qquad \text{(A.1-7)}$$

where $q(t)$ is a time-varying load. Provided the initial conditions are set to zero, Eq. (A.1-7), in the Laplace domain, takes the form

$$\rho s^2 \bar{u}(x,s) - E\frac{d^2\bar{u}(x,s)}{dx^2} + \frac{\mu\bar{u}(x,s)}{s+\alpha} = q(s) \tag{A.1-8}$$

Considering the assumed boundary conditions, one obtains

$$\bar{u}(x,s) = A\,q(s) - \frac{A\,q(s)}{(e^{Bl}+1)}e^{B(\frac{l}{2}-x)} + \frac{A\,q(s)}{(e^{Bl}+1)}e^{B(\frac{l}{2}+x)} \tag{A.1-9}$$

with

$$A = \frac{s+\alpha}{\mu+s^2\rho(s+\alpha)}$$

$$B = \frac{1}{\sqrt{E}\sqrt{A}} \tag{A.1-10}$$

Hence, the transfer function is

$$H(j\omega) = \frac{\bar{u}(x,s)}{q(s)} = A - \left.\frac{A\left[e^{B\left(\frac{l}{2}-x\right)}+e^{B\left(\frac{l}{2}+x\right)}\right]}{(e^{Bl}+1)}\right|_{s=j\omega\ ,\ x=x_0} \tag{A.1- 11}$$

## A.4. Modal analysis

Let us consider a similar system described by Eq. (A.1-7) with arbitrary boundary conditions. Expressing the longitudinal displacement in terms of normal modes $\phi_i$, we have

$$u(x,t) = \sum_i^\infty \phi_i(x)q_i(t) \tag{A.1-12}$$

Substitution of Eq. (A.1-12) into Eq. (A.1-7) results in

$$\rho\sum_i \phi_i\ddot{q}_i - E\sum_i q_i\phi''_i + \mu\int_{-\infty}^{t} P(t-\tau)\left[\sum_i \phi_i q_i\right]d\tau = q \tag{A.1-13}$$

Multiplying the Eq. (A.1-13) by $\phi_j$ and integrating over the length $l$, in the view of orthogonality relationships, the preceding reduces to

$$\ddot{q}_i + \omega_i^2 q_i + \tilde{\mu}(q_i * P) = \tilde{q}(t)\int_0^l \phi_i\,dx \tag{A.1-14}$$

where $\tilde{\mu} = \mu/\rho$ and $\tilde{q} = q/\rho$. Applying Fourier transform yields

$$Q_i(\omega) = \frac{\tilde{Q}(\omega)\int_0^l \phi_i dx}{\omega_i^2 - \omega^2 + \frac{\tilde{\mu}}{\alpha+j\omega}} \tag{A.1-15}$$

Thus, the signal may be reconstructed easily in the frequency domain as

$$u(x,\omega) = \tilde{Q}(\omega)\sum_i^\infty \frac{\phi_i(x)\int_0^l \phi_i dx}{\omega_i^2 - \omega^2 + \frac{\tilde{\mu}}{\alpha+j\omega}} \tag{A.1-16}$$

## A.5. Results and discussion

This section is devoted to investigating the propagation properties of an infinite waveguide in the presence of memory effects governed by the nondimensional parameter Γ. On the other hand, a frequency response analysis on the finite counterpart of the investigated system is performed.

### A.5.1. Wave propagation

Following the approach presented in section A.2, the propagation characteristics of infinite waveguide with non-instant interactions can be investigated. The imaginary component of the nondimensional wavenumber i.e., wave attenuation, with respect to the nondimensional frequency is plotted in Fig. A. 1, for different values of Γ. Based on the figure, such a waveguide may be employed as a potential medium for high-frequency energy transfer since the medium is significantly less attenuating at higher frequencies.

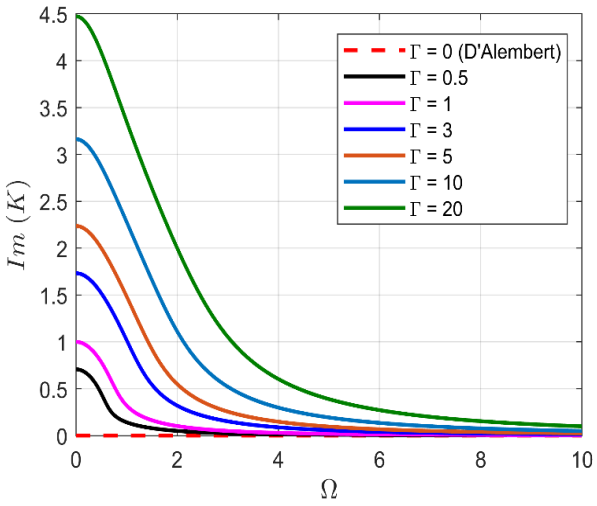


Fig. A. 1: The wave attenuation curves for the waveguide with non-instant interactions for various the nondimensional parameters Γ

Fig. A. 2 shows the phase velocity $C_\phi = \Omega/K_r(\Omega)$ against the nondimensional frequency for various values of Γ. Being the most obvious remarks, the system acts similarly to a conventional waveguide at higher frequencies. One may note that the amplitude of $C_\phi$ at the starting point of curve decreases for higher values of Γ. Furthermore, the phase velocity initially grows in a parabolic fashion with frequency and after reaching a maximum point, it decreases asymptotically to one.

Fig. A. 3 shows that the group velocity, at first, decreases rapidly to substantially rise straight afterwards. Finally, the value of $C_g$ manifests a monotonic drop immediately after reaching a certain frequency and approaches the response of the conventional waveguide. Note that, the fluctuations corresponding to the group velocity shows rather large variations (the distortion

belong to a range 0.5-2 with respect to the conventional speed) that can be purposely used to affect the propagation regimes, for example including control systems based on memory effects [130]. The propagation regimes associated to both time and space memory effect can in fact permit a surprising control of the wave pattern, even inducing wave-stopping or superluminal propagation which are already reported for systems affected by space and time nonlocality [109].

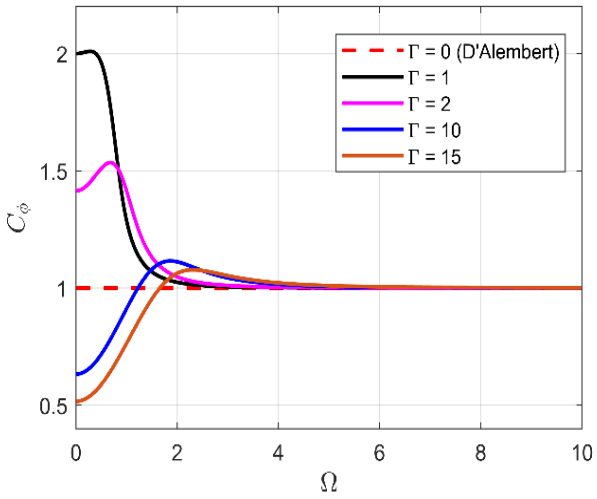


Fig. A. 2: The phase velocity curves for the waveguide with non-instant interactions for various the nondimensional parameters Γ

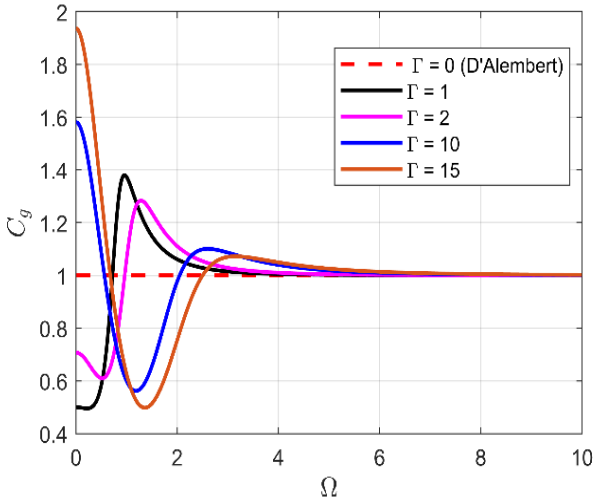


Fig. A. 3: The group velocity curves for the waveguide with non-instant interactions for various the nondimensional parameters Γ

## A.5.2. Frequency response analysis

Based on the mathematical framework developed in section A.3, the following graphical results for a finite waveguide of unit length with Young's modulus $E = 1$ and mass density $\rho = 1$, are provided. Note that the frequency response function is evaluated at the origin. Fig. A. 4 represents the amplitude of the complex frequency response for different values of $\alpha$ and $\mu$. From the figure, it is clear the value of $|H(j\omega)|$ decreases as the memory effect grows stronger. This, indeed, reflects the influence of induced damping due to the integral term $\int_{-\infty}^{t} P(t-\tau)\, u(x,t)\, d\tau$ when included into the conventional wave equation. The phase response of a waveguide with memory to an input signal with frequency content of sub-50 $rad/s$ is depicted in Fig. A. 5. The abruptness of the phase shift may be attributed to high damping at the corresponding frequency. Drastic changes in phase response of system is due to an increase in the memory gain $\mu$. Thus, temporal memory can cause a considerable delay of the input signal.

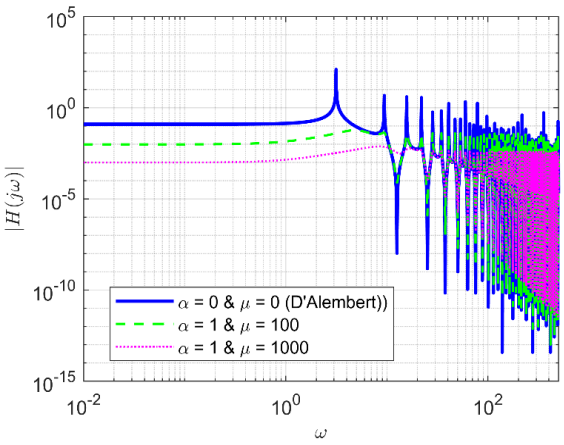


Fig. A. 4: The variation in the amplitude of the transfer function for the central point of a waveguide with non-instant interactions with respect to frequency for various values of $\alpha$ and $\mu$

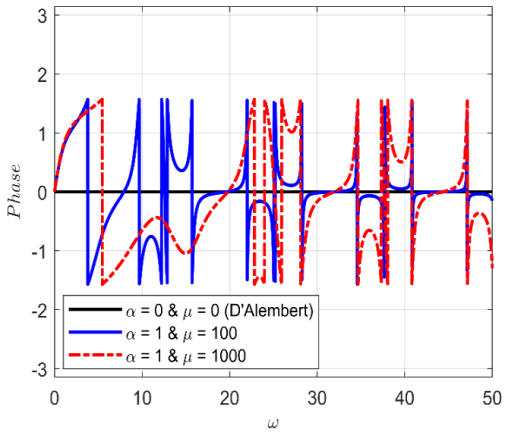


Fig. A. 5: The phase response for the central point of a waveguide with non-instant interactions with respect to frequency for various values of $\alpha$ and $\mu$

## A.6. Final remarks

The frequency response and wave propagation analysis for a waveguide with temporal memory is investigated in this study. The standard one-dimensional wave equation is modified by considering a supplementary term which describes the dependence of the system's response on the whole time-history. The spatiotemporal Fourier transform is applied to study the characteristics of waves in such a system with unbounded length and the dispersion relations is expressed in terms of nondimensional parameters. Results indicate the attenuation is significantly dependent upon the frequency. In the low frequency region, i.e. for $\Omega = \omega/\alpha$ about less than 5, i.e. for $\omega < 5\alpha$, the wave phase and group speeds are highly affected by the memory effects and can be reduced or increased of a factor up to 2. Furthermore, the imposed forcing term which introduces the memory effects, causes significant variations in phase response as the influence of memory grows stronger.

# References

[1] On the rotation of plane of polarisation of electric wave by a twisted structure, Proc. R. Soc. London. 63 (1898) 146–152.

[2] V.G. Veselago, The Electrodynamics of Substances with Simultaneously Negative Values of ∈ and μT, Sov. Phys. Uspekhi. 10 (1968) 509–514.

[3] J.B. Pendry, Negative refraction makes a perfect lens, Phys. Rev. Lett. 85 (2000) 3966–3969.

[4] D.R. Smith, W.J. Padilla, D.C. Vier, S.C. Nemat-Nasser, S. Schultz, Composite medium with simultaneously negative permeability and permittivity, Phys. Rev. Lett. 84 (2000) 4184–4187.

[5] Advances in Electromagnetics of Complex Media and Metamaterials, Springer Netherlands, 2002.

[6] T.J. Cui, R. Liu, D.R. Smith, Introduction to metamaterials, in: Metamaterials Theory, Des. Appl., Springer US, 2010: pp. 1–19.

[7] U. Leonhardt, Optical conformal mapping, Science (80-. ). 312 (2006) 1777–1780.

[8] J.B. Pendry, D. Schurig, D.R. Smith, Controlling electromagnetic fields, Science (80-. ). 312 (2006) 1780–1782.

[9] D. Schurig, J.J. Mock, B.J. Justice, S.A. Cummer, J.B. Pendry, A.F. Starr, D.R. Smith, Metamaterial electromagnetic cloak at microwave frequencies, Science (80-. ). 314 (2006) 977–980.

[10] V.I. Slyusar, Metamaterials on antenna solutions, Proc. Int. Conf. Antenna Theory Tech. 0 (2009) 19–24.

[11] S. Enoch, G. Tayeb, P. Sabouroux, N. Guérin, P. Vincent, A Metamaterial for Directive Emission, Phys. Rev. Lett. 89 (2002) 213902.

[12] O.F. Siddiqui, M. Mojahedi, G. V. Eleftheriades, Periodically Loaded Transmission Line with Effective Negative Refractive Index and Negative Group Velocity, IEEE Trans. Antennas Propag. 51 (2003) 2619–2625.

[13] J.D. Baena, J. Bonache, F. Martín, R.M. Sillero, F. Falcone, T. Lopetegi, M.A.G. Laso, J. García-García, I. Gil, M.F. Portillo, M. Sorolla, Equivalent-circuit models for split-ring resonators and complementary split-ring resonators coupled to planar transmission lines, IEEE Trans. Microw. Theory Tech. 53 (2005) 1451–1460.

[14] N. Fang, H. Lee, C. Sun, X. Zhang, Sub-diffraction-limited optical imaging with a silver superlens, Science (80-. ). 308 (2005) 534–537.

[15] A. Grbic, G. V. Eleftheriades, Overcoming the Diffraction Limit with a Planar Left-Handed Transmission-Line Lens, Phys. Rev. Lett. 92 (2004) 117403.

[16] J. Li, C.T. Chan, Double-negative acoustic metamaterial, Phys. Rev. E. 70 (2004) 055602.

[17] G.P. Srivastava, The Physics of Phonons, Routledge, 2019.

[18] M. Sigalas, E.N. Economou, Band structure of elastic waves in two dimensional

systems, Solid State Commun. 86 (1993) 141–143.

[19] F.R. Montero de Espinosa, E. Jiménez, M. Torres, Ultrasonic band gap in a periodic two-dimensional composite, Phys. Rev. Lett. 80 (1998) 1208–1211.

[20] I.E. Psarobas, N. Stefanou, A. Modinos, Scattering of elastic waves by periodic arrays of spherical bodies, Phys. Rev. B - Condens. Matter Mater. Phys. 62 (2000) 278–291.

[21] S. Yang, J.H. Page, Z. Liu, M.L. Cowan, C.T. Chan, P. Sheng, Focusing of sound in a 3D phononic crystal, Phys. Rev. Lett. 93 (2004) 024301.

[22] S. V. Sorokin, On propagation of plane symmetric waves in a periodically corrugated straight elastic layer, J. Sound Vib. 349 (2015) 348–360.

[23] R.B. Nielsen, S. V. Sorokin, Periodicity effects of axial waves in elastic compound rods, J. Sound Vib. 353 (2015) 135–149.

[24] A. Hvatov, S. Sorokin, Free vibrations of finite periodic structures in pass- and stop-bands of the counterpart infinite waveguides, J. Sound Vib. 347 (2015) 200–217.

[25] Z. Liu, X. Zhang, Y. Mao, Y.Y. Zhu, Z. Yang, C.T. Chan, P. Sheng, Locally resonant sonic materials, Science (80-. ). 289 (2000) 1734–1736.

[26] V. Fokin, M. Ambati, C. Sun, X. Zhang, Method for retrieving effective properties of locally resonant acoustic metamaterials, Phys. Rev. B - Condens. Matter Mater. Phys. 76 (2007) 144302.

[27] P.F. Pai, Metamaterial-based Broadband Elastic Wave Absorber, J. Intell. Mater. Syst. Struct. 21 (2010) 517–528.

[28] H. Sun, X. Du, P.F. Pai, Theory of metamaterial beams for broadband vibration absorption, J. Intell. Mater. Syst. Struct. 21 (2010) 1085–1101.

[29] P. Wang, F. Casadei, S. Shan, J.C. Weaver, K. Bertoldi, Harnessing buckling to design tunable locally resonant acoustic metamaterials, Phys. Rev. Lett. 113 (2014) 014301.

[30] G. Ma, P. Sheng, Acoustic metamaterials: From local resonances to broad horizons, Sci. Adv. 2 (2016) e1501595.

[31] C. Sugino, S. Leadenham, M. Ruzzene, A. Erturk, On the mechanism of bandgap formation in locally resonant finite elastic metamaterials, J. Appl. Phys. 120 (2016) 134501.

[32] S. Zhang, C. Xia, N. Fang, Broadband acoustic cloak for ultrasound waves, Phys. Rev. Lett. 106 (2011) 024301.

[33] D. Monroe, One-way Mirror for Sound Waves, Focus (Madison). 24 (2009).

[34] Acoustic “superlens” could mean finer ultrasound scans | New Scientist, (n.d.). https://www.newscientist.com/article/dn13156-acoustic-superlens-could-mean-finer-ultrasound-scans/ (accessed September 23, 2020).

[35] S. Zhang, L. Yin, N. Fang, Focusing ultrasound with an acoustic metamaterial network, Phys. Rev. Lett. 102 (2009) 194301.

[36] P. Kerrian, A. Hanford, B. Beck, D. Capone, Underwater acoustic ground cloak development and demonstration, J. Acoust. Soc. Am. 143 (2018) 1918–1918.

[37] Y. Dumeige, Stopping and manipulating light using a short array of active microresonators, EPL. 86 (2009) 14003.

[38] D.E. Chang, A.H. Safavi-Naeini, M. Hafezi, O. Painter, Slowing and stopping light using an optomechanical crystal array, New J. Phys. 13 (2011) 023003.

[39] D. Psaltis, Coherent optical information systems, Science (80-. ). 298 (2002) 1359–1363.

[40] M.F. Yanik, S. Fan, Dynamic photonic structures: stopping, storage, and time reversal of light, Stud. Appl. Math. 115 (2005).

[41] L.J. Wang, A. Kuzmich, A. Dogariu, Gain-assisted superluminal light propagation, Nature. 406 (2000) 277–279.

[42] A.D. Neira, G.A. Wurtz, A. V. Zayats, Superluminal and stopped light due to mode coupling in confined hyperbolic metamaterial waveguides, Sci. Rep. 5 (2015) 17678.

[43] A. Carcaterra, A. Akay, Transient energy exchange between a primary structure and a set of oscillators: Return time and apparent damping, J. Acoust. Soc. Am. 115 (2004) 683–696.

[44] A. Carcaterra, A. Akay, I.M. Koç, Near-irreversibility in a conservative linear structure with singularity points in its modal density, J. Acoust. Soc. Am. 119 (2006) 2141–2149.

[45] A. Carcaterra, A. Akay, Theoretical foundations of apparent-damping phenomena and nearly irreversible energy exchange in linear conservative systems, J. Acoust. Soc. Am. 121 (2007) 1971–1982.

[46] Eringen, A.Cemal, Edelen, D.G.B., On nonlocal elasticity, Int. J. Eng. Sci. 10 (1972) 233–248.

[47] A.C. Eringen, Plane waves in nonlocal micropolar elasticity, Int. J. Eng. Sci. 22 (1984) 1113–1121.

[48] A.C. Eringen, Linear Theory of Micropolar Elasticity, J. Math. Mech. 15 (1966) 909–923.

[49] A.C. Eringen, Linear theory of nonlocal elasticity and dispersion of plane waves, Int. J. Eng. Sci. 10 (1972) 425–435.

[50] A. Carcaterra, F. dell'Isola, R. Esposito, M. Pulvirenti, Macroscopic Description of Microscopically Strongly Inhomogenous Systems: A Mathematical Basis for the Synthesis of Higher Gradients Metamaterials, Arch. Ration. Mech. Anal. 218 (2015).

[51] A. Carcaterra, N. Roveri, A. Akay, Connectivity in waves and vibrations: One-to-six, one-to-all, all-to-all and random connections, in: Proc. ISMA 2018 - Int. Conf. Noise Vib. Eng. USD 2018 - Int. Conf. Uncertain. Struct. Dyn., 2018.

[52] A.D. Buckingham, Permanent and Induced Molecular Moments and Long-Range Intermolecular Forces, in: Adv. Chem. Phys. Intermol. Forces, Vol. 12, 2007: pp. 107–142.

[53] R. Grice, D.R. Herschbach, Long-range configuration interaction of ionic and covalent states, Mol. Phys. 27 (1974) 159–175.

[54] K.D. Jordan, M.N. Paddon-Row, Analysis of the Interactions Responsible for Long-Range Through-Bond-Mediated Electronic Coupling between Remote Chromophores Attached to Rigid Polynorbornyl Bridges, Chem. Rev. 92 (1992) 395–410.

[55] G.A. Victor, K. Sando, Long-rangee interaction between metastable helium and ground state helium [14], J. Chem. Phys. 55 (1971) 5421–5422.

[56] H. Fröhlich, Long-range coherence and energy storage in biological systems, Int. J. Quantum Chem. 2 (1968) 641–649.

[57] M.M. Pomerantz, N. Ahmadiyeh, L. Jia, P. Herman, M.P. Verzi, H. Doddapaneni, C.A. Beckwith, J.A. Chan, A. Hills, M. Davis, K. Yao, S.M. Kehoe, H.J. Lenz, C.A. Haiman, C. Yan, B.E. Henderson, B. Frenkel, J. Barretina, A. Bass, J. Tabernero, J. Baselga, M.M. Regan, J.R. Manak, R. Shivdasani, G.A. Coetzee, M.L. Freedman, The 8q24 cancer risk variant rs6983267 shows long-range interaction with MYC in colorectal cancer, Nat. Genet. 41 (2009) 882–884.

[58] S. Tanaka, H.A. Scheraga, Medium-and Long-Range Interaction Parameters between Amino Acids for Predicting Three-Dimensional Structures of Proteins, Macromolecules. 9 (1976) 945–950.

[59] E.M. Rauch, Y. Bar-Yam, Long-range interactions and evolutionary stability in a predator-prey system, Phys. Rev. E - Stat. Nonlinear, Soft Matter Phys. 73 (2006) 020903.

[60] F.A. Rihan, S. Lakshmanan, A.H. Hashish, R. Rakkiyappan, E. Ahmed, Fractional-order delayed predator–prey systems with Holling type-II functional response, Nonlinear Dyn. 80 (2015) 777–789.

[61] A. Gupta, T. Banerjee, P.S. Dutta, Increased persistence via asynchrony in oscillating ecological populations with long-range interaction, Phys. Rev. E. 96 (2017) 042202.

[62] A. Einstein, B. Podolsky, N. Rosen, Can quantum-mechanical description of physical reality be considered complete?, Phys. Rev. 47 (1935) 777.

[63] N. Kawakami, S.K. Yang, Finite-size scaling in one-dimensional quantum liquid with long-range interaction, Phys. Rev. Lett. 67 (1991) 2493–2496.

[64] F.D.M. Haldane, Z.N.C. Ha, J.C. Talstra, D. Bernard, V. Pasquier, Yangian symmetry of integrable quantum chains with long-range interactions and a new description of states in conformal field theory, Phys. Rev. Lett. 69 (1992) 2021.

[65] P. Richerme, Z.X. Gong, A. Lee, C. Senko, J. Smith, M. Foss-Feig, S. Michalakis, A. V. Gorshkov, C. Monroe, Non-local propagation of correlations in quantum systems with long-range interactions, Nature. 511 (2014) 198–201.

[66] W. Kolos, L. Wolniewicz, Variational Calculation Of The Long-Range Interaction Between Two Ground-State Hydrogen Atoms, Chem. Phys. Lett. 24 (1974) 457–460.

[67] D.D. Konowalow, J.L. Fish, Long-range interactions of Li(n = 2) states with each other and the long-range interaction of Li(2s2S) with Li(3s2S), Chem. Phys. 77 (1983) 435–448.

[68] J.O. Hirschfelder, P.O. Löwdin, Long-range interaction of two ls-hydrogen atoms expressed in terms of natural spin-orbitals, Mol. Phys. 2 (1959) 229–258.

[69] K. Smith, L.F. Mollenauer, Experimental observation of soliton interaction over long fiber paths: discovery of a long-range interaction, Opt. Lett. 14 (1989) 1284–1286.

[70] C. Rotschild, B. Alfassi, O. Cohen, M. Segev, Long-range interactions between optical solitons, Nat. Phys. 2 (2006) 769–774.

[71] J.K. Jang, M. Erkintalo, S.G. Murdoch, S. Coen, Ultraweak long-range interactions of solitons observed over astronomical distances, Nat. Photonics. 7 (2013) 657–663.

[72] J. Oppenheim, Thermodynamics with long-range interactions: From Ising models to black holes, Phys. Rev. E - Stat. Physics, Plasmas, Fluids, Relat. Interdiscip. Top. 68 (2003) 016108.

[73] C. Tsallis, Possible generalization of Boltzmann-Gibbs statistics, J. Stat. Phys. 52 (1988) pages479–487.

[74] F. Bouchet, S. Gupta, D. Mukamel, Thermodynamics and dynamics of systems with long-range interactions, Phys. A Stat. Mech. Its Appl. 389 (2010) 4389–4405.

[75] R.C. Fetecau, Y. Huang, T. Kolokolnikov, Swarm dynamics and equilibria for a nonlocal aggregation model, Nonlinearity. 24 (2011) 2681.

[76] D. Gorbonos, R. Ianconescu, J.G. Puckett, R. Ni, N.T. Ouellette, N.S. Gov, Long-range acoustic interactions in insect swarms: An adaptive gravity model, New J. Phys. 18 (2016) 073042.

[77] V. Zhdankin, J.C. Sprott, Simple predator-prey swarming model, Phys. Rev. E - Stat. Nonlinear, Soft Matter Phys. 82 (2010) 056209.

[78] A. Erramilli, O. Narayan, W. Willinger, Experimental queueing analysis with long-range dependent packet traffic, IEEE/ACM Trans. Netw. 4 (1996) 209–223.

[79] P. Shang, Y. Lu, S. Kamae, Detecting long-range correlations of traffic time series with multifractal detrended fluctuation analysis, Chaos, Solitons and Fractals. 36 (2008) 82–90.

[80] D. Helbing, A. Hennecke, V. Shvetsov, M. Treiber, Micro- and macro-simulation of freeway traffic, Math. Comput. Model. 35 (2002) 517–547.

[81] C. Dogbe, On the modelling of crowd dynamics by generalized kinetic models, J. Math. Anal. Appl. 387 (2012) 512–532.

[82] Y.W. Cheung, Long memory in foreign-exchange rates, J. Bus. Econ. Stat. 11 (1993) 93–101.

[83] V. V. Tarasova, V.E. Tarasov, Logistic map with memory from economic model, Chaos, Solitons and Fractals. 95 (2017) 84–91.

[84] V. V. Tarasova, V.E. Tarasov, Concept of dynamic memory in economics, Commun. Nonlinear Sci. Numer. Simul. 55 (2018) 127–145.

[85] W. Michiels, C.I. Morărescu, S.I. Niculescu, Consensus problems with distributed delays, with application to traffic flow models, SIAM J. Control Optim. 48 (2009) 77–101.

[86] C. Pignotti, I. Reche Vallejo, Asymptotic Analysis of a Cucker–Smale System with Leadership and Distributed Delay, in: Springer INdAM Ser., Springer International

Publishing, 2019: pp. 233–253.

[87] R. Sipahi, F.M. Atay, S.I. Niculescu, Stability of traffic flow behavior with distributed delays modeling the memory effects of the drivers, SIAM J. Appl. Math. 68 (2007) 738–759.

[88] H.I. Ene, M.L. Mascarenhas, J. Saint Jean Paulin, Fading memory effects in elastic-viscoelastic composites, Math. Model. Numer. Anal. 31 (1997) 927–952.

[89] Z. Abdessamad, I. Kostin, G. Panasenko, V.P. Smyshlyaev, Memory effect in homogenization of a viscoelastic kelvin-voigt model with time-dependent coefficients, Math. Model. Methods Appl. Sci. 19 (2009) 1603–1630.

[90] M.A. Ezzat, A.S. El-Karamany, A.A. El-Bary, Generalized thermo-viscoelasticity with memory-dependent derivatives, Int. J. Mech. Sci. 89 (2014) 470–475.

[91] I. Freund, M. Rosenbluh, S. Feng, Memory effects in propagation of optical waves through disordered media, Phys. Rev. Lett. 61 (1988) 2328.

[92] S. Feng, C. Kane, P.A. Lee, A.D. Stone, Correlations and fluctuations of coherent wave transmission through disordered media, Phys. Rev. Lett. 61 (1988) 834.

[93] S. Schott, J. Bertolotti, J.-F. Léger, L. Bourdieu, S. Gigan, Characterization of the angular memory effect of scattered light in biological tissues, Opt. Express. 23 (2015) 13505–13516.

[94] E. Kröner, Elasticity theory of materials with long range cohesive forces, Int. J. Solids Struct. 3 (1967) 731–742.

[95] M. Di Paola, M. Zingales, Long-range cohesive interactions of non-local continuum faced by fractional calculus, Int. J. Solids Struct. 45 (2008) 5642–5659.

[96] M. Di Paola, G. Failla, M. Zingales, Physically-Based Approach to the Mechanics of Strong Non-Local Linear Elasticity Theory, J. Elast. 97 (2009) 103–130.

[97] M. Di Paola, A. Pirrotta, M. Zingales, Mechanically-based approach to non-local elasticity: Variational principles, Int. J. Solids Struct. 47 (2010) 539–548.

[98] M. Zingales, M. Di Paola, G. Failla, The mechanically-based approach to 3D non-local linear elasticity theory: Long-range central interactions, Int. J. Solids Struct. 47 (2010) 2347–2358.

[99] M. Zingales, Wave propagation in 1D elastic solids in presence of long-range central interactions, J. Sound Vib. 330 (2011) 3973–3989.

[100] V.E. Tarasov, Continuous limit of discrete systems with long-range interaction, J. Phys. A. Math. Gen. 39 (2006) 14895.

[101] V.E. Tarasov, G.M. Zaslavsky, Fractional dynamics of systems with long-range interaction, Commun. Nonlinear Sci. Numer. Simul. 11 (2006) 885–898.

[102] V.E. Tarasov, G.M. Zaslavsky, Fractional dynamics of coupled oscillators with long-range interaction, Chaos. 16 (2006) 023110.

[103] V.E. Tarasov, Lattice model of fractional gradient and integral elasticity: Long-range interaction of Grünwald–Letnikov–Riesz type, Mech. Mater. 70 (2014) 106–114.

[104] A. Carcaterra, F. Coppo, F. Mezzani, S. Pensalfini, Metamaterials: Wave propagation

control, in: Proc. ISMA 2016 - Int. Conf. Noise Vib. Eng. USD2016 - Int. Conf. Uncertain. Struct. Dyn., 2016.

[105] F. Mezzani, F. Coppo, S. Pensalfini, N. Roveri, A. Carcaterra, Twin-waves propagation phenomena in magnetically-coupled structures, in: Procedia Eng., Elsevier Ltd, 2017: pp. 711–716.

[106] S. Pensalfini, F. Coppo, F. Mezzani, G. Pepe, A. Carcaterra, Optimal control theory based design of elasto-magnetic metamaterial, in: Procedia Eng., Elsevier Ltd, 2017: pp. 1761–1766.

[107] F. Coppo, A.S. Rezaei, F. Mezzani, S. Pensalfini, A. Carcaterra, Waves path in an elastic membrane with selective nonlocality, in: Proc. ISMA 2018 - Int. Conf. Noise Vib. Eng. USD 2018 - Int. Conf. Uncertain. Struct. Dyn., 2018.

[108] N. Roveri, S. Pensalfini, A. Carcaterra, Small-world based interactions in elastic metamaterials, in: Proc. ISMA 2018 - Int. Conf. Noise Vib. Eng. USD 2018 - Int. Conf. Uncertain. Struct. Dyn., 2018.

[109] A. Carcaterra, F. Coppo, F. Mezzani, S. Pensalfini, Long-Range Retarded Elastic Metamaterials: Wave-Stopping, Negative, and Hypersonic or Superluminal Group Velocity, Phys. Rev. Appl. 11 (2019) 014041.

[110] F. Mezzani, Elasto-magnetic waves in metamaterials: physics and modelling, Sapienza University of Rome, 2018.

[111] F. Coppo, Waves in elastic metamaterials, Sapienza University of Rome, 2018.

[112] S. Pensalfini, Long-range forces in controlled systems, Sapienza University of Rome, 2018.

[113] D. Beli, J.R.F. Arruda, M. Ruzzene, Wave propagation in elastic metamaterial beams and plates with interconnected resonators, Int. J. Solids Struct. 139–140 (2018) 105–120.

[114] E. Ghavanloo, S.A. Fazelzadeh, Wave propagation in one-dimensional infinite acoustic metamaterials with long-range interactions, Acta Mech. 230 (2019) 4453–4461.

[115] P.G. Luan, J.L. Wu, On the possibility of superluminal energy propagation in a hyperbolic metamaterial of metal-dielectric layers, AIP Adv. 8 (2018) 015106.

[116] A. Le Bot, Foundation of Statistical Energy Analysis in Vibroacoustics, Oxford University Press, 2015.

[117] S.T. Wei, C. Pierre, Localization phenomena in mistimed assemblies with cyclic symmetry part II: Forced vibrations, J. Vib. Acoust. Trans. ASME. 110 (1988) 439–449.

[118] C. Joannin, B. Chouvion, F. Thouverez, M. Mbaye, J.P. Ousty, Nonlinear Modal Analysis of Mistuned Periodic Structures Subjected to Dry Friction, J. Eng. Gas Turbines Power. 138 (2016) 072504.

[119] A. Culla, A. Carcaterra, Statistical moments predictions for a moored floating body oscillating in random waves, J. Sound Vib. 308 (2007) 44–66.

[120] A.H. Nayfeh, Perturbation Methods, Wiley, 2000.

[121] G. Hu, L. Tang, R. Das, Internally coupled metamaterial beam for simultaneous vibration suppression and low frequency energy harvesting, J. Appl. Phys. 123 (2018) 055107.

[122] L. Quan, A. Alù, Hyperbolic Sound Propagation over Nonlocal Acoustic Metasurfaces, Phys. Rev. Lett. 123 (2019) 244303.

[123] P.P. Pratapa, P. Suryanarayana, G.H. Paulino, Bloch wave framework for structures with nonlocal interactions: Application to the design of origami acoustic metamaterials, J. Mech. Phys. Solids. 118 (2018) 115–132.

[124] H. Zhu, S. Patnaika, T.F. Walsh, B.H. Jared, F. Semperlotti, Nonlocal elastic metasurfaces: Enabling broadband wave control via intentional nonlocality, Proc. Natl. Acad. Sci. U. S. A. 117 (2020) 26099–26108.

[125] Introduction to Solid State Physics, 8th Editio, Wiley, n.d.

[126] C. L. Morfey, The Dictionary of Acoustics , Academic Press , 2000.

[127] L. Cremer, M. Heckl, B.A.T. Petersson, Structure-borne sound: Structural vibrations and sound radiation at audio frequencies, Springer Berlin Heidelberg, 2005.

[128] J.B. Keller, Uniform solutions for scattering by a potential barrier and bound states of a potential well, Am. J. Phys. 54 (1986) 546–550.

[129] A.S. Rezaei, F. Mezzani, A. Carcaterra, Memory effect in wave propagation, in: 26th Int. Congr. Sound Vib. 2019, Montreal, 2019.

[130] E. Paifelman, G. Pepe, F. La Gala, A. Carcaterra, Control of Fluctuations of a Tethered Unmanned Underwater-vehicle, in: Proc. ISMA 2018 - Int. Conf. Noise Vib. Eng. USD 2018 - Int. Conf. Uncertain. Struct. Dyn., Leuven, 2018.